Synthesis of Gallium Phosphate Open Frameworks

A thesis presented by David Stephen Wragg B.Sc. to the University of St. Andrews in application for the degree of Doctor of Philosophy

October 2000

Declarations

I, David Stephen Wragg, hereby certify that this thesis has been composed by myself, that it is a record of my work and that it has not been accepted in partial or complete fulfilment of any other degree or professional qualification.

Signed Date 20/10/2000

I was admitted to the Faculty of Science of the University of St. Andrews under the Ordinance General No. 12 on the 1st October 1997 and as a candidate for the degree of Ph.D. on the 1st October 1998.

Signed Date 20/10/2000

I hereby certify that the candidate has fulfilled the conditions of the Resolution and Regulations appropriate to the degree of Ph.D.

Signed Date 9/1/2001

Declaration

In submitting this thesis to the University of St. Andrews, I understand that I am giving permission for it to be made available for its use in accordance with the regulations of the University library for the time being in force, subject to any copyright vested in the work not being affected thereby. I also understand that the title and abstract will be published, and that a copy of the work may also be made and supplied to any *bona fide* library or research worker.

Courses Attended

The Department of Chemistry requires that a number of lecture courses be attended by postgraduate students. these courses were: "Crystallography" (Dr P. Lightfoot), "Electronic and Magnetic Properties of Solids" (Dr P Slater), "Chemistry of Phosphorus and related compounds" (Dr R.A. Aitken), "NMR Spectroscopy" (Dr T. Rutherford), "Non-linear optical materials" (Dr R.E. Morris) and "Hot Topic in Catalysis" (Dr. J-A. M. Anderson).

Acknowledgements

I would like to thank Professor Russell Morris for his enthusiastic supervision of this project. I also thank Dr Paul Wright, Professor J.C. Walton, Dr Alex Slawin, Professor George Ferguson and Dr Nigel Poolton for technical help, constructive discussions and guidance. The Staff at the Synchrotron radiation Source, Daresbury (Dr's Simon Teat, Chiu Tang and Dave Taylor) and the European Synchrotron radiation Facility (Professor Åke Kvick and Dr Gavin Vaughn) also deserve credit for their help in the synchrotron X-ray diffraction experiments.

My thanks are also due to all the past and present members of the Morris group for their help and friendship over the past three years and to the technical staff of the department of chemistry for analytical services.

I thank all my friends "outside" for keeping me sane through music, mountaineering and just plain fun. I'll name no names, you know who you are.

Finally, I thank the EPSRC for funding this work.

Contents

Symbols and Abbreviations

AlPO	Aluminium phosphate
Å	Angstroms (10^{-5}m)
deg	Degrees
δ	Chemical Shift
D*n*R	Double *n* ring secondary building unit, *n* is an integer, commonly 4 or 6
DMAP	4-dimethylaminopyridine
ESR/EPR	Electron spin resonance or electron paramagnetic resonance (alternative names for same technique)
GaPO	Gallium phosphate
K	Kelvin
(MAS)NMR	(Magic angle spinning) nuclear magnetic resonance spectroscopy
PNBU	Pre-nucleation building unit
ppm	Parts per million
(SC/P)XRD	(Single crystal/ powder) X-Ray diffraction
SBU	Secondary building unit
SDA	Structure directing agent

Abstract

This thesis concerns the solvothermal synthesis of gallophosphate structures from non-aqueous media. The work is aimed firstly at the synthesis of new materials using amines as structure directing agents (SDAs) or templates and secondly at studying the mechanisms by which the materials are produced. The determination of structures by X-ray diffraction (XRD), nuclear magnetic resonance (NMR) spectroscopy and other techniques are also of great importance.

The first novel structure discussed is Cyclam-GaPO, which resulted from experiments in which the azamacrocycle cyclam was used as the organic SDA. This is the first example of an open-framework Gallophosphate material in which the organic part of the structure is covalently bonded to the framework. The structure was solved from single crystal XRD data collected from a very small crystal at a synchrotron source. The structure was further developed by the substitution of transition metals for gallium and the resulting phases were characterised by powder XRD and electron spin resonance (ESR) spectroscopy. Several other macrocycles were used as SDAs but did not lead to crystalline gallium phosphate products.

The second part of the thesis concerns the synthesis of gallophosphates with small, simple molecules as SDAs. The system in which pyridine acts as both solvent and template has proved particularly interesting, yielding four different and well characterised structures. Of these, three are produced in the presence of fluoride ions and one without. The structures of all four were determined by single crystal XRD and solid state NMR data is included for the previously unreported structures. A systematic study of synthesis conditions for these materials was carried out which helps to give some insight into the

mechanisms of synthesis for the materials and shows that production of some of the materials is favoured under certain conditions. Another new structure is also reported in this section, with 4-dimethylaminopyridine as the SDA. The structure of this material was solved from a very small single crystal and contains a structural unit related to that of one of the pyridine templated materials. The similarity of these units and their relationship to the double four ring unit which is found in several open framework structures is discussed.

CHAPTER 1

INTRODUCTION

1.1 Molecular Sieves

McBain defined molecular sieves in 1932 as a class of compounds, which demonstrate selective absorption properties, separating a chemical mixture on the basis of molecular size and shape differences.[1] It is now known that the reason for the properties of the molecular sieves is their "microporous" structure. For the most well known family of such compounds this consists of a framework of cations tetrahedrally coordinated to four oxygen atoms forming an ordered three-dimensional structure. The framework frequently forms voids and channels of similar size to small molecules, the micropores.

The best known of the many compounds which fall into McBain's definition are the zeolites, a family of minerals first discovered and named by A.F. Cronstedt in 1756.[2] These materials are defined as crystalline aluminosilicates based on an extensive 3D network of oxygen ions forming tetrahedral sites occupied by either Si^{4+} or Al^{3+} cations to give SiO_4 or AlO_4^- tetrahedra. The charge of the AlO_4^- groupings is balanced by the inclusion in the structure of low valence cations such as Na^+ and Mg^{2+}. About 40 natural zeolites are now known.[3] The first synthetic zeolites were prepared by Barrer and Milton in the 1940's.[4, 5] Zeolite-A[6] was patented by the Union Carbide company and this was quickly followed by zeolites X and Y. Since then many new synthetic zeolites have been prepared; some analogues of natural types, others with totally new structures.

Molecular sieves have found a variety of uses in industry including ion exchange and gas separation,[7] their most important application however is in catalysis where the shape selectivity of the porous structure is combined with the favourable

safety properties of solid over liquid acids (molecular sieves can be made acidic enough to replace some very strong acid solutions) and the ease of separation of a hetrogeneous catalyst. The best known use of microporous solid acid catalysts is in hydrocarbon cracking but they have found some uses in fine chemical synthesis and these applications seem set to increase in number.[8] Modified molecular sieves have also been found to have useful catalytic properties. The titanosilicates, for example, have been shown to catalyse a range of organic oxidations by stabilising peroxide species.[9]

Since the discovery of the useful properties of zeolites much work has been concentrated on modifying them to refine their useful characteristics. Various metal ions have been substituted for Si and Al and there are many publications,[10] but more pertinent to the work presented here 1982 saw the discovery of a truly novel family of synthetic molecular sieves, the aluminium phosphates (AlPOs). Since the discovery of AlPO-5 by Flannigen *et. al.*[11] many new aluminium and gallium phosphates have been synthesised. The materials generally have an $Al:PO_4$ ratio of 1:1 which means that no charge balancing cations are necessary in the structure. The gallium phosphates (GaPOs) are a logical next step from AlPOs (gallium being below aluminium in group III of the periodic table) and have proved interesting, particularly since gallium is less likely than aluminium to adopt a tetrahedral coordination in solids; the different polyhedra it adopts then allows a range of structural architectures to be formed. Again the literature contains examples of both previously known structures (e.g. the GaPO version of zeolite-A[12]) and completely new structures.[3] Metallophosphates have also been prepared using several other cations including iron, magnesium and vanadium.[13]

1.2 The structure of Molecular Sieves

Several types of material can be classified as molecular sieves under McBain's description, including pillared clays, porous charcoals and of course zeolites. The most simple classification of such structures is in terms of pore size, those with pore diameters of 3-20Å are called microporous, those with pore diameters of 20-50Å are known as mesoporous materials. This work concerns the synthesis of microporous molecular sieves which generally have a more ordered and crystalline nature than mesoporous systems.

The structures of zeolite-type microporous materials can be built up in three stages. Firstly the metal ions (Si, Al, Ga, P, etc) are tetrahedrally coordinated to four oxygen atoms. These MO_4 tetrahedra are known as the primary building units. Secondary building units (SBUs) are geometric groupings of the MO_4 units from which all zeolite structures can be generated. They are described in terms of the number of M atoms, for instance, a double four ring (D4R) unit is composed of two rings of four M atoms linked by oxygen into a cube (fig.1.1).

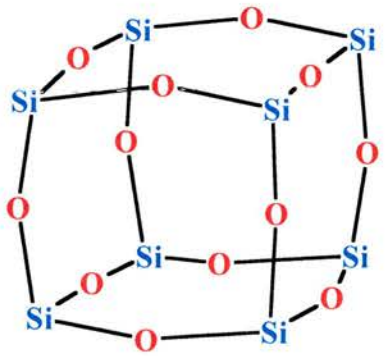

Figure 1.1 *A zeolite double four ring secondary building unit*

Other common SBUs include single four, six and eight rings, double six and eight rings and 4-1, 5-1 and 4-4-1 branched rings (fig. 1.2).

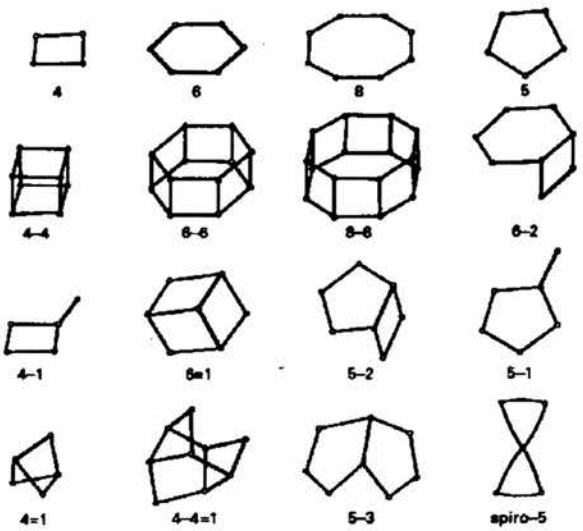

***Figure 1.2** Zeolite SBUs*

The fact that all possible zeolite structures can be built up from the SBU groupings has made them of great interest, firstly as a basis for theoretical predictions of possible zeolite structures[14] and secondly as a pathway for rational molecular sieve synthesis. This latter application has grow out of an initial interest in the so-called polyhedral oligameric silsesquioxanes (POSS) as model compounds for zeolite SBUs.[15] Cubic POSS resemble the D4R zeolite SBU, carrying a range of organic moieties on the corners. D6R POSS have also been synthesised as well as a range of group IV metal phosphonates of similar structures.[16] Recently Zhang and co workers have succeeded building hydride functionalised POSS cubes up into a porous structure using a hydrosilation reaction,[17] however, the materials produced are not crystalline and seem to be most comparable to the mesoporous silicates. The search for a true "crystal engineering" pathway to zeolite-type structures continues.

The third stage in zeolite structure development is the formation of tertiary units from the SBUs. Most tertiary units can be formed from more than one type of SBU and can be linked together to produce more than one type of framework

topology. A good example of this is the sodalite cage which can be formed from either four or six ring SBUs and which, by linking units in different ways can lead to the sodalite, zeolite-A, faujasite and EMC-2 structures (fig. 1.3).

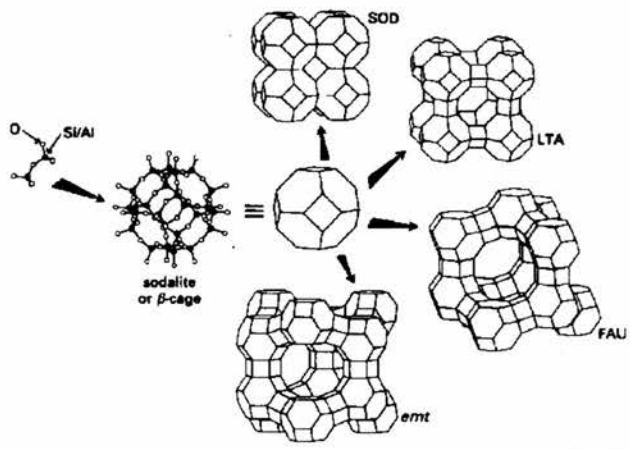

Figure 1.3 *Zeolite structures formed by linking sodalite cages in various ways*

1.3 Molecular Sieve Synthesis

1.3.1 background

Early attempts at zeolite synthesis used extremely high temperature and pressure to mimic the conditions under which the zeolite minerals formed in the earth's crust. The process was revolutionised by the work of Barrer,[4] who applied the process of hydrothermal synthesis to zeolite preparation. Hydrothermal synthesis uses the exceptional solvating properties of water under conditions of high temperature and autogeneous pressure in an autoclave as a medium for crystalising solids. In order to prepare open frameworks under such conditions it is normally necessary to add a structure directing agent or template to the reaction mixture, in early zeolite syntheses alkali and alkaline earth metal ions were used. In 1961 however, Barrer made a second important contribution by preparing zeolites using amine templates.[18] Since

then the use of organic templates in molecular sieve synthesis has been extensively developed.

The mechanisms of hydrothermal reactions are not well understood and are the subject of much research and speculation. Of particular interest is the template-framework interaction. A common simplification of the mechanism of zeolite formation is shown below (fig. 1.4), water molecules in the coordination sphere of the template are replaced by silicate species which then nucleate to form the extended microporous structure.

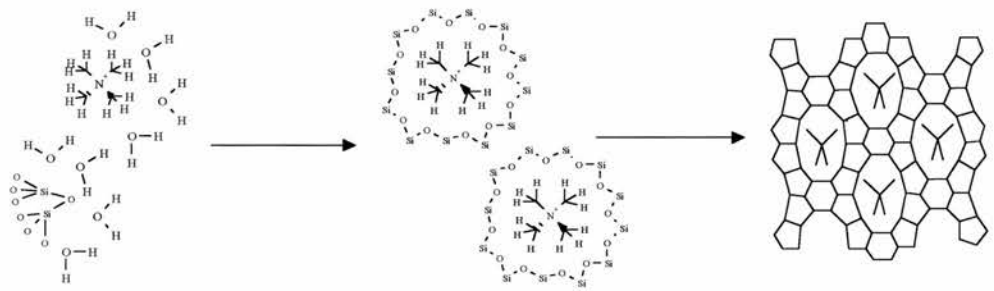

Figure 1.4 *Schematic illustration of siliceous zeolite formation. The hydrophobic hydration sphere of the template (in this case tetramethyl ammonium cations) are partially or fully replaced by silicate species. These inorganic-organic interactions form the basis of the geometric relationship between the template and the zeolite pores once nucleation and crystal growth have occurred.*

Three types of template-framework interaction have been proposed:

- True templating (in which the product adopts a structural and electronic configuration specifically dictated by the template that is retained on its removal).
- Structure direction (where a specific template leads to a specific structure, but there is no specific relationship between the shape of the void and that of the template).
- Space filling (which implies a gain in thermodynamic stability in the template-framework complex over the empty framework due to Van der Waals forces).

It is believed that most molecular sieve syntheses fall into the latter two categories (there is only one confirmed example of true templating in the literature to date[19]) however it is still possible to exert a degree of control over the product's architecture by template choice. Many unusual templates have been used. Zones and co workers have used propellanes and adamantanes to produce several new high silica zeolites (including SSZ-23, the first zeolite structure to contain seven-ring channels)[20] while Balkus has prepared molecular sieves using metal complexes as templates.[21] A number of groups have explored the use of specially designed templates. Camblor *et al* have prepared the ITQ-n series of high silica zeolites using modified quinuclidine templates in fluoride containing media[22] (the use of fluoride as a mineralising agent will be further discussed later in this chapter). Specially designed quinuclidine templates were also used in the synthesis of two new magnesium containing AlPOs, STA-1 and 2 by Noble and Wright,[13c, 23] however possibly the most significant contribution in this area has been by Catlow, Thomas and co workers at the Royal Institution of Great Britain. The work of this group of researchers has applied computational techniques to the design of templates for rational synthesis of

microporous materials, especially AlPOs and transition metal substituted AlPOs.[24] Recently they have published several papers on the application of De Novo design to molecular sieve synthesis, preparing templates to specifically target a particular open framework structure.[25] However, it must be remembered that despite some notable successes it is still not possible predict with certainty the product of a hydrothermal reaction. It is quite common for a carefully designed and painstakingly synthesised template to break down under the extreme conditions of hydrothermal synthesis or for the reaction to lead to a known phase of high stability.[26]

Several systematic studies have attempted to elucidate the factors which govern the template-framework relationship. One of the most commonly cited parameters is the balancing of framework charge by the template. Casci has demonstrated that the Al:Si:template ratio in zeolite syntheses can lead to different structures being formed around the same template.[27] The significance of the Al:Si ratio has also been investigated by Camblor and Villaescusa.[28] The importance of template-framework charge balancing in metal substituted AlPOs and GaPOs has been identified by Stucky and co workers, allowing the synthesis of a wide range of new transition metal substituted open frameworks using relatively simple templates in non aqueous media (to be discussed below).[29]

It seems that the reaction conditions are crucial to the outcome of a hydrothermal preparation, systematic studies such as those mentioned above have identified pH, water content, temperature and heating time as of great importance, Ozin *et al* have used an argument based on hydrolysis and condensation to explain the different products which can be obtained from the JDF-20 reaction mixture when the amount of water is varied.[30] In addition to this Mortlock, Bell and Radke have reported NMR investigations of the species present in Aluminophosphate synthesis gels prior to

hydrothermal treatment and their dependence on pH.[31] More recently Ozin has reported a new model for aluminophosphate formation in which linear AlPO chains are converted to chain, layer and framework structures by twisting, hydrolysis and condensation, based in part on the observations made in the JDF-20 system.[32] This mechanism is based on chains of four or six-ring units (some such chains have been isolated as solid AlPOs) which can, by hydrolysis and condensation, twist into a variety of forms. These chains are then linked to form sheets and 3 dimensional structures (fig. 1.5). In the case of the material UT-6 (see below) the chains are linked by a unit consisting of two octahedrally coordinated aluminium atoms linked by fluorine, however, this unit itself has not been isolated.

Several mechanisms for zeolite synthesis based on the formation of structures from SBUs have been reported.[10] Férey has extended this to GaPOs, in which he suggests the secondary building units formed are dictated by the necessity of balancing the charge of the amine template. The neutral pre-nucleation building units (PNBUs; amine-SBU complexes), whose structure is related to the final material, then condense to produce the final framework. The results of *in situ* NMR and XRD studies (discussed below) are offered in support of the hypothesis.[33] Recently an NMR study of the synthesis of AlPO-CJ2 revealed clear evidence of the isomerisation of a PNBU to form the SBU of the final structure.[34]

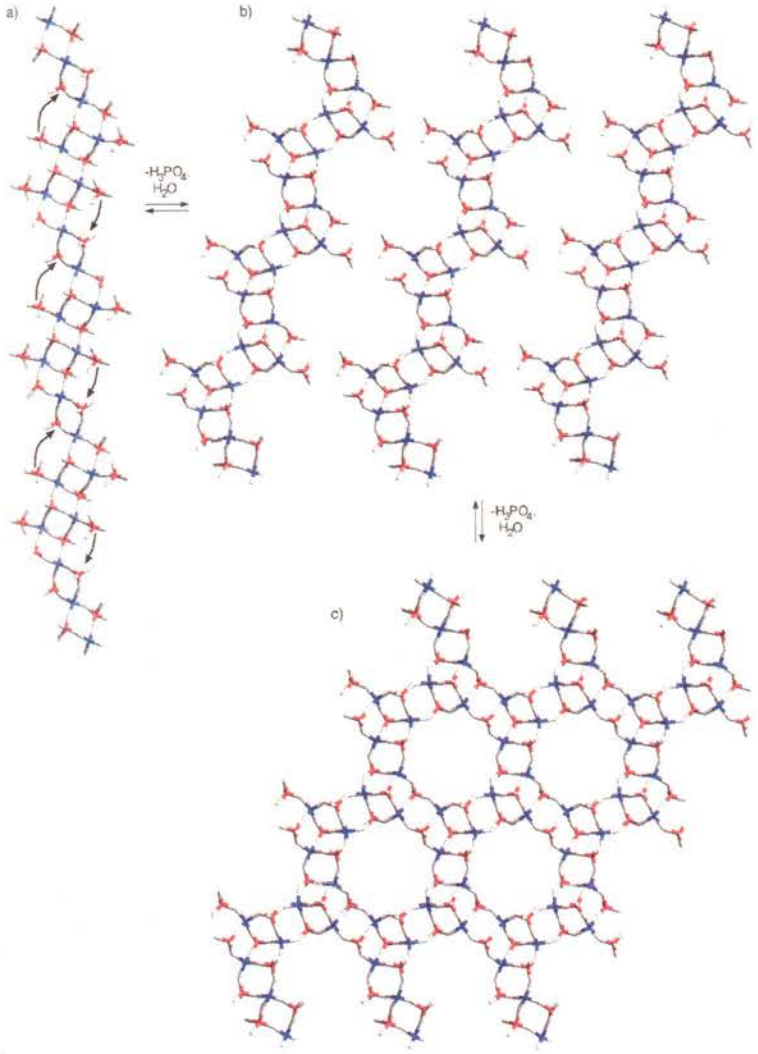

Figure 1.5 *Ozin's chain to layer transformation mechanism for AlPO synthesis. The parent chain (a) is twisted and hydrolysed to produce the chain precursor (b). These chains are then linked to form the sheet structure. Reproduced from reference 32, the example is an AlPO-5 type structure*

The reaction within the autoclave, however, remains mysterious. Recent *in situ* time resolved energy dispersive synchrotron XRD studies (fig. 1.6) carried out by O'Hare and co-workers have demonstrated the formation of molecular sieves by two pathways. In the first case the product appears spontaneously as the first crystalline

phase after a short incubation period, in the second an unidentified crystalline intermediate is formed after the incubation period and then converted to the final product. For the GaPO ULM-5 it was found that the same product could crystallise via both mechanisms depending on the phosphorous source. In both cases it was noted that the products had reached their peaks of crystallinity after about two hours, challenging the conventional wisdom that crystal growth in molecular sieve systems is encouraged by longer heating times.[35]

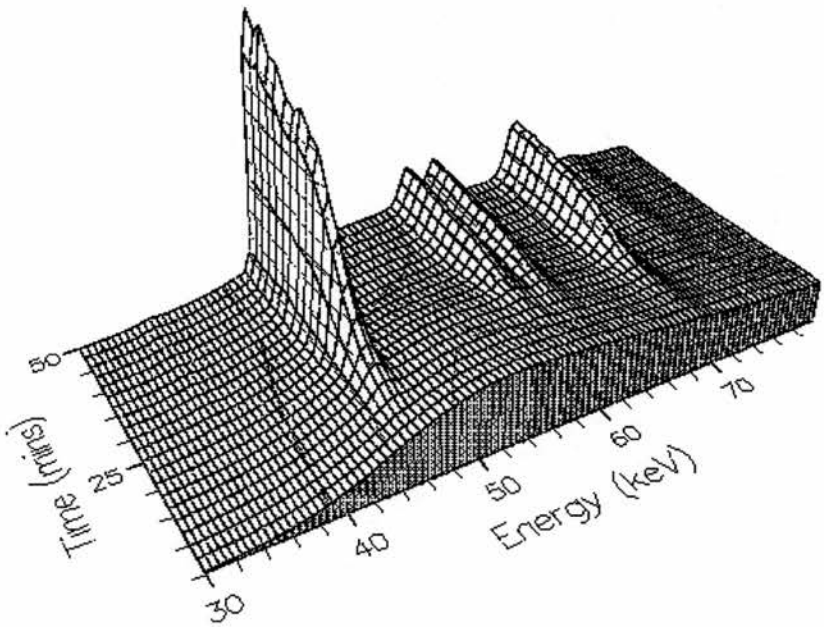

Figure 1.6 *A typical time resolved in situ XRD pattern.*

1.3.2 Non-aqueous synthesis

Water is the most common solvent in open framework synthesis,[3] indeed, until 1985 when Bibby and Dale reported the synthesis of Sodalite structures from ethylene glycol and propan-1-ol solvents,[36] it seems that the idea of using other solvents had been ignored. The rationale of non aqueous molecular sieve synthesis is that the strongly hydrogen bonding nature of water may interfere with the formation of template-framework complexes, due to the water coordinating the template more

strongly than the framework species in solution. In theory therefore, by using more weakly hydrogen bonding solvents a higher template-framework correlation may be achieved. It has also been experimentally observed that non-aqueous solvent systems often yield larger crystals than equivalent hydrothermal preparations.

Although it has been shown that many zeolite syntheses can work equally well in aqueous or non-aqueous solvothermal preparations[37] no new zeolite structures have been isolated specifically under non-aqueous conditions and the use of non-aqueous solvents for the preparation of zeolites remains rare. The area of metal phosphate open framework synthesis by contrast has developed greatly thanks to the use of non-aqueous solvents.

The first AlPO phases to be prepared by non-aqueous routes were known phases (AlPO-5, AlPO-11 and AlPO-21),[38] however, new phases which could not be prepared in aqueous media were soon identified.[39] Probably the most interesting of these was the extra large pore material JDF-20[40] (reported in collaboration by Xu of the university of Jillin, China and Thomas of the Royal Institution of Great Britain, fig. 1.7). The pores of JDF-20 are the same size as those of Cloverite,[41] the largest of any microporous material so far discovered.

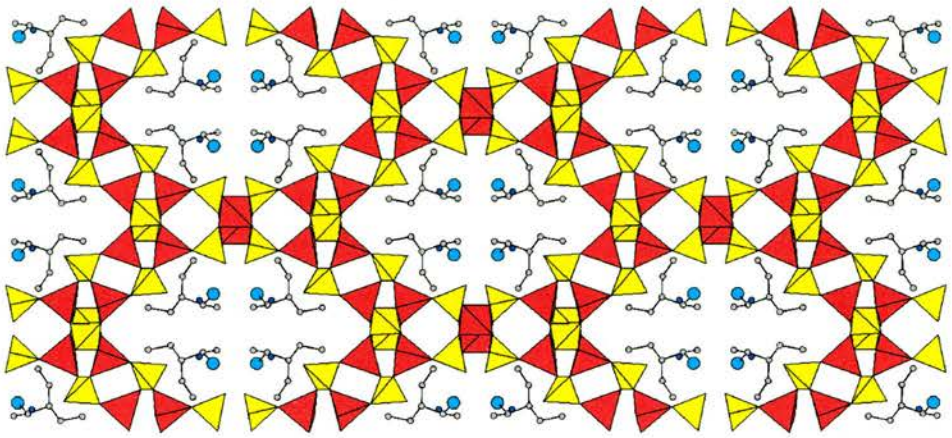

Figure 1.7 *The large oval pores of JDF-20. AlO_4 terahedra shown in red, PO_4 in yellow. The triethylamine template miolecules are shown in the pores.*

The product of the JDF-20 preparation is highly dependent on conditions, at higher temperatures or after long periods of heating AlPO-5 is crystallised rather than the desired product. The structure of JDF-20 has some unusual features. The ratio of Al:P is 5:6 rather than 1:1 as is normally found, it also has an "interrupted" structure, meaning that some of the Al atoms, rather than being linked to four PO_4 tetrahedra carry terminal OH groups. It has been suggested in a recent review that these features my prove of great importance in the future development of extra large pore microporous materials.[42] Another interesting feature of this reaction is that it is the only example of a solvothermal synthesis which will proceed entirely in the absence of water, working even if the water in which the phosphoric acid is dissolved is distilled off.

As previously discussed Ozin and co workers have presented a model for the formation of layered and 3 dimensional AlPO frameworks from chain structures (such as the mono dimensional AlPO $et_3NH^+(H_2ALP_2O_8)$[38]).[32] In the course of their

investigation they also discovered several new AlPO structures, including the parent chain structures and some new 3D structures, for example the fluorinated AlPO UT-6 which transforms to the Chabasite structure on heating.[43] UT-6 is templated by pyridine but is not the only structure which can be formed around this molecule. A second pyridine templated AlPO phase has been reported by Chippindale *et al*[44] synthesised by a conventional hydrothermal preparation, they have also prepared layered AlPO and GaPO phases with pyridine in the interlayer region by an unusual technique of ambient temperature synthesis using tetraethylorthosilicate (TEOS) gels.[45]

During the 1990s Chippindale and co workers have prepared a large number of new AlPO and GaPO structures. Recently they have reported the synthesis of the first transition metal substituted GaPOs,[46] these solvothermal preparations used TEOS as a mineralising agent. Metal subsituted AlPOs (with a transition metal centre replacing the aluminium) have been known for some time and have been the subject of much of the research on structure direction by Catlow *et al* mentioned in the previous section.

Bu, Feng and Stucky, have recently reported some important developments in the non-aqueous synthesis of metal substituted AlPO and GaPO materials. Initially they reported a method for the synthesis of small pore transition metal based zeolite analogues,[29a] then as discussed above, they were able to extend their methodology to the preparation of large cage structures with multidimensional 12-ring channels.[29b] The structures reported include both previously known zeolite topologies and completely novel frameworks formed around a variety of templates in a mixed solvent system of ethylene glycol and water. Recently they have also prepared zeolite type

materials which consist almost totally of cobalt phosphate with only tiny amounts of Al^{3+} or Ga^{3+} cations being necessary for the synthesis to work.[47]

A final interesting piece of research in non-aqueous GaPO synthesis is the approach of cooperative amine templates by Cheetham and co workers. By using two amine templates they isolated the first directly synthesised zeolite-type structure to contain 14-ring pores (Fig. 1.8;the only other framework of this type known at the time, $AlPO_4$-8 is prepared by thermal treatment of VPI-5 and contains a high level of defects).[48] In this structure the 14-ring windows are filled with alternate layers of 4,4'-dipyridyl and pyridine (with pairs of pyridine rings aligned under the rings of the bipyridyl molecules). A second material containing 12 and 8 membered rings has also been prepared in which the two templates (pyridine and tris-(aminoethyl)amine) are separated between the two different channel systems.[49] The same authors have additionally reported another phase, present as a side product in both cases, which can be templated by either pyridine or trimethylamine.[50]

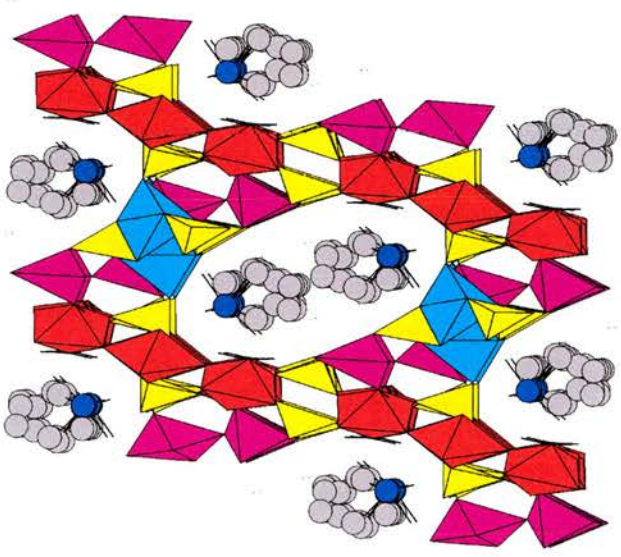

Figure 1.8 *The 14 T-atom ring of DIPYR-GaPO. Four coordinate phosphorus yellow; four, five and six coordinate gallium purple, cyan and red respectively.*

1.3.3 Synthesis of open frameworks from fluoride media

The mineralising effects of fluoride ions in hydrothermal synthesis were first noted by Patton and Flannigen in the 1970's[51] and since then many new phases have been synthesised using these methods. Ozin and co-workers extended the principle to the use of HF-pyridine and HF-alkylamine solvents to prepare "giant" single crystals of several zeolites,[52] and more recently Camblor *et al* have used fluoride containing systems to prepare the ITQ-n series of zeolites previously mentioned (section 1.3.1).[22] As for non-aqueous synthesis, however, the greatest impact of this methodology has been in metal phosphate synthesis.

It is thought that F^- ions act in solution to form reactive fluoride precursors in place of the usual oxo-linked species. Because of this fluorine is often incorporated into the final product, most commonly inside D4Rs in which they may be bonded to two, three or four of the metal atoms, stabilising the structure. Interestingly the fluorine atoms are almost always found to link Al or Ga atoms directly in metal phosphate structures contrary to Lowenstiens rule which states that direct Al-Al linkages should never exist in this type of material (several other exceptions to this rule are also known, however). Fluorine can also be incorporated into structures that do not contain D4Rs, often leading to five and six coordinate metal centres as seen in UT-6[43] and PYR-GaPO.[50]

The effectiveness of fluoride ions as mineralising agents in the preparation of GaPOs was first demonstrated in 1986 by Kessler and co workers.[53] In 1990 Kessler, Estermann *et al* reported the synthesis of Cloverite,[41] still the largest pore molecular sieve structure known, from a fluorine containing synthesis gel. Cloverite is named after it's unusually shaped 20 T-atom pores (which resemble four leafed clovers, fig. 1.9) and like JDF-20 (which has the same pore size) is an interrupted structure.

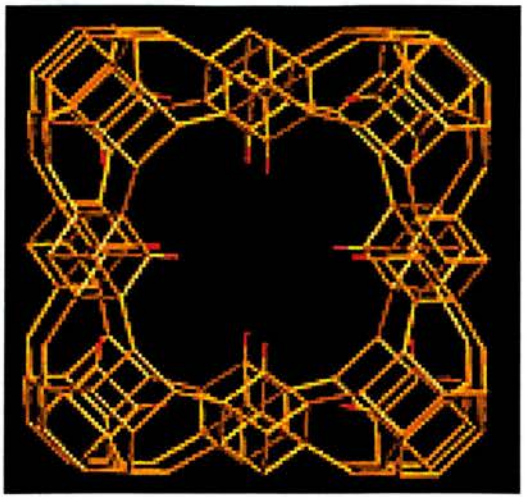

Figure 1.9 *The Pore structure of Cloverite. Note the –OH groups of the interrupted structure protruding into the pores.*

The contribution of Férey to the area of fluoride mineralised open framework synthesis is extensive. The ULM-n series of materials synthesised during his tenure at the Université Le Mans, France includes a huge range of metal phosphate structures, particularly fluorinated GaPOs.[33] The most significant of these new materials is ULM-5, a GaPO with 16 T-atom pore openings.[54] Férey has also postulated a mechanism (discussed earlier) for the formation of the ULM-n type materials based on their common SBUs.[33,55] Recently the broad research into open frameworks by Férey and his co-workers has continued with the MIL-n series of inorganic-organic hybrids.[56]

References

1. J.W. McBain, *The Sorption of Gases and Vapours by Solids*, Rutledge and Sons, London, 1932, Ch. 1.
2. A.F. Cronstedt, *Akad. Handl. Stockholm,* 1756, **17**, 120.
3. M.E. Davies and R.F. Lobo, *Chem. Mater.*, 1992, **4**, 756.
4. R.M. Barrer, *J. Chem. Soc.,* 1948, 127.
5. R.M. Milton, *U.S. Patent 2 882 423,* 1959.
6. R.M. Szostak, *Handbook of Molecular Sieves,* Van Nostrand Rienhold, New York, 1992.
7. D.F. Shriver, P.W. Atkins and C.H. Langford, *Inorganic Chemistry*, Oxford University Press, Oxford, 1994, Ch. 11.
8. J.M. Thomas, *Angew Chem. Int. Ed. Engl.*, 1994, **33**, 913.
9. (a) R. Murugavel and H.W. Roesky, *Angew. Chem. Int. Ed. Engl.,* 1997, **36**, 477. (b) P.T. Tanev, M. Chivebe, T.J. Pinnavala, *Nature,* 1994, **368**, 321.
10. R.M. Szostak, *Molecular Sieves, Principles of Synthesis and Identification,* Van Nostrand Rienhold, New York, 1989, Ch. 1.
11. S.T. Wilson, B.M. Lok, C.A. Messina, T.R. Cannan, E.M. Flannigen, *J. Am. Chem. Soc.,* 1982, **104**, 1146.
12. H. Kessler, J. Patarin, C. Schottdarie, *Stud. Surf. Sci. Catal.*, 1994, **85**, 75.
13. (a) M. Cavellec, C. Egger, J. Linares, M. Nogues, F. Varret and G. Férey, *J. Solid State Chem.*, 1997, **134**, 349. (b)C. Ninclaus, D. Riou and G. Férey, *Acta Cryst. C,* 1996, **52**, 512. (c) G.W. Noble, P.A. Wright and Å. Kvick, *J. Chem Soc., Dalton Trans.,* 1997, **23**, 4485.

14. (a) N. Engel, *Acta Cryst. B*, 1991, **47**, 849. (b) M.M.J. Treacy, K.H. Randall, S. Rao, J.A. Perry and D.J. Chadi, *Ziet. Fur. Krist.*, 1997, **212**, 768.

15. P.G. Harrison, *J. Organometallic Chem.*, 1997, **542**, 141, *and references contained therein.*

16. (a) R. Murugavel, V. Chandrasekhar and H.W. Roesky, *Acc. Chem. Res.*, 1996, **29**, 183. (b) M. G. Walawalkar, H.W. Roesky and R. Murugavel, *Acc. Chem. Res.*, 1999, **32**, 117.

17. C. Zhang, F. Babonneau, C. Bonhomme, R.M. Laine, C.L Soles, H.A. Hristov and A.F. Yee, *J. Am. Chem. Soc.*, 1998, **120**, 8380.

18. R.M. Barrer and P.J. Denny, *J. Chem. Soc.*, 1961, 971.

19. S.L. Lawton and W.J. Rhorburgh, *Science*, 1990, **247**, 1319.

20. (a) S.I. Zones, *Eur. Pat. Appl. 231018*, 1987. (b) S.I. Zones, M.M. Olmstead and D.S. Santilli, *J. Am. Chem. Soc.*, 1992, **114**, 4195. (c) S.I. Zones, *J. Am. Chem. Soc.*, 1996, **118**, 7558. (d) S.I. Zones, *J. Am. Chem. Soc.*, 1997, **119**, 4195.

21. (a) K.J. Balkus, *J. Am. Chem. Soc.*, 1997, **119**, 8474. (b) K.J. Balkus, Stud. Surf. Sci. Catal., **105**, 415.

22. (a) M.A. Camblor, A. Corma, M.J. Diaz-Cabanas and Ch. Baerlocher, *J. Phy. Chem. B*, 1998, **102**, 44. (b) M.A. Camblor, A. Corma, P. Lightfoot, L.A. Villaescusa and P.A. Wright, *Angew. Chem. Int. Ed.*, 1997, **36**, 2659. (c) P.A. Barrett, M.A. Camblor, A. Corma, R.H. Jones and L.A. Villaescusa, *J. Phys. Chem. B*, 1998, **102**, 4147. (d) L.A. Villaescusa, P.A. Barrett and M.A. Camblor, *Angew. Chem. Int. Ed.*, 1999, **38**, 1997.

23. G.W. Noble, P.A. Wright, P. Lightfoot, R.E. Morris, K.J. Hudson, Å. Kvick and H. Graafsma, *Angew. Chem. Int. Ed. Engl.*, 1997, **36**, 81.

24. (a) D.W. Lewis, C.R.A. Catlow and J.M. Thomas, *Chem. Mater.*, 1996, 8, 1112. (b) D.W. Lewis, C.R.A. Catlow and J.M. Thomas, Faraday Discuss., 1997, 451.

25. (a) D.W. Lewis, D.J. Willock, C.R.A. Catlow, J.M. Thomas and G.J. Hutchings, *Nature*, 1996, **382**, 604. (b) D.J. Willock, D.W. Lewis, C.R.A. Catlow, G.J. Hutchings and J.M. Thomas, *J. Mol. Catal. A-Chem.*, 1997, **119**, 415. (c) D.W. Lewis, G. Sankar, J.K. Wyles, J.M. Thomas, C.R.A. Catlow and D.J. Willock, *Angew. Chem.Int. Ed.*, 1997, **36**, 2675.

26. D.S. Wragg and R.E. Morris, *unpublished results.*

27. J.L. Casci, *Stud. Surf. Sci. Catal.*, 1994, **84**,133.

28. (a) L.A. Villaescusa, *PhD Thesis*, Universidad polytéchnica de Valencia, 1999. (b) M.A. Camblor, L.A. Villaescusa, M.J. Diaz-Cabanas, *Top. Catal.*, 1999, **9**, 59.

29. (a) P. Feng, X. Bu, and G.D. Stucky, *Nature,* 1997, **388**, 735. (b) X. Bu, P. Feng and G.D. Stucky, *Science*, 1997, **278**, 2080.

30. S. Oliver, A. Kuperman, A. Lough, G.A. Ozin, J.A. Garces, M.M.Olken and P. Rudolf, *Stud. Surf. Sci. Catal.*, 1994, **84**, 219.

31. R.F. Mortlock, A.T. Bell and C.J. Radke, *J. Phys. Chem.*, 1993, **97**, 775.

32. S. Oliver, A. Kuperman and G.A. Ozin, *Angew. Chem. Int. Ed.*, 1998, **37**, 46.

33. G. Férey, *C. R. Acad. Sci. Ser. C.*, 1998, **1**, 1.

34. F. Taulelle, M. Pruski, J.P. Amoureaux, D. Lang, A. Bailly, C. Hugenard, M. Haouas, C. Geradin, T. Lousieau and G. Férey, *J. Am. Chem. Soc.,* 1999, **121**, 12148.

35. R.J. Francis and D. O'Hare, *J. Chem Soc., Dalton Trans.*, 1998, 3133.

36. D.M. Bibby and M.P. Dale, *Nature*, 1985, **317**, 157.

37. (a) Q.S. Huo, S.H. Feng and R.R. Xu, *Acta Chimica Sinica*, 1990, **48**, 639. (b) Q. Huo, S. Feng and R. Xu, *J. Chem Soc., Chem. Commun.,* 1988, 1486.

38. Q. Huo and R. Xu, *J. Chem Soc., Chem. Commun.*, 1990, 783.

39. R.H. Jones, J.M. Thomas, Q. Huo, R. Xu, M.B. Hursthouse and J. Chen, *J. Chem Soc., Chem. Commun.*, 1991, 1520.

40. (a) Q. Huo, R. Xu, S. Li, Z. Ma, J.M. Thomas, R.H. Jones and A.M. Chippindale, *J. Chem Soc., Chem. Commun.*, 1992, 875. (b) R.H. Jones, J.M. Thomas, J. Chen, R. Xu, Q. Huo, S. Li, Z. Ma, and A.M. Chippindale, *J. Solid State Chem.*, 1993, **102**, 204.

41. M. Estermann, L.B. McCusker, C. Baerlocher, A. Merrouche and H. Kessler, *Nature*, 1991, **352**, 320.

42. R.E. Morris and S.J. Weigel, *Chem. Soc. Rev.*, 1997, **26**, 309.

43. S. Oliver, A. Kupermann, A. Lough and G.A. Ozin, *J. Mater. Chem.*, 1997, **7**, 807.

44. A.M. Chippindale, A.V. Powell, L.M. Bull, R.H. Jones, A.K. Cheetham, J.M. Thomas and R. Xu, *J. Solid State chem.*, 1992, **96**, 199.

45. (a) M.A. Leech, A.R. Cowley, K. Prout and A.M. Chippindale, *Chem. Mater.*, 1998, **10**, 451; (b) A.M. Chippindale, S.J. Brech, *J. Chem Soc., Chem. Commun.*, 1996, 2781.

46. A.M. Chippindale, A.R. Cowley, *Microporous And Mesoporous Mater.*, 1998, **212**, 71.

47. X.H. Bu, T.E. Gier, P.Y. Feng and G.D. Stucky, *Chem.Mater.*, 1998, **102**, 546.

48. S.J. Weigel, R.E. Morris, G.D. Stucky and A.K. Cheetham, *J. Mater. Chem.*, 1998, **8**, 1607.

49. S.J. Weigel, S.C. Weston, A.K. Cheetham and G.D. Stucky, *Chem. Mater.*, 1997, **9**, 1293.

50. S.J. Wiegel, T. Louiseau, G. Férey, V. Munch, F. Taulelle, R.E. Morris, G.D. Stucky and A.K. Cheetham, *Proc. 12th Intl. Zeolite Conference*, 1999, 2453.

51. R.L. Patton and E.M. Flannigen, *U.S. Patent 4 073 865*, 1978.

52. (a) A. Kuperman, S. Nadimi, S. Oliver, G.A. Ozin, J.A. Garces and M.M. Olken, *Nature*, 1993, **365**, 23. (b) S. Nadimi, S. Oliver, A. Kuperman, A. Lough, G.A. Ozin, J.A. Garces, M.M. Olken and P. Rudolf, *Stud. Surf. Sci. Catal.*, 1994, **84**, 93.

53. J.L. Guth, H. Kessler and R. Wey, *Stud. Surf. Sci. Catal.*, 1986, **28**, 121.

54. T. Louiseau and G. Férey, *J. Mater. Chem.*, 1996, **6**, 1073.

55. G. Férey, *J. Fluorine Chem.*, 1995, **7**, 187.

56. C. Paulet, C. Serre, T. Loiseau, D. Riou and G. Ferey, *C. R. Acad. Sci. Ser C*, 1999, **2**, 631.

CHAPTER 2

AIMS OF THIS PROJECT

2.1 Synthesis of Novel Gallium Phosphate Open Frameworks From Non-aqueous Media

The driving force for this project is the search for a better understanding of open framework synthesis. It is hoped that this will eventually lead to a methodology for rational synthesis of molecular sieve materials for catalysis. As discussed in the previous chapter the use of non-aqueous solvothermal synthesis has led to many interesting new open-framework materials (see chapter 1). It is thought that this is due to solvent-template and solvent-framework interactions being minimised by the use less coordinating solvents than water.[1] The first objective is to prepare new materials from non-aqueous media. From the results of these experiments it may subsequently be possible to make deductions about the nature of the structure directing effects influencing the framework architecture. By experimenting with similar series of templates the changes in template structure may be related to the framework (similar studies have been carried out in the past for other series of molecular sieve materials, for example the STA-n magnesium AlPOs[2]), the influence of synthesis conditions may also be investigated by systematic alterations to the initial conditions.

2.2 Characterisation of New Materials

An important part of this work will be the characterisation of the materials prepared by a range of techniques. Most significant of these will be microcrystal diffraction, a novel technique by which single crystal X-ray diffraction (SCXRD) data may be collected from extremely small crystals using extremely high flux synchrotron X-rays.[3] The application of this technique has been of great value in the field of

microporous materials as the growth of large crystals for SCXRD using solvothermal synthesis can be very difficult.[4] In addition to this a wide range of other techniques familiar to the solid state chemist will be used, including magic angle spinning solid state nuclear magnetic resonance spectroscopy (MASNMR), thermal gravimetry (TGA) and powder XRD. The theory and practice of these techniques will be discussed in the next chapter.

References

1. R.E. Morris and S.J. Wiegel, *Chem. Soc. Rev.*, 1997, **26**, 309.
2. G.W. Noble, *PhD Thesis*, University of St. Andrews, 1998.
3. R.J. Cernik, W. Clegg, C.R.A. Catlow, G. Bushnell-Wye, J.V. Flaherty, G.N. Greaves, I. Burrows, D.J. Taylor, S.J. Teat and M. Hamichi, *J. Synchrotron Rad.*, 1997, **4**, 279.
4. (a) M. Estermann, L.B. McCusker, C. Baerlocher, A. Merrouche and H. Kessler, *Nature*, 1991, **352**, 320. (b) M.A. Cablor, M. Diaz-Cabañas, J. Perez-Pariente, S.J. Teat, W. Clegg, I.J. Shannon, P. Lightfoot, P.A. Wright and R.E. Morris, *Angew. Chem. Int. Ed. Engl.*, 1998, **37**, 2122.

CHAPTER 3

Experimental Techniques

3.1 Solvothermal Synthesis

Solvothermal synthesis is the main technique by which zeolite-type open framework materials are prepared.[1] The process consists of three stages, formation of the gel, ageing of the gel and solvothermal treatment. A typical gel for the preparation of an AlPO might consist of a 1:2 molar ratio of Alumina and phosphoric acid (i.e. a 1:1 ratio of Al:P) dissolved in 80 molar equivalents of water with 0.5 molar equivalents of a structure directing amine. The gel is stirred until homogeneity is achieved, the ageing process, which may take as little as a few minutes or as much as two hours. After this it is transferred to a Teflon lined stainless steel autoclave and heated at a temperature generally between 100°C and 220°C for up to 15 days. Within the autoclave the reagents develop autogeneous pressure due to the boiling solvents and it is under these conditions that the open framework materials are crystallised.

The gels from which molecular sieve materials can be crystallised range from clear solutions to very thick and viscous gels,[2] in some cases materials of interest have been prepared from mixtures in which the solid reagents are suspended rather than fully dissolved. In general, the ageing process does not seem to be crucial to the product of a reaction, however the influence of heating time on certain systems is well documented. In zeolite syntheses in particular it is common for an open framework product to be obtained after short heating times only to transform to a dense phase after longer periods of heating (this change from a large pore through small pore to dense material is known as Ostwald ripening).[3]

The pH of the gel is very important. Zeolites are synthesised in basic systems, at pHs of around 10-14, while metal phosphates are normally prepared from mildly

acidic gels, pH 4-6.[1] As pH is highly important in processes of hydrolysis and condensation it is sited as of great importance in the mechanism of AlPO formation proposed by Ozin.[4] The pH of the mixture will also have an influence on the amine template which, will be protonated at low pH but not in more basic conditions. The pH's of the synthesis mixtures were measured with narrow range indicator paper or in some cases a pH electrode.

The products of the reactions were recovered by vacuum filtration, washed and dried (normally at room temperature in air). In some cases, the samples were sonicated in distilled water to separate larger crystallites from powder.

3.2 X-ray Diffraction

When electromagnetic radiation is incident on a repetitive lattice in which the lattice spacings are of a similar order of magnitude to the wavelength of the radiation it is diffracted. A crystal is a lattice in which the spacings correspond to the chemical bonds between the atoms of its structure. It is made up of an infinitely repeated unit known as the unit cell. The wavelength of X-rays is of the same order of magnitude as chemical bonds (Ca. 10^{-9}m), therefore they are diffracted by the crystal lattice.[5] When radiation is diffracted by a lattice the diffracted beams interfere to create a pattern, this pattern is described by Bragg's law:

$$n\lambda = 2d\sin\theta \qquad (3.1)$$

This relationship predicts whether constructive or destructive interference will occur between two diffracted beams of an incident angle θ. The spacing of two Miller

planes is denoted by d and λ is the wavelength of the radiation. Its derivation is shown in figure 3.1.

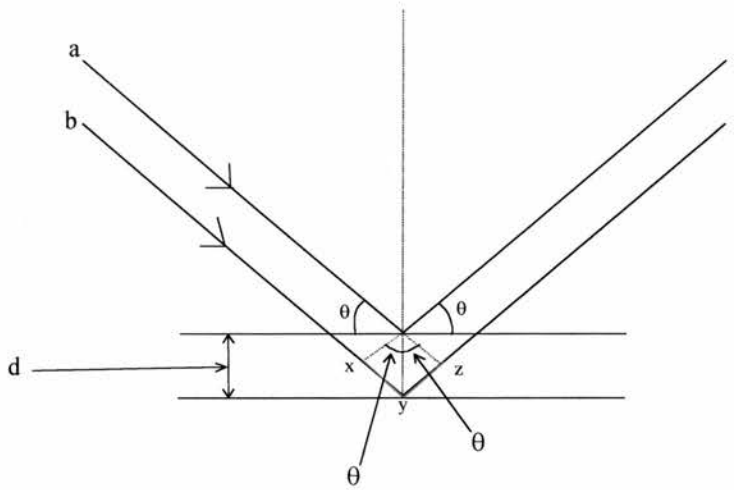

Figure 3.1 *The derivation of Bragg's law. Two waves a and b are incident at an angle θ upon an array of crystalline planes with a spacing d. Wave a is diffracted by the top plane and wave b by a second, dÅ below it. It is clear that wave b travels further than wave a; this extra distance (xyz) is referred to as a path difference. The distance xyz is equal to 2dsinθ. If the path difference is equal to an integral number of wavelengths nλ then constructive interference occurs between waves a and b and a diffracted beam is observed.*

The X-rays are scattered by the electrons surrounding the atomic nuclei. The degree of scattering from an atom is known as the scattering factor and is determined mainly by the number of electrons around the nucleus, it therefore increases with atomic number. The reflections correspond to the planes of atoms by which the X-ray beam is diffracted, these are denoted by the so called Miller indices (hkl). These

consist of three numbers h, k and l which describe how the plane of atoms intersects with the axes of the unit cell. Some examples of miller planes are shown in figure 3.2.

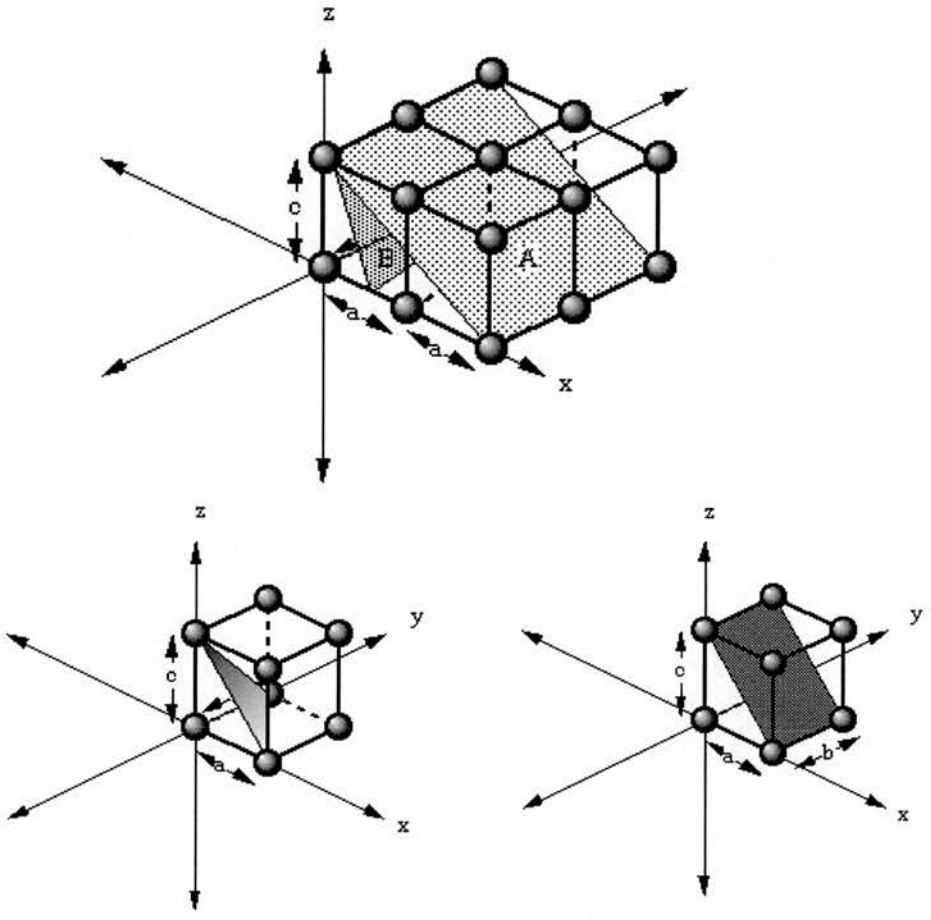

Figure 3.2 *Miller Planes. Clockwise from top: (102) (A) and (201) (B) planes; (101) plane and (111) plane (Diagrams by P. Schroeder, University of Georgia).*

The pattern created by the interference of the diffracted beams is, then clearly related to the structure of the crystal lattice. The problem of X-ray structure solution is that the data from the diffraction pattern cannot be converted directly back to the lattice structure. It is therefore necessary to guess a model for the structure and then

refine it against the X-ray data by comparing the calculated and observed patterns using the method of least squares.[6]

The intensities of the X-rays in the diffraction pattern are influenced by several factors. The one directly related to the structure of the crystal is called the "structure factor" (F(*hkl*)), this is described in terms of a single unit cell (the smallest repetitive unit of the crystal lattice) by equation 3.2.

$$F(hkl) = \sum_{j=1}^{N} f_j \exp[2\pi i(hx_j + ky_j + lz_j)] \qquad (3.2)$$

Where the position of the j^{th} atom, whose scattering factor is f_j, is given by the coordinates (x_j, y_j, z_j) and it is part of a structure with N atoms. The structure factors represent diffracted beams which have the wave properties of amplitude |F(hkl)| and relative phase ϕ(hkl).

The reason that the diffraction pattern cannot be directly converted to the structure is that phases cannot be directly observed and determined. For single crystal XRD data it is now generally routine to perform structure solution by statistical "direct methods"[7] in order to obtain a starting model for the structure. For powder XRD however there are sometimes too few data to obtain a really good model by direct methods, making solving structures from powder data very difficult.

Direct methods use the fact that the amplitude and phase of a structure factor are related to one another by the electron density. If the phases are known then the intensity could be predicted from the electron density and *vice versa*. By making several sensible assumptions about the nature of the structure's electron density the predicted solution can be improved. Principle among these are:

1. Atoms are discrete centres of electron density
2. Electron densities cannot be negative ($\rho(x) \geq 0$)
3. $\int \rho^3(x)\, dV = \text{max}$
4. Atoms are equal

These assumptions apply certain constraints to the electron densities predicted in the solution. The first removes the effects of atomic shape from the observed structure factors F_{obs}, giving normalised structure factors (E's). When used in the phase determining formulae these give a predicted electron density map of the structure as point atoms (if the electron density of the structure does not consist of atomic peaks, however, this has no meaning). The second assumption is perhaps self evident but helps by allowing one to disregard phases which would lead to $\rho(x)$ being a negative value for some value of x. This is only really useful if the structure factor in question represents a significant proportion of the scattering energy. A more powerful constraint is given by the third assumption. It applies across the entire volume of the unit cell and discriminates against negative electron density while encouraging the formation of positive peaks, both natural features of the true electron density. It also leads directly to the probability relationships among phases and the tangent formula, which form the basis of direct methods. The fourth assumption is used to give exact relationships between the structure factors. Because of this assumption direct methods may not be suitable for the solution of some structures containing heavy atoms. These may be solved by Patterson methods (which were used in crystal structure solution prior to the development of direct methods) which determine the heavy atom positions from the vectors between them.

Several other assumptions are also used in modern direct methods calculations, but it is from the above that most of the phase information is determined and refined to give the electron density map and figures of merit, from which the most suitable solution may be chosen.

In order to obtain physical parameters such as atom types and positions and bond lengths and angles from the electron density map, which direct methods produces the structure must be refined. As previously mentioned this is done by the method of least squares, which compares the experimentally observed diffraction pattern to that calculated for the model.

The method of least squares itself is a statistical method for solving simultaneous equations. Its most simple form is the linear case, commonly used to determine the straight line of best fit through a number of points (x_i, y_i), this line would have the equation:

$$y_i = mx_i + c \qquad (3.3)$$

or

$$\varepsilon_i = y_i - mx_i - c \qquad (3.4)$$

Where ε_i is called the residual of the equation. The line of best fit has values of m and c, which minimise $\sum\varepsilon_i^2$. This may be expressed in terms of vectors:

$$\begin{pmatrix} x_1 & 1 \\ x_2 & 1 \\ x_3 & 1 \\ .. & 1 \\ .. & 1 \\ x_i & 1 \end{pmatrix} \begin{pmatrix} m \\ c \end{pmatrix} = \begin{pmatrix} y_1 \\ y_2 \\ y_3 \\ .. \\ .. \\ y_i \end{pmatrix} \qquad (3.5)$$

Or more concisely as:

$$\mathbf{A\,x = b} \qquad (3.6)$$

Where **A** is the left-hand-side matrix containing the x values, **x** is the vector of unknowns m and c and **b** is the right-hand-side matrix of y values. The matrix **A** is known as the design matrix. The least squares solution for these equations is found by premultiplying both sides of (3.5) by the transpose of **A**:

$$\mathbf{A^T A\,x = A^T b} \qquad (3.7)$$

And solving the resulting equations for **x**. These values are known as the normal solutions for least squares. This method may be generalised for more complex non-linear systems, for example, the parameters of a crystal structure. The best fit is defined as the solution which minimises the function:

$$\Sigma w(F_o^2 - F_c^2) \qquad (3.8)$$

Where F_o is the observed structure factor and F_c is the calculated structure factor and each reflection is given a weight w (see below).

For least squares solution to be possible, it is necessary to have an excess of observational equations over unknowns. This means that the least squares matrices for a crystal structure are very large. Because of this it is common to utilise certain statistical techniques to improve the least squares fit. These include weighting (lending increased significance in the least squares calculation to more reliable

observations), restraints (treated as experimental observations, a weight dictates how strongly the restraint is applied) and constraints (must be fulfilled exactly, e.g. making the angles of a triangle add up to 180°).

The progress of a refinement is followed by the value of the so called "minimisation function". This is expressed by several "residual factors" (R factors). The R factor most closely related to the minimisation procedure is wR^2:

$$wR^2 = \sum w(F_o - F_c)^2 / \sum wF_o^2 \qquad (3.9)$$

Which takes into account the reflection weightings, however, it is also common to quote R:

$$R = \sum||F_o| - |F_c|| / \sum|F_o| \qquad (3.10)$$

Using the |F| values of "observed" reflections (those for which $F_o^2 > 2\sigma(F_o^2)$). This index was used in the past when it was more common to refine data against F than F^2. It gives smaller values than wR^2 and is less sensitive to changes in the weighting scheme so is still commonly quoted alongside wR^2.

Another measure of the worth of the refinement is the goodness of fit, S:

$$S = \{\sum w(F_o - F_c)^2 / (N - P)\}^{½} \qquad (3.11)$$

Where N is the number of data and P that of parameters. If the weights are correct, S should be close to unity.

There are several structural parameters which may be refined:

1. Atomic coordinates – Three for each atom in a general position, if an atom occupies a special position one or more of these may be fixed
2. Thermal displacement parameters – Isotropic or anisotropic. Isotropic atoms have a single displacement value in all directions, so are described by a single parameter (U or B). The anisotropic model describes thermal motion in three dimensions with arbitrarily oriented axes, giving six U values for refinement.
3. Overall scale factor – Brings the observed and calculated intensities to the same scale.
4. Site occupancies (not normally refined) – Normally an atom in a general position has an occupancy of one, however in disordered structures the disorder may be modelled by the use and refinement of non-unit occupancies.
5. Atom type – Incorrect atom assignments lead to incorrect scattering factors for calculation of F_c. This has a knock on effect on the refinement of the other parameters.

Estimated standard deviations (esd's) for the structural parameters are calculated from the least squares matrix. Standard deviations are normally associated with systems for which a single parameter is measured several times. In these cases, the standard deviation (σ) is the average deviation of the measured values from the mean:

$$\sigma = \frac{1}{N}\sqrt{\sum_{i=1}^{n}(x_i - \bar{x})^2} \qquad (3.12)$$

Where N is the number of measurements and (x bar) is the average of the measurements, x_i. However, for a crystal structure there is only one measurement of each parameter, therefore standard deviations must be estimated. This is possible because of the excess of data over parameters. The esd for a refined parameter P_j depends on three things:

1. The minimisation of the function $w_i(F_o^2{}_i - F_c^2{}_i)$ (referred to below as $w_i\Delta_i$)
2. The numbers of data and parameters
3. The diagonal terms of the inverse least squares matrix $\mathbf{A}^{-1}$

The esd is given by:

$$\sigma(p_j) = \sqrt{\left((\mathbf{A}^{-1})_{jj} \frac{\sum_{i=1}^{N} w_i \Delta_i^{\,2}}{N - P} \right)} \qquad (3.13)$$

The esd's for the bond lengths, angles and torsions are derived from the refined parameter esd's unless constrained in the refinement.

3.2.1 Single crystal X-ray diffraction

Thanks to modern computing power SCXRD is now a routine tool for obtaining detailed structures with a large amount of information. By collecting data from a single crystal in a range of orientations, data may be obtained for the full 3-dimensional lattice structure. This is commonly done in the laboratory using the four-circle diffractometer system (fig 3.3) which allows three degrees of rotational freedom for the crystal and one for the detector, using which all possible crystal orientations may be obtained.[8]

The detectors used in this type of diffractometer must find a peak in the diffraction pattern then scan around it to measure the intensity, being able only to detect a single diffracted beam. This makes data collection on a four-circle diffractometer a long process, particularly for structures with low crystallographic symmetry, recently this problem has been solved by the development of area detectors. Area detectors are not a new thing, in fact the first XRD patterns were recorded using an area detector, photographic paper; however the development of inexpensive, reliable, high resolution CCD (charge coupled device) chips has recently led to a tremendous increase in the speed of X-ray data collection.[9] Since area detectors can gather many diffracted beams in a single exposure not only is the time necessary for data collection reduced but also the crystal mounting may be simplified to a two-circle set-up. The intensities of the diffracted beams are separated from background by thresholding software and measured by integration of the intensities.

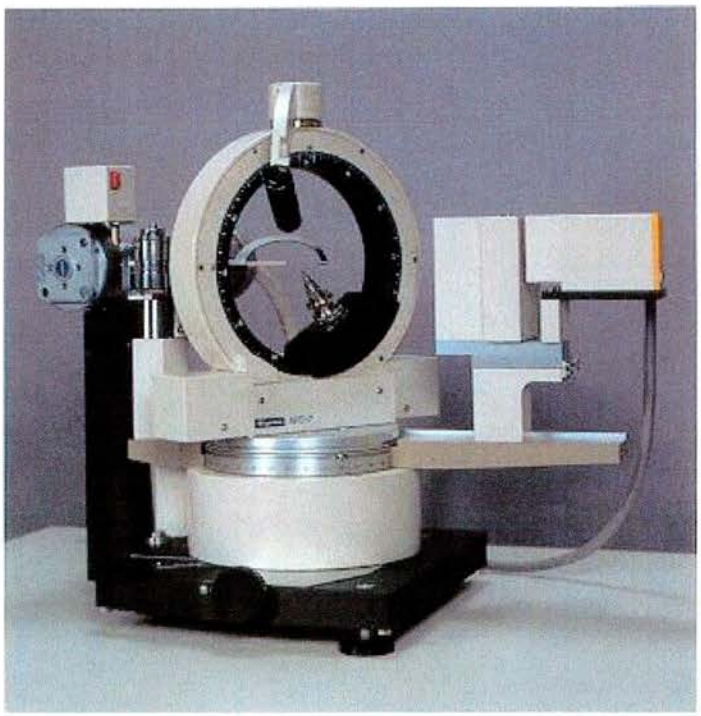

Figure 3.3 *A Rigaku AFC7S 4-circle single crystal X-ray diffractometer. A similar instrument was used for data collection in several of the structures presented here.*

As discussed above structure solution by direct methods from SCXRD data with fast modern computers is now routine in most cases. Crystal growth however, is still a problem, particularly in solvothermal synthesis. Two alternatives when suitably sized single crystals cannot easily be obtained are discussed below.

SCXRD data were collected in St. Andrews on Rigaku 4-circle and Bruker AXS SMART CCD area detector diffractometers using either molybdenum or copper K_α X-rays from sealed tube sources.

3.2.2 Powder X-ray diffraction

The powder forms of many materials are composed of tiny crystallites, which diffract X-rays in the same way as a single crystal; it can therefore provide structural

information when no large single crystals are present. However, the random orientation of the crystallites in the powder sample means that the diffraction pattern obtained is an average of all crystal orientations (except in some cases, where the crystallites have a preferred orientation), the three dimensional data of the single crystal diffraction pattern is compressed into two dimensions. Because of this compression, peaks from the 3-D diffraction pattern overlap and data is lost, the lack of data makes *ab initio* structure solution from powder profiles very difficult (though nonetheless possible in some cases).[10]

Sometimes a known model can be applied or adapted to fit the data, it may then be refined by the Rietveld method.[11] This is a specially developed method for the refinement of a model against powder data. Essentially this involves calculated model being compared with the observed data as in the refinement of single crystal data. However, the Rietveld method allows the refinement not only of the atom positions, thermal parameters and site occupancies (as in a single crystal refinement) but also of various "profile parameters" relevant to the powder XRD pattern. These parameters include the diffractometer zero point, peak shape and background. The profile parameters are refined first with the structural parameters only being refined when the fit to the profile is already good. There are normally too few data in a PXRD pattern to allow full refinement of the structural parameters for all atoms, in particular it is very rare to allow anisotropic refinement of temperature factors in a Rietveld refinement. In order to make up for the lack of data much use is also made of restraints such as known bond lengths and angles from similar materials to the sample. It is also possible to refine only the profile parameters (a structure free refinement). The most common form of this is the Le Bail method, which is often

used to obtain a single crystal-like data set from the powder profile for structure solution.

Like a single crystal refinement, the progress of Rietveld refinements is monitored by several figures of merit. The weighted profile R factor (R_{wp}) is derived in a similar manner to wR^2 for a single crystal refinement but is based on the intensities at each step in the powder pattern:

$$R_{wp} = \{\sum w_i [y_i(obs) - y_i(calc)]^2 / \sum w_i [y_i(obs)]^2\}^{½} \qquad (3.14)$$

Where $y_i(obs)$ and $y_i(calc)$ are the observed and calculated intensities at a step i and w_i is the weight. It should be noted that the value of R_{wp} is highly dependent on the treatment of the background in the refinement and so does not always provide a good way of comparing refinements. Ideally, the final R_{wp} should approach the statistically expected R value, R_{exp}:

$$R_{exp} = \sqrt{\left\{(N-P) / \sum_{i}^{N} w_i y_i(obs)^2\right\}} \qquad (3.15)$$

Where N is the number of data points and P is the number of refined parameters. This value reflects the quality of the data. The approach of the two R factors is monitored by the goodness of fit χ^2, this is given by

$$\chi^2 = R_{wp} / R_{exp} \qquad (3.16)$$

As the refinement is completed, the value of χ^2 should approach unity. Unusually small or large values of χ^2 may be caused by poor data collection. Plots of the observed, calculated and difference profiles are also extremely useful in assessing the success of a refinement. With experience, it is possible to spot the problems in a refinement by studying the difference plot.[12]

The Rietveld method is often used to check that SCXRD structures correspond to the bulk sample.

Because of the problem of peak overlap, it is important to obtain the highest resolution possible when powder data are being collected with a view to structure solution; this is discussed in the next section. The main use of powder XRD, however, is as a quick method of identifying inorganic structures. As such, it is the most important screening tool in the synthesis of open framework materials, allowing one to quickly determine whether the desired structure has been obtained.

Powder XRD data were collected on STOE stadip and Phillips Xpert diffractometers. The Phillips diffractometers uses flat plate samples in a reflective collection mode, while the samples for the STOE diffractometer are mounted between Mylar discs and spun with transmitted diffracted beams being collected.

3.2.3 Synchrotron radiation

When electrons are accelerated to high speeds in a circle high energy X-ray photons are emitted at a tangent to the electron current. A synchrotron achieves this by directing the accelerated electrons in a circle using powerful magnets. The energy of the X-ray photons emitted is dependent on the radius of the circle, in order to obtain X-rays of different energy levels the accelerated beam is also passed through magnets with greater or lesser degrees of curvature than the main accelerator ring

(these are known as "wigglers" and "undulators" respectively). A device called the "Klystron" is used to maintain the speed of the circling electrons (around 200mph) as they lose energy. The energy of the electron beam decays over time due to electron-electron interactions and collisions with gas molecules in the ring. Because of this, the ring is "refilled" with high-energy electrons twice to three times per day.[13] A schematic representation of a synchrotron is shown in figure 3.4.

The X-rays emitted by the synchrotron encompass the full range of X-ray wavelengths and are known as a "white beam" (by analogy with the visible spectrum). Specific wavelengths are selected for different applications using crystals (for instance the wavelengths used for single crystal diffraction at station 9.8 of the synchrotron radiation source (SRS) at Daresbury are selected by a silicon (111) crystal) or gratings, in some cases the white beam itself is used directly.[14]

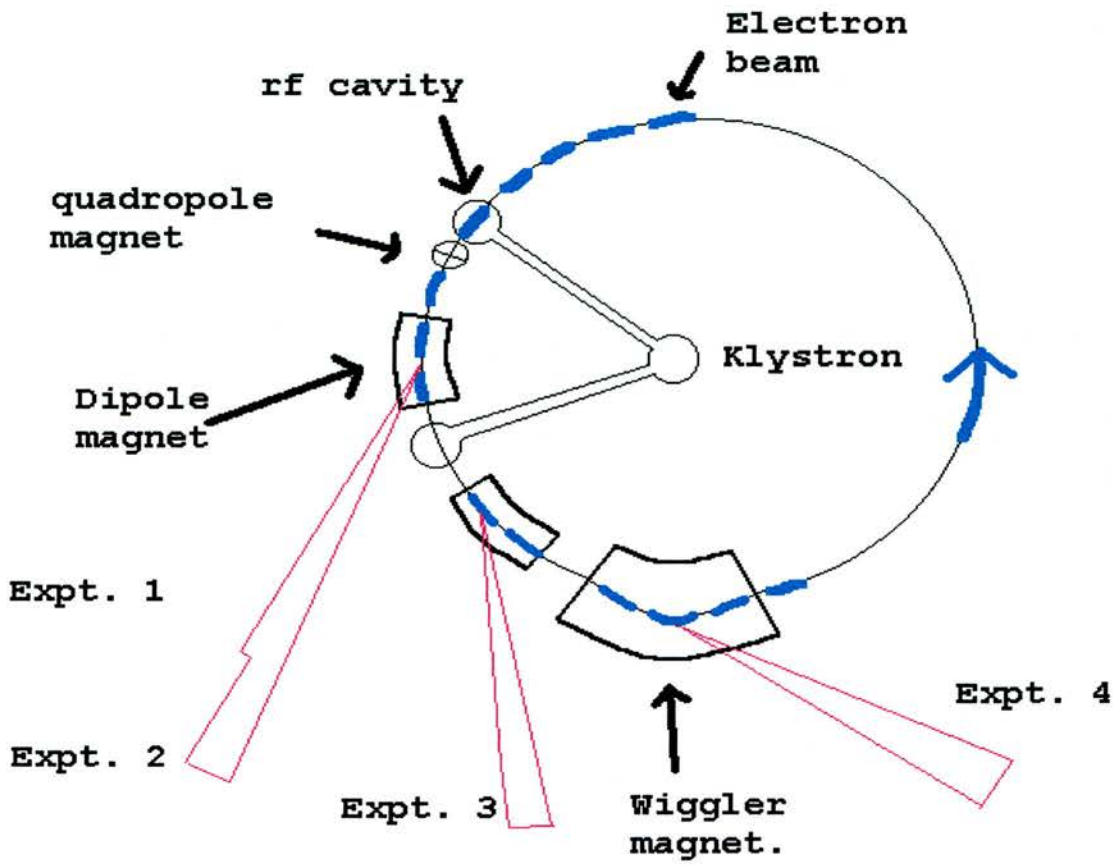

Figure 3.4 *schematic diagram of a synchrotron.*

A vast range of experiments is available to the synchrotron scientist. Due to the continuous spectrum of X-ray wavelengths, synchrotron radiation can be used for X-ray spectroscopy techniques like XPS (X-ray photoelectron spectroscopy). Absorption methods such as EXAFS (extended X-ray absorption fine structure) can be used to probe atom environments and or to probe surfaces and a range of scattering techniques are also available. The experiment of relevance here is, however, traditional XRD.

3.2.3.1 Microcrystal X-ray diffraction

The intensity of synchrotron radiation has long been used by protein crystallographers as a tool for collecting data from weakly diffracting crystals, but until the recent advances in CCD area detectors discussed above was little used in small molecule crystallography.

The SRS in Daresbury now has a dedicated station (station 9.8, fig. 3.5) for microcrystal diffraction studies, facilities are also available at the European synchrotron radiation facility (ESRF, beamline ID 11).

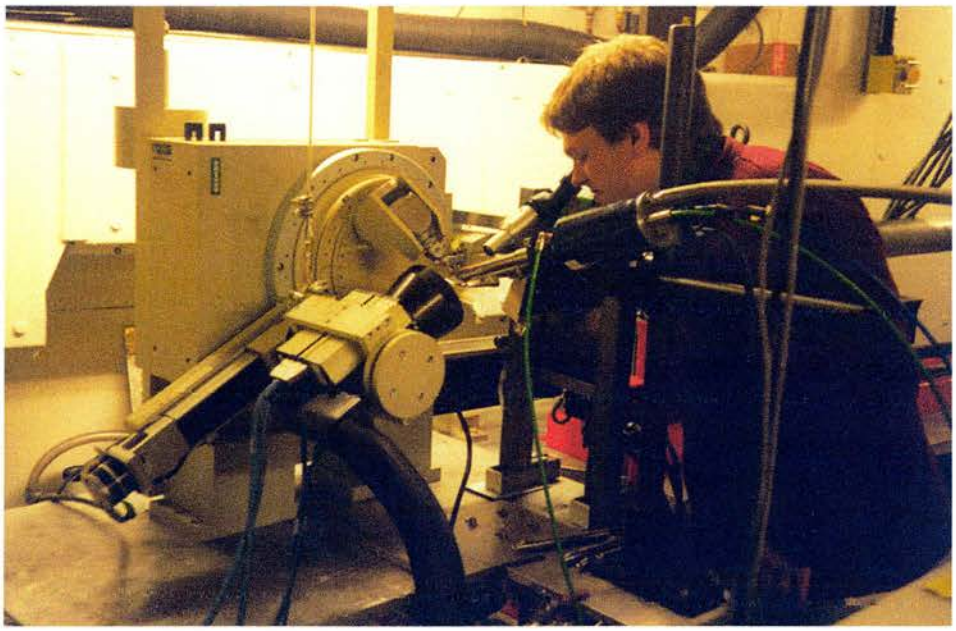

Figure 3.5 *Dr Gary Hix Aligning a crystal on the SMART diffractometer of station 9.8*

Data collection at station 9.8 (the high-flux microcrystal-diffraction facility of the SRS) is with a Bruker AXS SMART CCD area-detector mounted on a two circle diffractometer. The experiment normally uses X-rays with a wavelength of approximately 0.69Å (although this can be varied for experiments in anomalous

dispersion or absolute structure determination) selected by a horizontally focusing silicon (111) monochromator and vertically focussed by a cylindrically bent palladium-coated zerodur mirror.[15] The intensity of the synchrotron beam decays during the timescale of the experiment as the electrons lose energy, this is compensated for by computational methods as part of the inter-frame scaling procedure of the area detector.[16] To improve the quality of data collected from complex structures the diffractometer is fitted with a cryostat which can cool the sample to temperatures as low as 100K. A furnace system for collecting data at high temperatures is also available; this has been used for *in situ* SCXRD studies of the calcination of molecular sieves.[17]

The highly intense X-rays allow collection of data from crystals as small as 5x10x15μm, also X-rays are scattered more strongly at high values of 2θ giving a higher number of observed data (this has allowed the solution of structures with several hundred independent atoms[9]). It is also possible to collect data from weakly scattering crystals, such as those of very large organic molecules.

3.2.3.2 High resolution powder diffraction

The problem of peak overlap in PXRD can be reduced somewhat by collecting data at the highest possible resolution. The high collimation of synchrotron X-rays give exceptionally resolution and therefore very sharp peaks in the diffraction pattern, minimising overlap. Synchrotron high-resolution powder diffraction (HRPD) is the data collection method of choice for powder X-ray structural studies and is considered almost essential in structure solution.

The HRPD data used in this project was collected on station 2.3 of the SRS. This station uses variable X-ray wavelengths. Diffracted intensities are measured with

a position sensitive detector controlled by the PINCER control software.[18] Samples were packed in capillaries to avoid preferred orientation effects and mounted on a modified STOE spinner.

Indexing of the patterns (to determine lattice parameters and crystal system) where necessary was done with the program TREOR 90.[19] Rietveld refinements were carried out with the GSAS suite[20] and the EXPO[21] combined Le Bail extraction and direct methods package was used for structure solution.

3.3 Nuclear Magnetic Resonance Spectroscopy

In addition to XRD, several other analytical techniques have proved valuable in the characterisation of porous solids. Nuclear Magnetic Resonance spectroscopy (NMR) allows the chemist to probe the environment of nuclei with spin ½. It is generally considered the most valuable analytical tool of the synthetic organic chemist, and many excellent texts are available on the subject.[22] NMR spectra contain three sources of chemical information. The chemical shift (measured in parts per million), shown by the peak position in the spectrum, gives information about the environment of the nucleus from the amount of "shielding" it gains from surrounding electrons. The multiplicity of the lines shows the number of other spin ½ nuclei surrounding the nucleus corresponding to the central peak. Sometimes to simplify spectra the technique of decoupling is used to remove this splitting, especially to remove C-H coupling in ^{13}C NMR spectra. The distances between the lines of a multiplet give the "coupling constants" which can give geometric information.

In the solid state the technique encounters two problems, chemical shift anisotropy (CSA), caused by the directional nature of the shielding of the nuclei, and dipole-dipole interactions which are not averaged out by the molecular tumbling

inherent in the solution state, leading to excessive line broadening. These problems are remedied by two techniques. "Magic angle spinning" (MAS) reduces line broadening due to CSA by setting the local magnetic field in the sample to zero. The local magnetic field (B_{loc}) is defined by the equation:

$$B_{loc}=\pm\mu_y r_{xy}^{-3}(3\cos^2\theta_{xy}-1) \qquad (3.14)$$

The sample is spun at a speed of the order of the static line width (typically *ca.* 6000-10 000 Hz) and tilted at an angle (θ_{xy}) of 54°44' (the so called "magic angle") to the applied magnetic field. This sets $3\cos^2\theta_{xy}=1$ in equation 3.2 and therefore the value of B_{loc} becomes zero and the splitting due to CSA is negated and dipole-dipole broadening is reduced. Dipolar decoupling, a technique similar to the proton decoupling methods common in solution NMR but using higher energy is also used to reduce dipole-dipole interactions. With a combination of these methods the line broadening in solid state NMR spectra can be reduced to acceptable levels. MASNMR studies of several microporous systems have given some useful data.[23] The MASNMR results from St. Andrews were obtained from a Bruker MSL500 NMR spectrometer, with results generally being acquired at two different spinning speeds in order to differentiate side bands from actual peaks. ^{19}F and ^{31}P MASNMR spectra were also collected by the EPSRC solid state NMR service at Durham University. Solution ^{1}H NMR spectra were recorded on a Bruker AM300 spectrometer.

3.4 Electron Paramagnetic Resonance Spectroscopy

Electron paramagnetic resonance (EPR) is a similar technique to NMR but instead of studying nuclei, it probes electrons. Electrons necessarily have spin ½ and can therefore be caused to resonate in the same way as spin ½ nuclei in a magnetic field. Bonding electrons are not caused to resonate and so the technique is only useful for systems containing unpaired electrons, for example free radical reactions and compounds containing paramagnetic transition metal ions.

Like the nucleus in NMR the spin of an electron in EPR may be aligned parallel or antiparallel to the applied magnetic field (spin +½ or spin –½) and may absorb a quantum of energy hμ (where h is Planck's constant and μ is the frequency) to change between the two energy levels (fig. 3.5).[24]

The energy required to excite a single free electron from the low energy (spin –½) to high energy (spin +½) level is given by the equation:

$$h\mu = g\beta_e B \qquad (3.15)$$

Where g is the Zeeman splitting constant for a free electron (~2), β_e is the Bhor magneton and B is the applied magnetic field. The values of hμ required to activate these transitions are within the microwave region of the electromagnetic spectrum.

In real systems the g value is effected by the local magnetic field and can be used in a similar way to the chemical shift in NMR. Light atoms such as 1st row transition elements with a single unpaired electron can have g values close to 2, however, heavier atoms and those with more than one unpaired electron have g values very different from 2. As in NMR the EPR signals can be split due to the influence of

surrounding spin ½ centres. This "hyperfine splitting" can give further information about the environment of the unpaired electron.

Unlike NMR no special apparatus are required to collect solid state EPR spectra. It is, however, necessary to cool the samples to a low temperature using liquid helium or nitrogen (for the work presented here liquid nitrogen was cold enough). Samples were packed in sealed dropping pipettes and data were collected at 100K on a Bruker ES073 spectrometer.

3.5 Thermal Analysis

Thermogravimetric analysis (TGA) is commonly used in the characterisation of molecular sieves. This technique involves heating a small sample of the unknown material at a controlled rate, often in an inert atmosphere, and observing the changes in mass which occur during heating. Observed mass losses can be related to the loss from the structure of solvent and template molecules or to structural transformations[25] (in the case where a mass change occurs). It is also sometimes possible to deduce the molecular formula of the compound.[26]

Differential temperature analysis (DTA) data is commonly obtained at the same time as TGA and gives information on the energy changes at a thermal event. All of the TGAs so far in this project were carried out on a TA instruments combined TGA-DTA instrument heating to 1200°C in an atmosphere of flowing nitrogen or oxygen (flow rate 100mL $minute^{-1}$) in alumina crucibles against a reference of pre-calcined alumina.

3.6 Other Useful Techniques

3.6.1 Infra red spectroscopy

In the characterisation of metal phosphates infra red (IR) spectroscopy may be used as a general structural probe, with samples being run as KBr discs containing *ca.* 1% sample. It is possible to gain information about the organic template by this method, also features of the framework may be observed (for example pendant –OH groups). Spectra in this project were collected on a Perkin Elmer PE1710 Fourier transform IR spectrometer.

3.6.2 Microanalysis

C, H, N Microanalysis can provide some interesting data on the amount of template molecule present in the material. Microanalysis was carried out with a Carlo Erba model 1106 elemental analyser.

3.6.3 Nitrogen adsorption

The final technique that has been used so far in the work presented here is nitrogen adsorption. This is a method for determining the surface area of molecular sieves (related, obviously, to the void size) and is particularly useful in the characterisation of mesoporous materials, which are difficult to characterise by crystallography due to their lack of long range order. It is a low pressure technique. The material to be analysed is first held at reduced pressure ($4x10^{-3}$ Torr) and heated at 100°C for some time in order to remove any adsorbed water already in the matrix or on the surface. For the adsorption measurement the temperature of the sample is reduced to 160K with liquid nitrogen. This increases the time for which the weakly bound gas atoms will remain on the surface of the sample to a value for which the

atmosphere and the adsorbed gas can equilibrate. A pressure of nitrogen gas (typically ~30 Torr) is then released into the vacuum line with the sample sealed off and the pressure in the line ($P_{initial}$) is measured. The line is then opened to the sample and after a period of equilibration the pressure of the whole system is measured (P_{final}) and the sample sealed off again. This process is continued until the difference between $P_{initial}$ and P_{final} becomes negligibly small (~2-3 Torr). After this, the process is repeated in reverse with the line pressure being reduced by the vacuum pump before each exposure of the sample to the line. The collected data set of $P_{initial}$ and P_{final} values are then processed to give a curve known as an isotherm. The isotherm is obtained by plotting $P_{final} / \sigma(P_{initial} - P_{final})$ against $P_{initial} / P_{final}$ with the parameter σ representing the surface coverage of nitrogen atoms. σ is determined from the volume of nitrogen adsorbed and the molecular volume of nitrogen.[27]

3.6.4 Magnetic measurements

Magnetic properties in materials arise from the ordering of the spins of unpaired electrons in a crystal lattice. The spins become ordered when information about the spin state of an atom can be passed on to neighbouring atoms. This may occur by several mechanisms. Direct exchange occurs when the atoms with unpaired electrons are close enough in space to influence each others orbital structure, indirect exchanges can occur by other atoms linking the spin centres. the most common types of magnetic ordering are ferromagnetism and antiferromagnetism. In a ferromagnet all the unpaired electron spins are aligned in a single direction leading to an inherent magnetic moment (for example ferromagnetic iron), in an antiferromagnet the spins alternate giving a net magnetic moment of zero. Many materials which have unpaired

electrons do not have any magnetic ordering with the spins being randomly arranged. These are known as paramagnets.

By making measurements of magnetic susceptibility (χ) against temperature it is easy to determine whether the material in question has any type of magnetic ordering. The simplest way to determine which category the material falls into is to plot $1/\chi$ against temperature. For an idealised paramagnet this gives a straight line which intercepts the axes at the origin (under real conditions the line does not quite reach the origin). For a ferromagnet a straight line which intercepts the T axis at a positive value is obtained. Antiferromagnetic materials give a stright line which intecepts the T axis at a negative value. Since temperature is measured on a kelvin scale this is an imaginary value which known as the Weiss temperature.[28]

References

1. R.M. Szostak, *Molecular Sieves, Principles of Synthesis and Identification,* Van Nostrand Rienhold, New York, 1989, Ch. 1.
2. R.H. Jones, J.M. Thomas, J. Chen, R. Xu, Q. Huo, S. Li, Z. Ma, and A.M. Chippindale, *J. Solid State Chem.*, 1993, **102**, 204.
3. V.V. Slezov, J. Schmelzer and J. Moller, *J. Cryst. Growth,* 1993, **132**, 419.
4. S. Oliver, A. Kuperman and G.A. Ozin, *Angew. Chem. Int. Ed.*, 1998, **37**, 46.
5. A. Guinier, *X-ray Diffraction*, Wm Freeman and Co., San Francisco, 1963, 121.
6. D. Viterbo in *Fundamentals of Crystallography*, C. Giacovazzo Ed., 1992, Oxford University Press, Oxford, Ch. 5.
7. *Ibid.*
8. H.L. Monaco in *Fundamentals of Crystallography*, C. Giacovazzo Ed., 1992, Oxford University Press, Oxford, Ch. 4.
9. A.M.Z. Slawin, *Chem. Brit.*, 1998, **34**, 31.
10. K.D.M. Harris and M. Tremayne, *Chem. Mater*, 1996, **8**, 2554.
11. (a) H.M. Rietveld, *Acta Cryst.,* 1967, **22**, 151. (b) H.M. Rietveld, *J. Appl. Cryst.,* 1969, **2**, 65.
12. L.B. McCusker, R.B. Von Dreele, D.E. Cox, D. Louer and P. Scardi, *J. Appl. Cryst.*, 1999, **32**, 36.
13. G.N. Greaves and C.R.A. Catlow in *Applications of Synchrotron radiation*, G.N. Greaves and C.R.A. Catlow Ed., 1990, Blackie and Son, Glasgow, Ch1.
14. *Ibid.*
15. R.J. Cernik, W. Clegg, C.R.A. Catlow, G. Bushnell-Wye, J.V. Flaherty, G.N. Greaves, I. Burrows, D.J. Taylor, S.J. Teat and M. Hamichi, *J. Synchrotron Rad.,* 1997, **4**, 279.

16. SADABS absorption correction software, G.M. Sheldrick, University of Göttingen, Germany, 1997.

17. G. Muncaster, G. Sankar, C.R.A. Catlow, J.M. Thomas, R.G. Bell, P.A. Wright, S. Coles, S.J. Teat, W. Clegg and W. Reeve, Chem. Mater., 1999, **11**, 158.

18. C.C. Tang, *SRS Station 2.3 Documentation*, 1998.

19. TREOR90, P.E. Werner, University of Stockholm, Sweden, 1990.

20. GSAS, R.B. Von Dreele and A.C. Larson, University of California, USA, 1995.

21. EXPO, A. Altomare, M.C. Burla, B. Carrozzini, G. Cascarano, C. Giacovazzo, A. Guagliardi, A.G.G. Moliterni, G. Polidori and R. Rizzi, University of Bari, Italy, 1997.

22. D.M. Grant and R.K. Harris (Eds), *Encyclopaedia of Nuclear Magnetic Resonance Spectroscopy,* John Wiley and Sons, New York, 1996.

23. (a) S.J. Weigel, J.C. Gabriel, E.G. Puebla, A.M. Bravo, N.J. Henson, L.M. Bull and A.K. Cheetham, *J. Am. Chem. Soc.,* 1996, **118**, 2427. (b) R.E. Morris, S.J. Weigel, N.J. Henson, L.M. Bull, M.T. Janicke, B.F. Chmelka, A.K. Cheetham, *J. Am. Chem. Soc.,* 1994, **116**, 11849.

24. (a) J.W. Orton, *Electron paramagnetic resonance*, London Iliffe Books, London, 1968. (b) J. Weil, J. Bolton and J. Wertz, *Electron Paramagnetic Resonance*, Wiley Interscience, London, 1994.

25. S. Oliver, A. Kupermann, A. Lough and G.A. Ozin, *J. Mater. Chem.*, 1997, **7**, 807.

26. P.R. Slater and C. Greaves, *Physica C,* 1991, **175**, 172.

27. G.A. Somorjai, *Introduction to Surface Science and Catalysis,* John Wiley and Sons, New York, 1994, Ch. 3.

28. C. Kittel, *Introduction to Solid state physics*, John Wiley and Sons, New York, 1996, Ch. 15.

CHAPTER 4

MACROCYCLES AS TEMPLATES FOR GALLOPHOSPHATES

4.1 Macrocycles in Zeolite Synthesis

The use of oxygen containing "crown-ether" macrocycles as templates in zeolite synthesis was first reported in1992 by Guth *et al.*[1] Since then several other researchers have published work in which macrocycles are used as structure directing agents (SDAs).[2]

Macrocycles offer several interesting properties as SDAs. Firstly they may be prepared with a range of C:N ratios and different shapes, allowing modification of the charge density of the SDA and the level of steric hindrance around the nitrogen atoms. Second, they have quite rigid structures, meaning that the nitrogen atoms should be firmly held in position, this is advantageous when trying to work up from a template to a specific framework. The well documented coordinating powers of macrocycles are also of interest in the synthesis of substituted frameworks and inorganic-organic hybrids.

Only a few simple macrocycles were used in the studies presented here, however, further work is currently under way to investigate more complex macrocycles. The macrocycles investigated are shown in figure 4.1 below. The results of their use are discussed in the following sections.

4.2 CYCLAM-GaPO: A New Class of Inorganic-Organic Hybrid

4.2.1 Synthesis

During the investigation of the use of 1,4,8,11-tetraazacyclodecane (cyclam) as a structure directing agent for GaPO open frameworks a new type of inorganic-

organic hybrid material was prepared in which the macrocycle is covalently bonded to the framework.

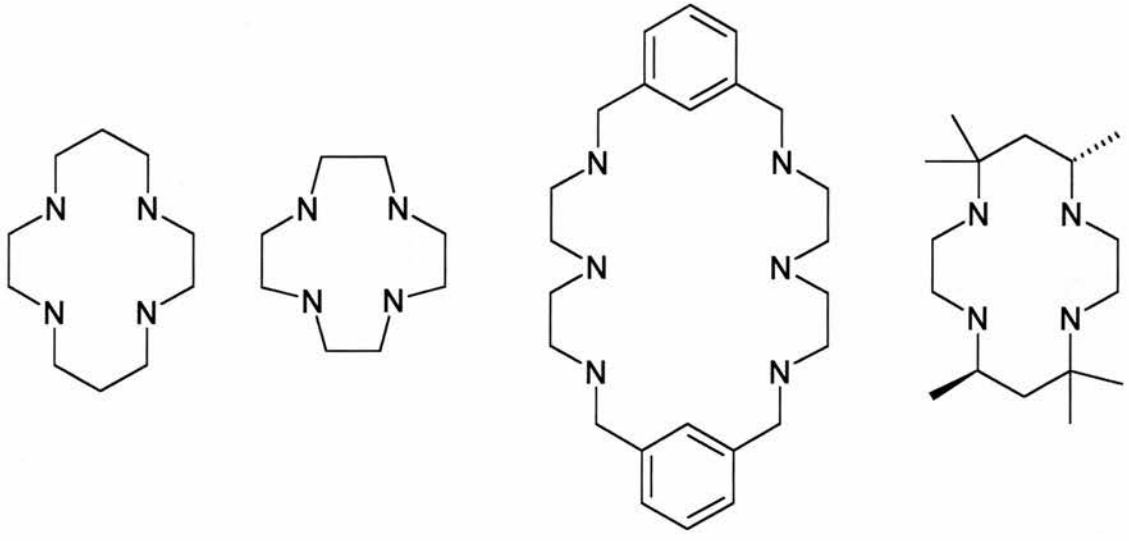

Figure 1. *Macrocyclic templates used in the synthesis of gallophosphates. Cyclam, cyclen, macrocycle 1 and tet-a.*

Cyclam-GaPO may be prepared from a range of solvents provided fluoride ions are present, however it was found that when pyridine was used the product was obtained in the form of tiny crystals. The approximate composition of the synthesis gel was P_2O_5: Ga_2O_3: 70 pyridine: HF: 0.5 CYCLAM, no water was added to the mixture although some was present in the phosphoric acid. Gallium sulfate (99.8%, Aldrich) and CYCLAM (98%, Strem) were slurried in pyridine (Fischer) and stirred vigorously. To this mixture phosphoric acid (85% weight aqueous solution, Aldrich) and HF (70% weight in pyridine, Aldrich) were added. The pH was adjusted to ~5 with trimethylamine (TMA, ~3mL, 40% aqueous solution, Aldrich), aged at 25°C for one hour, transferred to a Teflon lined stainless steel autoclave and heated at 135°C for 72 hours. The product was recovered by suction filtration and washed with acetone and water to reveal small colourless crystals.

4.2.2 Structural Characterisation

The crystals of the product were too small (max. size 30x30x15 μm) for single crystal XRD on a standard laboratory four circle diffractometer, so data were collected at the high-flux microcrystal-diffraction facility (station 9.8) of the SRS at Daresbury. In order to improve the chances of determining the position of the organic part of the material (which is often difficult to pinpoint due to molecular motion) data were collected at low temperature (160K). Details of the data collection and structure solution are given in table 4.1.

Table 4.1 *Crystal data and refinement details for cyclam-GaPO*

Identification code	Cyclam-GaPO
Empirical formula	$GaPO_4(OH)_2F.Ga(C_{10}N_4H_{24})$
Formula weight	489.816
Temperature	160(2) K
Wavelength	0.6849 Å
Crystal system, space group	Orthorhombic, P_{bcn}
Unit cell dimensions	a = 13.2785(2) Å α = 90°
	b = 10.4467(2) Å β = 90°
	c = 18.4550(3) Å γ = 90°
Volume	2560.01(7) $Å^3$
Z, Calculated density	14, 2.532 Mg/m^3
Absorption coefficient	5.544 mm^{-1}
F(000)	1904
Crystal size	0.03 x 0.03 x 0.015 mm
Theta range for data collection	2.48 to 28.05°
Limiting indices	$-16 \le h \le 17, -13 \le k \le 13, -20 \le l \le 23$
Reflections collected / unique	14162 / 2891 [R(int) = 0.0556]
Completeness to theta	28.05, 93.0 %
Refinement method	Full-matrix least-squares on F^2
Data / restraints / parameters	2891 / 0 / 189
Goodness-of-fit on F^2	1.065
Final R indices [I>2sigma(I)]	R1 = 0.0407, wR^2 = 0.1213
R indices (all data)	R1 = 0.0427, wR^2 = 0.1224
Largest diff. peak and hole	1.228 and -1.782 e.$Å^{-3}$

4.2.3 Structure

The final unit cell of cyclam-GaPO refined to values of a = 13.2558(5) Å, b = 10.4321(5) Å, c = 18.4382(9) Å, volume = 2549.7(2) Å^3 at T = 160K, spacegroup *P*bcn, ρ_{calc} = 2.542g cm^{-3}. Full atomic coordinates, bond lengths and angles and thermal displacement parameters are given in tables 4.2 to 4.4.

The structure of cyclam-GaPO consists of inorganic GaPO layers linked by a gallium-cyclam complex; its asymmetric unit is shown in figure 4.2.

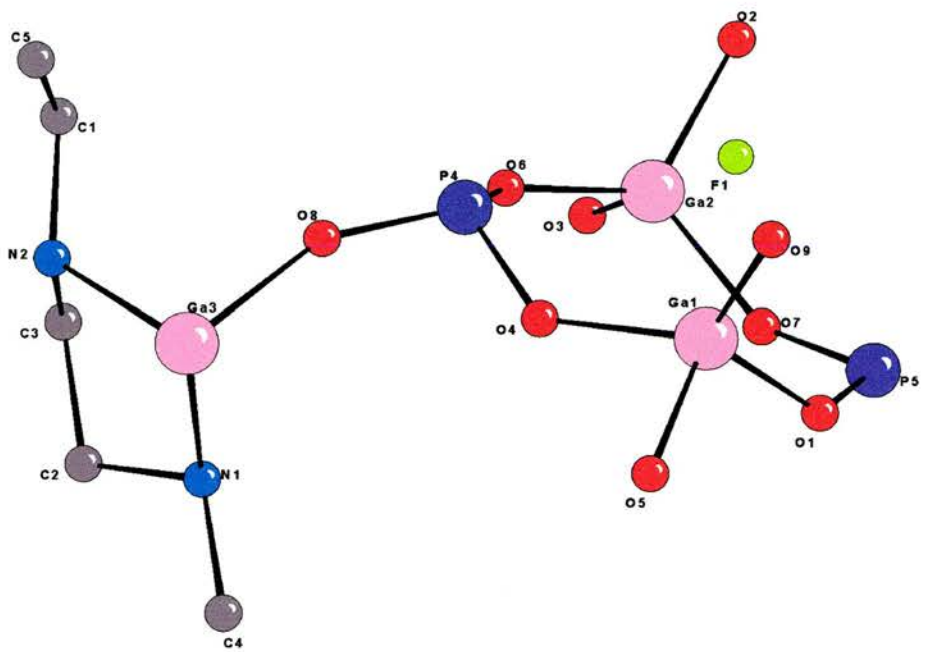

Figure 4.2 *The asymmetric unit of cyclam-GaPO*

The structure of the GaPO part is closely related to that of many molecular sieves and can be described using the terminology discussed in section 1.2. The basic structural motif is a D4R unit (fig. 4.3) which, as is often the case for GaPOs synthesised in the presence of HF, contains a fluorine atom inside the cage. This

feature is observed in cloverite[3] and several of the ULM-n[4] materials, with the fluorine atom having been reported in the exact centre of the cage, or displaced towards either two or three of the gallium atoms. In this case the fluorine lies closer to two of the gallium atoms (crystallographically equivalent), making relatively long contacts of 2.286Å.

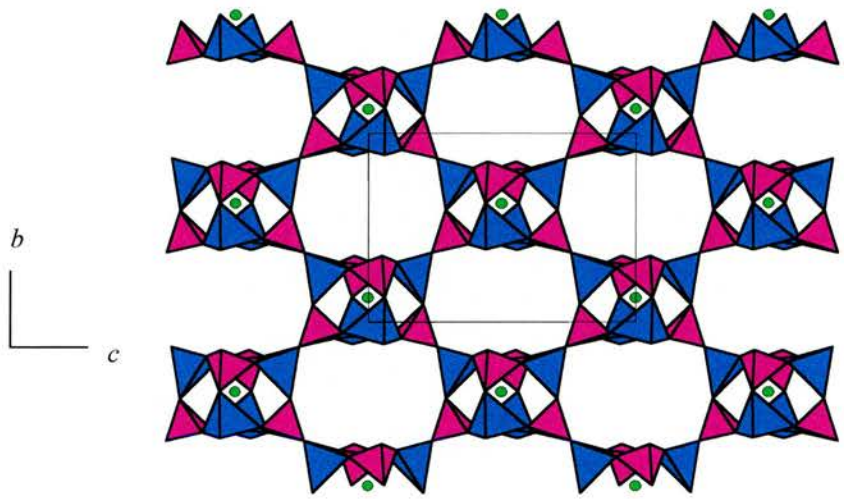

Figure 4.3 *The layer structure of CYCLAM-GaPO viewed parallel to the (100) direction. The D4R units and the ten-ring windows which they define are clearly visible. GaO_4 units are represented by purple tetrahedra and PO_4 by blue, the fluorine atom is shown as a green sphere.*

The bond angles around these two gallium atoms are distorted away from the tetrahedral towards those which would be expected for a trigonal bipyramidal atom, indicating that the fluorine atoms are close enough to affect the position of the oxygen atoms. The O-Ga-O bond angles around the other two gallium atoms remain close to their ideal tetrahedral values.

The D4R units are linked through the oxygen atoms of two GaO_4 and two PO_4 tetrahedra to form planar layers, which are perpendicular to the (100) direction of the unit cell. The sheets have ten tetrahedral atom ring windows defined by four D4R units. This arrangement of D4R units is similar to that of ACP-14, a CoAPO first reported by Stucky *et.al.*[5] Whereas in ACP-14 the D4Rs are linked together to form a zeolite-type structure, the layers in cyclam-GaPO are joined by a six coordinate gallium-cyclam complex (fig. 4.4).

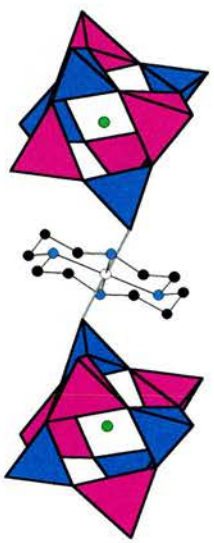

Figure 4.4 *Two D4R units linked by a gallium-CYCLAM complex. Colour scheme as for fig. 4.3, the hydrogen atoms of the macrocyclic ligand are omitted for clarity.*

Four of the six coordination sites of the gallium are taken by the nitrogen atoms of the macrocycle while the other two are occupied by oxygen atoms from PO_4 tetrahedra of D4Rs in adjacent layers (fig. 4.5). Two of the oxygens attached to gallium atoms in the D4R units are not coordinated to any other atom, and from bond valence and charge balancing considerations these have been assigned as hydroxyl

groups. The cyclam complex adopts the trans III conformation, which is the most thermodynamically favourable for this system.

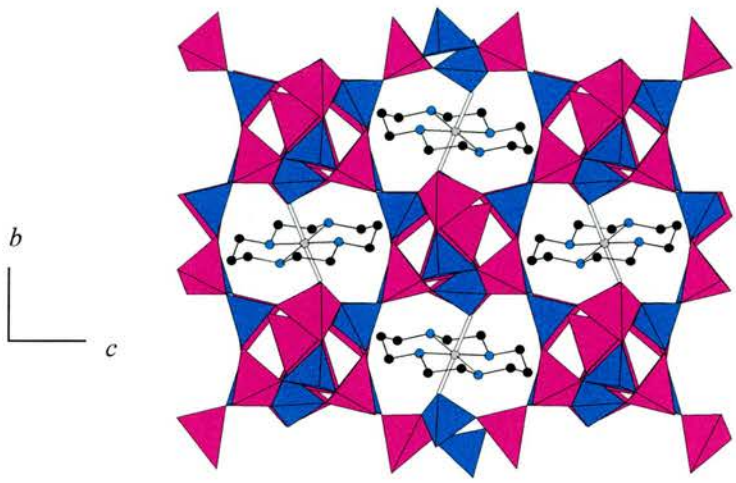

Figure 4.5 *The structure of CYCLAM-GaPO viewed parallel to the (100) direction.*

Table 4.2 *Atomic coordinates (x 10^4) and equivalent isotropic displacement parameters ($Å^2$ x 10^3) for cyclam-GaPO. U(eq) is defined as one third of the trace of the orthogonalized U_{ij} tensor.*

	x	y	z	U(eq)
Ga(1)	8583(1)	2488(1)	7303(1)	8(1)
Ga(2)	10337(1)	-202(1)	6406(1)	16(1)
Ga(3)	10000	5000	5000	8(1)
P(4)	10374(1)	2721(1)	6224(1)	8(1)
P(5)	8284(1)	-443(1)	7243(1)	9(1)
O(1)	7915(2)	950(3)	7294(2)	13(1)
O(2)	11244(3)	-865(3)	7044(2)	19(1)
O(3)	10584(3)	-1154(3)	5626(2)	14(1)
O(4)	9271(2)	2866(3)	6470(2)	15(1)
O(5)	7593(2)	3694(3)	7060(2)	13(1)
O(6)	10619(3)	1335(3)	6045(2)	20(1)
O(7)	9036(3)	-574(3)	6619(2)	17(1)
O(8)	10529(2)	3529(3)	5560(2)	12(1)
O(9)	8922(3)	3191(3)	8171(2)	18(1)
F(1)	10000	1289(4)	7500	22(1)
N(1)	9197(3)	3769(4)	4353(2)	12(1)
N(2)	11158(3)	4718(4)	4283(2)	10(1)
C(1)	12173(3)	4600(5)	4616(3)	14(1)
C(2)	9757(4)	3713(5)	3652(2)	14(1)
C(3)	10872(4)	3604(5)	3822(3)	15(1)
C(4)	8108(2)	4030(4)	4255(2)	17(1)
C(5)	12437(2)	5814(4)	5024(2)	17(1)

Table 4.3 *Bond lengths [Å] and angles [°] for cyclam-GaPO.*

Ga(1)-O(9)	1.819(3)	O(7)-Ga(2)-O(2)	114.13(18)
Ga(1)-O(4)	1.830(3)	O(8)-Ga(3)-O(8)#1	180.00(15)
Ga(1)-O(1)	1.834(3)	O(8)-Ga(3)-N(2)#1	92.34(14)
Ga(1)-O(5)	1.875(3)	O(8)-Ga(3)-N(2)	87.66(14)
Ga(1)-F(1)	2.290(2)	N(2)#1-Ga(3)-N(2)	180.000(1)
Ga(2)-O(6)	1.778(4)	O(8)-Ga(3)-N(1)#1	89.91(15)
Ga(2)-O(3)	1.781(3)	N(2)#1-Ga(3)-N(1)#1)	85.63(15
Ga(2)-O(7)	1.814(3)	N(2)-Ga(3)-N(1)#1	94.37(15)
Ga(2)-O(2)	1.820(3)	O(8)-Ga(3)-N(1)	90.09(15)
Ga(3)-O(8)	1.981(3)	N(2)-Ga(3)-N(1)	85.63(15)
Ga(3)-N(2)	2.050(4)	N(1)#1-Ga(3)-N(1)	180.00(17)
Ga(3)-N(1)	2.053(4)	O(8)-P(4)-O(6)	109.21(19)
P(4)-O(8)	1.502(3)	O(8)-P(4)-O(9)#2	109.29(19)
P(4)-O(6)	1.520(3)	O(6)-P(4)-O(9)#2	109.4(2)
P(4)-O(9)#2	1.538(3)	O(8)-P(4)-O(4)	108.43(18)
P(4)-O(4)	1.541(3)	O(6)-P(4)-O(4)	111.1(2)
P(5)-O(5)#3	1.511(3)	O(9)#2-P(4)-O(4)	109.4(2)
P(5)-O(2)#2	1.522(3)	O(5)#3-P(5)-O(2)#2	109.72(19)
P(5)-O(7)	1.531(3)	O(5)#3-P(5)-O(7)	106.34(19)
P(5)-O(1)	1.539(3)	O(2)#2-P(5)-O(7)	110.9(2)
N(1)-C(4)	1.483(5)	O(5)#3-P(5)-O(1)	109.41(19)
N(1)-C(2)	1.493(6)	O(2)#2-P(5)-O(1)	110.6(2)
N(2)-C(1)	1.487(6)	O(7)-P(5)-O(1)	109.8(2)
N(2)-C(3)	1.490(6)	P(5)-O(1)-Ga(1)	132.5(2)
C(1)-C(5)	1.516(6)	P(5)#2-O(2)-Ga(2)	136.1(2)
C(2)-C(3)	1.517(7)	P(4)-O(4)-Ga(1)	134.5(2)
C(4)-C(5)#1	1.523(7)	P(5)#4-O(5)-Ga(1)	152.6(2)
		P(4)-O(6)-Ga(2)	137.2(2)
O(9)-Ga(1)-O(4)	121.88(17)	P(5)-O(7)-Ga(2)	139.9(2)
O(9)-Ga(1)-O(1)	118.77(16)	P(4)-O(8)-Ga(3)	144.4(2)
O(4)-Ga(1)-O(1)	115.00(16)	P(4)#2-O(9)-Ga(1)	131.4(2)
O(9)-Ga(1)-O(5)	96.44(15)	Ga(1)#2-F(1)-Ga(1)	113.68(18)
O(4)-Ga(1)-O(5)	90.25(14)	C(4)-N(1)-C(2)	112.8(3)
O(1)-Ga(1)-O(5)	104.34(15)	C(4)-N(1)-Ga(3)	117.5(3)
O(9)-Ga(1)-F(1)	82.96(12)	C(2)-N(1)-Ga(3)	105.7(3)
O(4)-Ga(1)-F(1)	80.87(11)	C(1)-N(2)-C(3)	113.7(4)
O(1)-Ga(1)-F(1)	85.39(14)	C(1)-N(2)-Ga(3)	115.1(3)
O(5)-Ga(1)-F(1)	169.02(13)	C(3)-N(2)-Ga(3)	106.8(3)
O(6)-Ga(2)-O(3)	99.34(15)	N(2)-C(1)-C(5)	110.2(4)
O(6)-Ga(2)-O(7)	118.33(17)	N(1)-C(2)-C(3)	108.0(4)
O(3)-Ga(2)-O(7)	103.29(16)	N(2)-C(3)-C(2)	108.0(4)
O(6)-Ga(2)-O(2)	116.56(18)	N(1)-C(4)-C(5)#1	112.2(4)
O(3)-Ga(2)-O(2)	100.90(16)	C(1)-C(5)-C(4)#1	114.4(4)

Table 4.4 *Anisotropic displacement parameters ($Å^2$ x 10^3) for cyclam-GaPO. The anisotropic displacement factor exponent takes the form:*
$-2\pi^2 [h^2 a^{*2} U_{11} + ... + 2 h k a^* b^* U_{12}]$

	U_{11}	U_{22}	U_{33}	U_{23}	U_{13}	U_{12}
Ga(1)	9(1)	9(1)	7(1)	-1(1)	1(1)	-1(1)
Ga(2)	13(1)	15(1)	22(1)	4(1)	-1(1)	0(1)
Ga(3)	7(1)	13(1)	5(1)	-2(1)	0(1)	0(1)
P(4)	6(1)	13(1)	7(1)	0(1)	0(1)	2(1)
P(5)	8(1)	8(1)	10(1)	0(1)	-1(1)	-1(1)
O(1)	10(2)	8(2)	21(2)	1(1)	-1(1)	0(1)
O(2)	22(2)	17(2)	18(2)	-6(1)	-12(1)	9(1)
O(3)	18(2)	8(2)	15(2)	-2(1)	1(1)	-1(1)
O(4)	7(2)	24(2)	13(2)	7(1)	3(1)	7(1)
O(5)	11(2)	14(2)	14(2)	1(1)	1(1)	5(1)
O(6)	30(2)	14(2)	16(2)	-3(1)	10(2)	5(2)
O(7)	9(2)	18(2)	24(2)	-8(1)	6(1)	-5(1)
O(8)	9(1)	18(2)	8(1)	3(1)	2(1)	2(1)
O(9)	17(2)	20(2)	16(2)	-9(1)	-9(1)	9(1)
F(1)	27(2)	19(2)	19(2)	0	-7(2)	0
N(1)	11(2)	16(2)	9(2)	-3(1)	-3(1)	0(2)
N(2)	8(2)	14(2)	8(2)	-2(1)	2(1)	-1(1)
C(1)	10(2)	21(2)	13(2)	3(2)	2(2)	2(2)
C(2)	17(2)	16(2)	10(2)	-4(2)	0(2)	-1(2)
C(3)	16(2)	15(2)	14(2)	-6(2)	5(2)	0(2)
C(4)	12(2)	23(2)	15(2)	-1(2)	-6(2)	-3(2)
C(5)	9(2)	25(2)	19(2)	2(2)	-2(2)	-4(2)

4.2.4 Thermal Properties

TGA in an atmosphere of flowing nitrogen showed that the bulk sample of CYCLAM-GaPO was stable up to a temperature of ~500°C at which it underwent a 11% mass loss which we believe to be due to the removal of the organic part. The residue was amorphous when studied by XRD, suggesting that, in common with many GaPOs reported in the literature, the structure of CYCLAM-GaPO collapses on removal of the organic part. This implies that the CYCLAM complex fulfils a space filling role in the formation of the product despite the fact that it is no longer simply a template for the structure as it is covalently bound to the inorganic matrix. When the observed mass loss is compared to that calculated for the loss of the organic part from the crystal structure it is found to be less than expected (calc. value = 41.4%). This shows that the material is

not phase pure in its bulk form, microanalysis (C, H, N) also suggested the presence of impurities, with a poor match between calculated and observed structural formulae. It is suspected that an amount of amorphous material is present in the bulk accounting for the large difference between observed and calculated results for the whole sample compared to the single crystal. However, Rietveld refinement of the model against synchrotron powder data gives a very good fit (fig. 4.6) indicating that the crystalline bulk material is in fact pure cyclam-GaPO. The results of the Rietveld refinement are given in tables 4.5, 4.6 and 4.7.

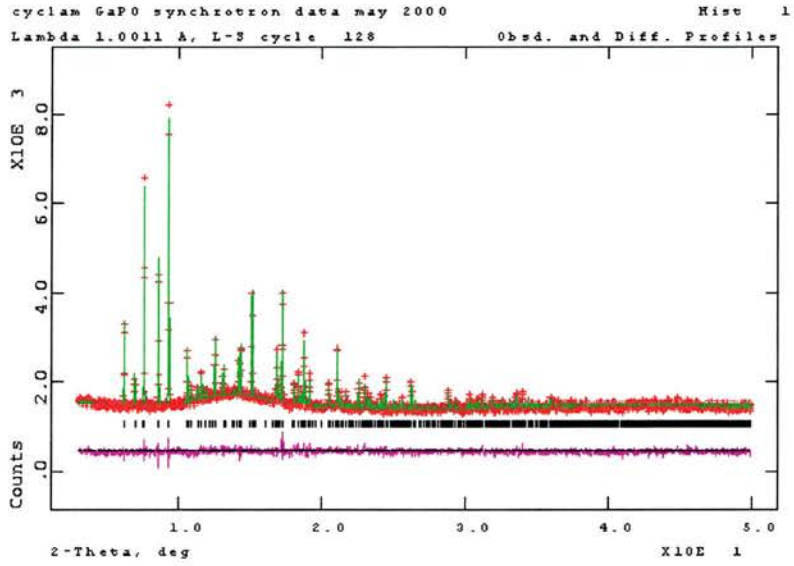

Figure 4.6 *Rietveld profile for cyclam-GaPO at room temperature. Red crosses indicate the observed profile, green line calculated, purple difference*

Table 4.5 *Rietveld refinement details for cyclam-GaPO*

Diffractometer type	SRS station 2.3
Wavelength/Å	1.0011
Temperature/K	298
2 θ range / °	3 - 40
Step size / °	0.1
Chemical formula	$GaPO_4(OH)_2F.Ga(C_{10}N_4H_{24})$
Formula weight	489.816
Calculated density/gcm^{-3}	2.468
Space group	*P*bcn
Unit cell dimensions/Å	a = 13.28646(31)
	b = 10.48778(21)
	c = 18.45645(45)
Z	14
Number of reflections	844
Final R values (all data)	wRp = 0.0336
	Rp = 0.0261
	RF^2 = 0.4123
Background method	Fixed background

Table 4.6 *Atom positions and isotropic thermal displacement parameters from Rietveld refinement of cyclam-GaPO*

	x	y	z	U_{iso}
Ga(1)	0.8566(8)	0.247(1)	0.7317(7)	0.047(2)
Ga(2)	1.034(9)	-0.020(1)	0.636(5)	0.047(2)
Ga(3)	1.000000	0.500000	0.500000	0.047(2)
P(4)	0.033(2)	0.279(2)	0.616(1)	0.052(8)
P(5)	0.829(2)	-0.036(2)	0.730(2)	0.052(8)
O(6)	0.790(3)	0.124(4)	0.724(3)	0.068(9)
O(7)	0.126(3)	-0.095(4)	0.700(2)	0.068(9)
O(8)	0.054(4)	-0.134(4)	0.562(2)	0.068(9)
O(9)	0.919(3)	0.300(5)	0.650(2)	0.068(9)
O(10)	0.759(3)	0.386(4)	0.694(3)	0.068(9)
O(11)	1.050(4)	0.152(4)	0.601(2)	0.068(9)
O(12)	0.914(3)	-0.071(4)	0.659(2)	0.068(9)
O(13)	1.062(3)	0.373(4)	0.553(2)	0.068(9)
O(14)	0.890(3)	0.310(4)	0.823(2)	0.068(9)
F(15)	1.000000	0.121(3)	0.750000	0.05(2)
N(16)	0.910(4)	0.387(6)	0.428(3)	0.033(5)
N(17)	1.128(4)	0.452(6)	0.430(3)	0.033(5)
C(18)	12173(3)	4600(5)	4616(3)	0.019(1)
C(19)	9757(4)	3713(5)	3652(2)	0.019(1)
C(20)	10872(4)	3604(5)	3822(3)	0.019(1)
C(21)	8108(2)	4030(4)	4255(2)	0.019(1)
C(22)	12437(2)	5814(4)	5024(2)	0.019(1)

Table 4.7 *Bond lengths (Å) and angles (°) from Rietveld refinement of cyclam-GaPO*

Ga(1)-O(9)	1.900(7)	O(3)-Ga(2)-O(2)	98.1(14)
Ga(1)-O(4)	1.836 (8)	O(7)-Ga(2)-O(2)	114.1(2)
Ga(1)-O(1)	1.889(17)	O(8)-Ga(3)-O(8)#1	180.0(2)
Ga(1)-O(5)	1.955(7)	O(8)-Ga(3)-N(2)	86.7(9)
Ga(1)-F(1)	2.334(7)	O(8)#1-Ga(3)-N(2)	93.3(9)
Ga(2)-O(6)	1.876(7)	N(2)#1-Ga(3)-N(2)	180.000(1)
Ga(2)-O(3)	1.870(8)	O(8)-Ga(3)-N(1)#1	89.4(15)
Ga(2)-O(7)	1.861(7)	O(8)#1-Ga(3)-N(1)#1	90.6(15)
Ga(2)-O(2)	1.888(8)	N(2)-Ga(3)-N(1)#1	94.358(2)
Ga(3)-O(8)	1.854(6)	N(2)-Ga(3)-N(1)	85.642(6)
Ga(3)-N(2)	2.05083(4)	O(8)-P(4)-O(6)	116.1(20)
Ga(3)-N(1)	2.05695(3)	O(8)-P(4)-O(9)#2	108.0(23)
P(4)-O(8)	1.550(9)	O(6)-P(4)-O(9)#2	101.2(20)
P(4)-O(6)	1.550(32)	O(8)-P(4)-O(4)	108.4(17)
P(4)-O(9)#2	1.550(8)	O(6)-P(4)-O(4)	125.8(17)
P(4)-O(4)	1.662(28)	O(9)#2-P(4)-O(4)	92.6(15)
P(5)-O(5)#3	1.625(12)	O(5)#3-P(5)-O(2)#2	116.9(12)
P(5)-O(2)#2	1.617(10)	O(5)#3-P(5)-O(7)	88.59(12)
P(5)-O(7)	2.069(31)	O(2)#2-P(5)-O(7)	103.1(13)
P(5)-O(1)	1.792(23)	O(5)#3-P(5)-O(1)	114.3(12)
N(1)-C(4)	1.483(5)	O(2)#2-P(5)-O(1)	122.1(11)
N(1)-C(2)	1.493(6)	O(7)-P(5)-O(1)	103.4(9)
N(2)-C(1)	1.487(6)	P(5)-O(1)-Ga(1)	116.7(8)
N(2)-C(3)	1.490(6)	P(5)#2-O(2)-Ga(2)	110.3(12)
C(1)-C(5)	1.516(6)	P(4)-O(4)-Ga(1)	134.7(7)
C(2)-C(3)	1.517(7)	P(5)#4-O(5)-Ga(1)	134.1(11)
C(4)-C(5)#1	1.523(7)	P(4)-O(6)-Ga(2)	129.6(16)
		P(5)-O(7)-Ga(2)	115.8(11)
O(9)-Ga(1)-O(4)	110.5(6)	P(4)-O(8)-Ga(3)	145.3(21)
O(9)-Ga(1)-O(1)	105.9(8)	P(4)#2-O(9)-Ga(1)	129.7(8)
O(4)-Ga(1)-O(1)	139.8(10)	Ga(1)#2-F(1)-Ga(1)	113.7(2)
O(9)-Ga(1)-O(5)	103.7(5)	C(4)-N(1)-C(2)	112.8(3)
O(4)-Ga(1)-O(5)	84.6(9)	C(4)-N(1)-Ga(3)	117.5(3)
O(1)-Ga(1)-O(5)	103.1(6)	C(2)-N(1)-Ga(3)	105.7(3)
O(9)-Ga(1)-F(1)	81.7(4)	C(1)-N(2)-C(3)	113.7(4)
O(4)-Ga(1)-F(1)	83.8(4)	C(1)-N(2)-Ga(3)	115.1(3)
O(1)-Ga(1)-F(1)	85.0(4)	C(3)-N(2)-Ga(3)	106.8(3)
O(5)-Ga(1)-F(1)	168.4(8)	N(2)-C(1)-C(5)	110.2(4)
O(6)-Ga(2)-O(3)	108.7(6)	N(1)-C(2)-C(3)	108.0(4)
O(6)-Ga(2)-O(7)	118.3(2)	N(2)-C(3)-C(2)	108.0(4)
O(3)-Ga(2)-O(7)	103.3(2)	N(1)-C(4)-C(5)#1	112.2(4)
O(6)-Ga(2)-O(2)	126.2(9)	C(1)-C(5)-C(4)#1	114.4(4)

4.2.5 Nitrogen adsorption

A nitrogen adsorption isotherm was collected for the bulk sample of CYCLAM-GaPO. The isotherm was of type 4; meaning that only surface absorption of nitrogen takes place and the structure is not porous.[6]

4.3 Modifying Cyclam-GaPO

The cyclam-GaPO structure offers several possibilities for modification. Firstly, it is possible to substitute other metal atoms into the gallium sites. This may be achieved either by replacing a proportion of the original gallium with another type of metal atom or by using pre-prepared metal-cyclam complexes in the synthesis described in section 4.2.1 above. Metal substituted frameworks may have interesting magnetic or catalytic properties. The second possible area of modification is the macrocycle itself. This is currently the subject of further research.

4.3.1 Substitutions on the Gallium Sites

The substitution of transition metals such as zinc and manganese in open framework gallophosphate and aluminophosphate materials has been widely reported (see section 1.3.2). In the case of cyclam-GaPO the substitutional metal atoms may show a preference for framework or cyclam-complex sites, depending on their chemical and geometric properties. Generally the samples were synthesised by the simple method of replacing a percentage of the initial gallium sulfate with a transition metal salt, however some work has also been carried out using a manganese-cyclam complex prepared by the

method of Daugherty *et. al.*[7] It was hoped that the substitutions would lead to materials with interesting magnetic properties or potential as catalysts.

4.3.2 Synthesis of substituted cyclam-GaPO

Initially a synthesis gel was prepared as described in section 4.1.1 above. To this an M^{2+} transition metal salt (Cobalt (II) carbonate hydrate, 98%, Aldrich; Manganese (II) chloride hydrate, obtained locally; copper (II) chloride dihydrate, 99.9%, Aldrich; Nickel (II) chloride hexahydrate, 99.99%, Aldrich) was added along with a small amount of phosphoric acid to maintain the correct M : P ratio. Samples were prepared in which 5%, 10%, 20%, 30%, 40% and 50% of the M sites were occupied by the transition metals. In all cases the products were powders, those containing copper being pink, cobalt blue (with some pink colour at higher levels of substitution) and nickel and manganese colourless. The products were recovered by standard filtration washing and drying techniques.

The reaction using a pre-prepared manganese-cyclam complex was slightly different. $Mn(cyclam)Cl_2.5H_2O$, was synthesised by dissolving cyclam (2.4g, 98%, Strem) in ethanol (60ml) and adding $MnCl_2.4H_2O$ (0.2364g, obtained locally). The resulting solution was stirred for 3 hours, extracted into 20ml of distilled water and acidifed with 20ml of 4 mol dm^{-3} hydrochloric acid. Green needle like crystals were recovered (microanalysis: C, found 30.25%, calc 28.9%; H, found 8.63%, calc 7.3%, N, found 13.97%, calc 13.5%) by filtration and dried at room temperature in air.

For the Gallophosphate preparation phosphoric acid (0.5g, 85% weight aqueous solution, Aldrich) was dissolved in pyridine (10ml, Fischer) and to this solution gallium

sulfate (0.5g, 99.8%, Aldrich) and the manganese complex (0.9g) were added. HF (70% solution in pyridine, Aldrich) was then added giving an approximate oxide gel composition of Ga_2O_3 : P_2O_5 : 2F : 2Mn-cyclam : 70 pyridine, the pH of the mixture was 7. After stirring for 30 minutes the gel was transferred to a Teflon lined stainless steel autoclave and heated at 170°C for 72 hours. The product, an off white powder was recovered by vacuum filtration, washed with water and acetone and dried at room temperature in air.

4.3.3 Results

The colour of the cobalt and copper substituted samples combined with powder XRD studies of the products of these preparations suggest that incorporation of the transition metal ions into the cyclam-GaPO structure has taken place. Changes in peak position are apparent from comparisons of the XRD patterns of the substituted materials. Unit cell parameters obtained from Le Bail extractions and full Rietveld refinements also show systematic variation, suggesting that substitution has occurred. Each substituted metal is now considered in turn.

4.3.3.1 Copper Substitution

The materials obtained when up to 20% copper is substituted for gallium in cyclam-GaPO were pink in colour, at higher levels of substitution some purple material was observed in addition to the pink. Pink is the colour of copper (II) ions coordinated by nitrogen donor ligands,[8] suggesting that at low levels of substitution copper ions are

situated in the cyclam complex site. This simple observation is supported by several other results.

Initial powder XRD examination of samples containing up to 50% substitution of copper for gallium showed that at up to 20% substitution the most intense peak (d = 6.15Å) was shifted to higher angle with greater substitution (fig 4.7), while above 20% the peak positions returned to their original values with a second phase becoming increasingly dominant in the powder pattern (fig 4.8).

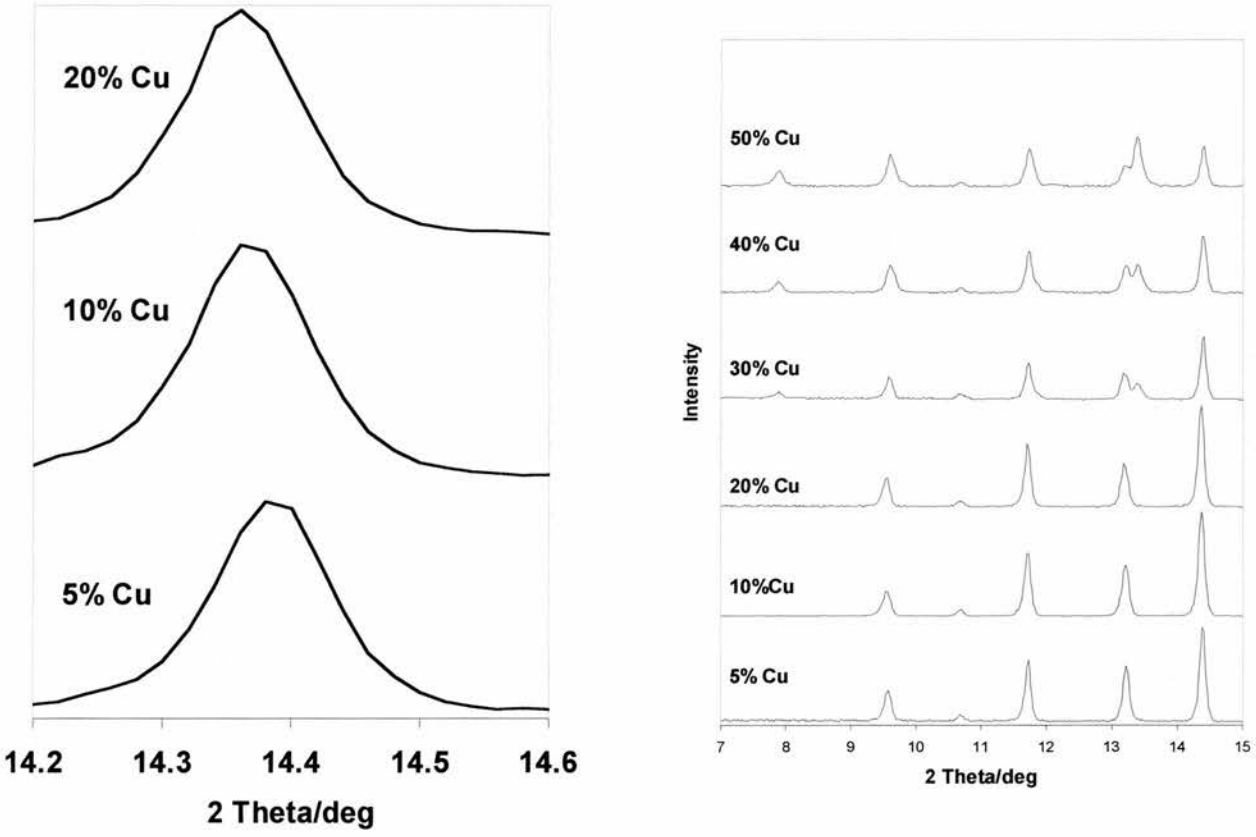

Figures 4.7 and 4.8 *Powder XRD data for Cu substituted cyclam-GaPO. The shifting of the main peak with increasing substitution is shown on the left, the emergence of a second phase on the right*

This may be explained by the phenomenon of phase segregation, with all of the copper forming the second phase as soon as it appears, leaving the cyclam-GaPO unsubstituted. Refinement of the lattice parameters of the 5, 10 and 20% Cu samples by the Le Bail method (model free refinement) from high resolution synchrotron powder data showed that the *a* and *b* axes increase in length with increasing Cu substitution while the *c* axis contracted (fig 4.9).

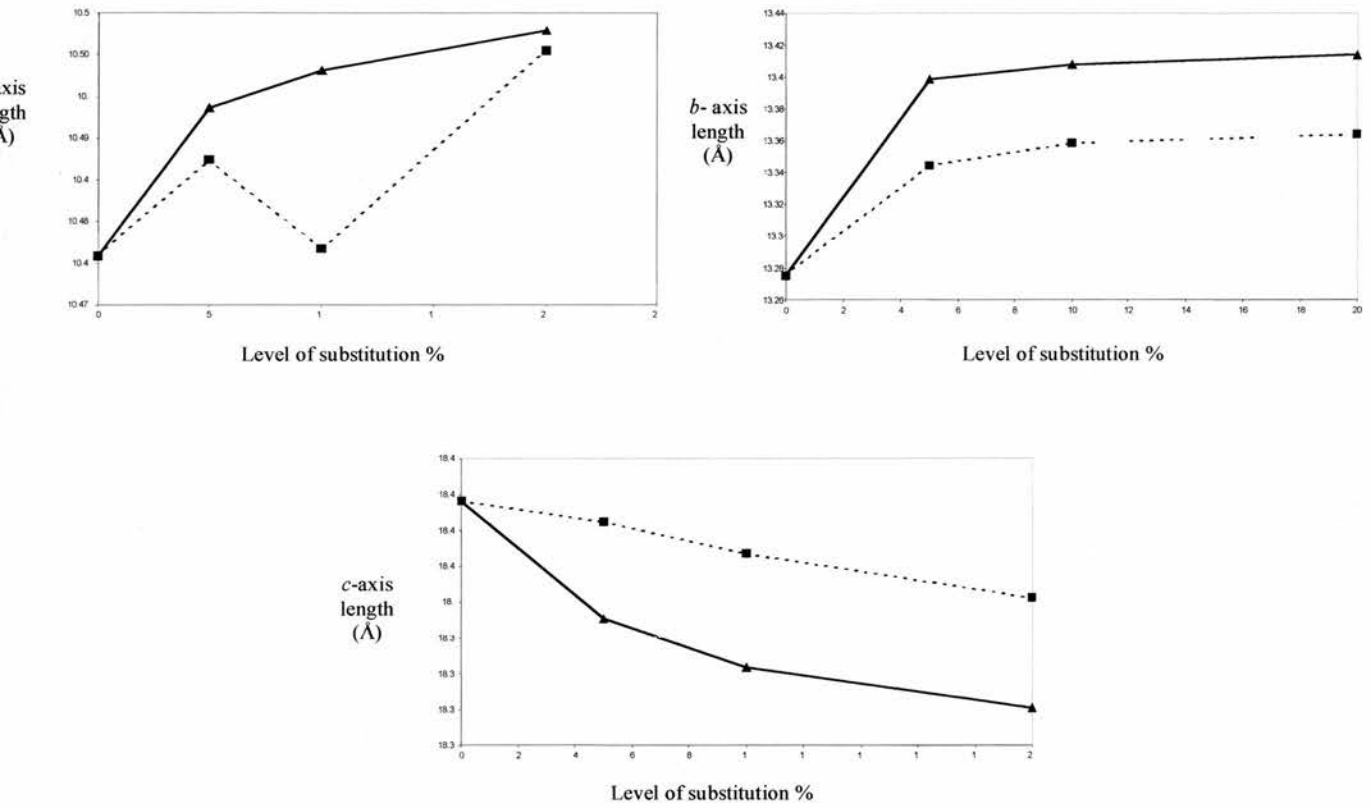

Figure 4.9 *Trends in axis length for Cu and Mn substituted cyclam GaPO. The copper substituted material is denoted by a dotted line, Mn substituted solid. The a and b axes extend (top graphs, left and right) while the c axis contracts (bottom graph), also note that the degree of change is greater for Mn substitution than for Cu.*

By using a model in which gallium and copper shared occupancy of the cyclam complex site (1, ½, ½) it was possible to carry out Rietveld refinements whose result concurred with those of the Le Bail fits to the powder data. The cyclam-GaPO structure has three gallium sites, two in the framework with general positions (multiplicity 1) and one in the cyclam complex in a special position on the face of a unit cell (multiplicity ½). This means that 80% of the gallium sites are in the framework and 20% in the complex and hence 20% copper substitution potentially leads to complete occupancy of the cyclam complex site by Cu. Using the data collected from the 20% copper sample it was possible to refine the atomic coordinates of the model in which the (1, ½, ½) position was occupied entirely by copper (fig 4.10).

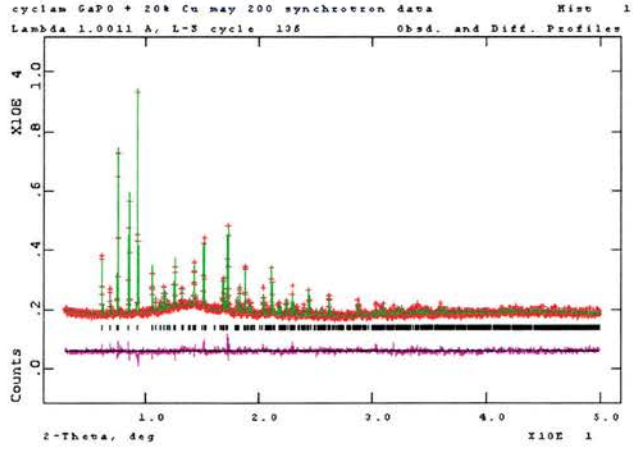

Figure 4.10 *Rietveld profile for cyclam-GaPO substituted with 20% Cu. Colour scheme as for fig. 4.6.*

In order to avoid refinement instability the bond lengths and angles of the D4R cages and the cyclam macrocycle were constrained to known values and the Cu-O bond

length was constrained to an average of literature values for cyclam complexes obtained from the Cambridge crystallographic database. The results of the refinement are given in tables 4.8, 4.9 and 4.10.

Table 4.8 *Rietveld refinement details for cyclam-GaPO substituted with 20% Cu*

Diffractometer type	SRS station 2.3
Wavelength/Å	1.0011
Temperature/K	298
2 θ range / °	3 - 40
Step size / °	0.1
Chemical formula	GaPO4(OH)2F.Cu(C10N4H24)
Formula weight	483.609
Calculated density/gcm^{-3}	2.443
Space group	*P*bcn
Unit cell dimensions/Å	a = 13.36463(34)
	b = 10.49766(22)
	c = 18.40175(50)
Z	14
Number of reflections	812
Final R values (all data)	wRp = 0.0302
	Rp = 0.0231
	RF^2 = 0.2345
Background method	Fixed background

Table 4.9 *Atomic coordinates from the Rietveld refinement of cyclam-GaPO substituted with 20% Cu.*

	x	y	z	U_{iso}
Ga(1)	0.8574(6)	0.2469(9)	0.7321(6)	0.011(3)
Ga(2)	1.0319(7)	-0.0252(8)	0.6380(4)	0.011(3)
Cu(3)	1.0000	0.5000	0.5000	0.025(5)
P(4)	1.0272(18)	0.2792(18)	0.6162(10)	0.031(7)
P(5)	0.8302(13)	-0.0457(18)	0.7295(13)	0.031(7)
O(1)	0.7939(20)	0.0950(23)	0.7278(26)	0.068(9)
O(2)	1.1218(27)	-0.0950(30)	0.7019(16)	0.068(9)
O(3)	1.0575(30)	-0.129(4)	0.5530(14)	0.068(9)
O(4)	0.9221(27)	0.298(4)	0.6509(19)	0.068(9)
O(5)	0.7602(28)	0.3682(33)	0.7033(25)	0.068(9)
O(6)	1.0501(32)	0.1323(23)	0.6022(15)	0.068(9)
O(7)	0.9040(22)	-0.064(4)	0.6646(18)	0.068(9)
O(8)	1.0765(24)	0.3371(33)	0.5479(20)	0.068(9)
O(9)	0.8965(28)	0.308(4)	0.8187(17)	0.068(9)

Table 4.9 continued

	x	y	z	U_{iso}
F(1)	1.0000	0.1289(14)	0.7500	0.01(2)
N(1)	0.9211(30)	0.393(5)	0.4325(23)	0.004(9)
N(2)	1.1178(28)	0.455(5)	0.4341(23)	0.004(9)
C(1)	1.215(4)	0.466(6)	0.4576(30)	0.004(9)
C(2)	0.969(4)	0.398(5)	0.3806(27)	0.004(9)
C(3)	1.090(4)	0.361(6)	0.3850(32)	0.004(9)
C(4)	0.811(4)	0.402(6)	0.4314(30)	0.004(9)
C(5)	1.2411(34)	0.575(6)	0.5033(33)	0.004(9)

Table 4.9 *Bond lengths and angles from the Rietveld refinement of cyclam-GaPO substituted with 20% Cu*

Ga(1)-O(9)	1.795(22)	O(6)-Ga(2)-O(7)	120.9(16)
Ga(1)-O(4)	1.809(23)	O(3)-Ga(2)-O(7)	100.2(13)
Ga(1)-O(1)	1.808(21)	O(6)-Ga(2)-O(2)	117.4(11)
Ga(1)-O(5)	1.895(26)	O(3)-Ga(2)-O(2)	100.2(13)
Ga(1)-F(1)	2.297(9)	O(7)-Ga(2)-O(2)	112.92(1)
Ga(2)-O(6)	1.798(22)	O(8)-Cu(1)-O(8)#1	180.0(2)
Ga(2)-O(3)	1.937(24)	O(8)-Cu(1)-N(2)	78.678(2)
Ga(2)-O(7)	1.823(22)	O(8)#1-Cu(1)-N(2)	101.322(2)
Ga(2)-O(2)	1.834(22)	N(2)#1-Cu(1)-N(2)	180.000(1)
Cu(1)-O(8)	2.179(12)	O(8)-Cu(1)-N(1)#1	101.734(2)
Cu(1)-N(2)	2.042(32)	O(8)#1-Cu(1)-N(1)#1	78.266(2)
Cu(1)-N(1)	1.976(33)	N(2)-Cu(1)-N(1)#1	84.7(13)
P(4)-O(8)	1.543(12)	N(2)-Cu(1)-N(1)	95.3(19)
P(4)-O(6)	1.593(26)	O(8)-P(4)-O(6)	99.6(20)
P(4)-O(9)#2	1.602(26)	O(8)-P(4)-O(9)#2	105.3(26)
P(4)-O(4)	1.556(25)	O(6)-P(4)-O(9)#2	100.3(20)
P(5)-O(5)#3	1.583(26)	O(8)-P(4)-O(4)	132.0(19)
P(5)-O(2)#2	1.508(25)	O(6)-P(4)-O(4)	111.5(24)
P(5)-O(7)	1.560(24)	O(9)#2-P(4)-O(4)	104.1(21)
P(5)-O(1)	1.555(25)	O(5)#3-P(5)-O(2)#2	112.5(22)
N(1)-C(4)	1.48(5)	O(5)#3-P(5)-O(7)	100.4(24)
N(1)-C(2)	1.15(6)	O(2)#2-P(5)-O(7)	109.3(21)
N(2)-C(1)	1.37(5)	O(5)#3-P(5)-O(1)	107.3(21)
N(2)-C(3)	1.39(5)	O(2)#2-P(5)-O(1)	118.4(29)
C(1)-C(5)	1.47(5)	O(7)-P(5)-O(1)	107.4(27)
C(2)-C(3)	1.66(5)	P(5)-O(1)-Ga(1)	133.6(19)
C(4)-C(5)#1	1.41(5)	P(5)#2-O(2)-Ga(2)	132.7(19)
		P(4)-O(4)-Ga(1)	137.1(21)
O(9)-Ga(1)-O(4)	119.2(16)	P(5)#4-O(5)-Ga(1)	145.3(31)
O(9)-Ga(1)-O(1)	119.3(17)	P(4)-O(6)-Ga(2)	143.6(21)
O(4)-Ga(1)-O(1)	116.9(17)	P(5)-O(7)-Ga(2)	140.4(20)
O(9)-Ga(1)-O(5)	102.0(19)	P(4)-O(8)-Cu(1)	106.35(5)
O(4)-Ga(1)-O(5)	84.0(16)	P(4)#2-O(9)-Ga(1)	141.5(21)
O(1)-Ga(1)-O(5)	105.0(15)	Ga(1)#2-F(1)-Ga(1)	113.59(4)
O(9)-Ga(1)-F(1)	79.8(11)	C(4)-N(1)-C(2)	123.0(5)
O(4)-Ga(1)-F(1)	83.3(11)	C(4)-N(1)-Cu(1)	120.4(33)
O(1)-Ga(1)-F(1)	85.4(10)	C(2)-N(1)-Cu(1)	101.6(34)
O(5)-Ga(1)-F(1)	166.3(14)	C(1)-N(2)-C(3)	121.0(4)
O(6)-Ga(2)-O(3)	101.3(15)	C(1)-N(2)-Cu(1)	121.5(31)

Table 4.10 Continued

C(3)-N(2)-Cu(1)	110.1(28)	N(2)-C(3)-C(2)	97.0(4)
N(2)-C(1)-C(5)	118.0(5)	N(1)-C(4)-C(5)#1	119.0(5)
N(1)-C(2)-C(3)	120.0(5)	C(1)-C(5)-C(4)#1	120.0(5)

The refined atom positions show the principal axis of the cyclam complex tilting towards the *a* and *b* axes (leading to their extension) and away from the *c* axis (the angle between O8 and the *c*-axis increases from 47.7° to 67.3°, fig. 4.11). This leads to a reduction in separation of the D4R layers from 8.034Å to 7.884Å (P4 to P4 distance), and hence the contraction of the *c*-axis.

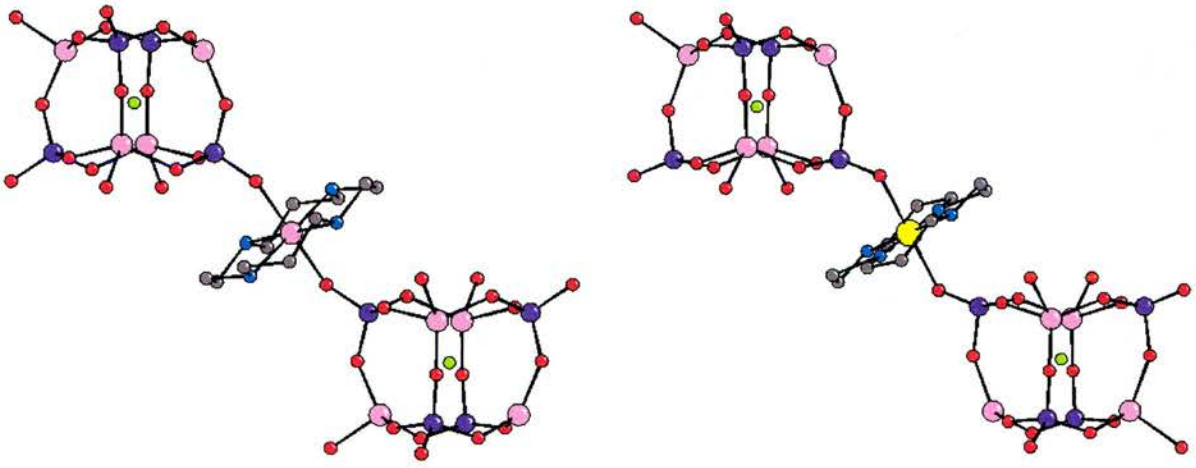

Figure 4.11 *Comparison of the gallium-cyclam and copper-cyclam complex sites in cyclam-GaPO and cyclam-GaPO substituted with 20% Cu. The twisting of the principal axis is clearly illustrated. The colour scheme is as in fig. 4.2 with Cu shown as a yellow sphere.*

The validity of the assumption that copper occupies the cyclam complex site is further supported by ESR spectroscopy. The spectrum obtained from a solid state sample

of cyclam-GaPO prepared with 20% copper was successfully simulated with the program Simfonia[9] (fig.4.12). The signal for a Cu^{2+} ion (d^9, single free electron, spin 3/2) is axially symmetric with $g_{||}$ = 2.1823 and $g_{\perp}$= 2.05, suggesting that the Cu is in either an axially compressed tetrahedral site or an axially strained octahedral site.

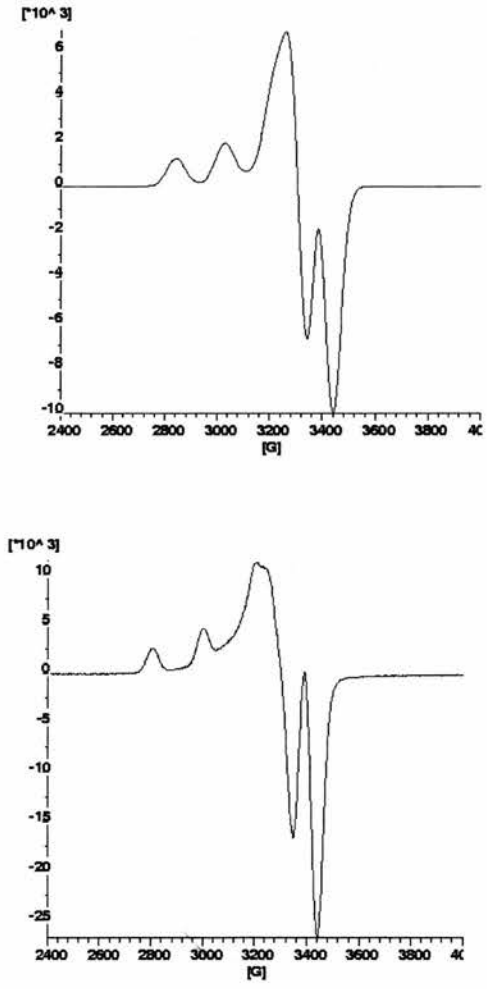

Figure 4.12 *Observed (bottom) and simulated (top) ESR spectra for cyclam-GaPO containing Cu.*

Since it would be unusual to find Cu^{2+} in an axially compressed tetrahedral site, this supports the above evidence. The axial extension is explained by the Jahn-Teller effect, well documented for Cu^{2+}, similar g values are also observed for other d^9 ions with this site geometry (table 4.11).[10] The main component of the hyperfine coupling is parallel to the principle axis of the site with J = 200 cm^{-1}other components are close to zero.

Table 4.11 *$g_{//}$and $g_{\perp}$for d^9 ions in axially strained octahedral geometries*

Ion	Host	$g_{\|\|}$	$g_{\perp}$
Cu^{2+}	Copper phthalocyanine	2.165	2.045
Ag^{2+}	KCl	2.193	2.035
Cu^{2+}	**Cyclam-GaPO**	**2.182**	**2.05**
Au^{2+}	ZnSe	2.183	2.033

Magnetic susceptibility measurements on Cu substituted cyclam-GaPO show that it is a paramagnet (fig. 4.13), however the signal observed is very weak (an unusually high field, 2 Tesla, must be applied for the effect to be observed). This paramagnetic behaviour is as expected from the crystal structure, since the separation between the magnetic centres is large (minimum 8.448Å).

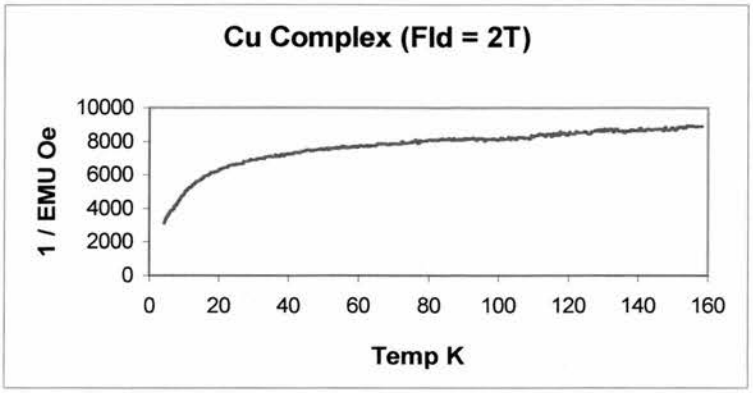

Figure 4.13 *Plot of $1/\chi$ against temperature for Cu substituted cyclam-GaPO, the behaviour is paramagnetic*

At 120K the behaviour of the sample under a varying magnetic field was extremely unusual, this has not yet been explained but could be due to the very weak signal being measured (fig. 4.14).

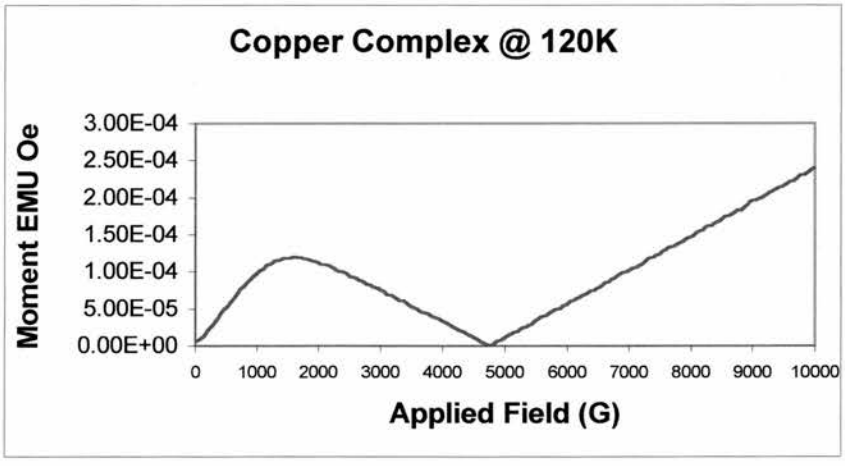

Figure 4.14 *Unusual behaviour of Cu substituted cyclam-GaPO under a varying magnetic field at 120K. Plot of χ against applied magnetic field.*

4.3.3.2 Manganese Substitution

Powder XRD analysis of samples of cyclam-GaPO prepared with manganese substituted for gallium showed similar trends in peak position variation to copper substituted samples. Again, the samples appeared to be single phase for levels of substitution up to 20%, however, rather than a second crystalline phase appearing at higher levels of substitution the intensity of the main cyclam-GaPO phase is reduced and an amorphous background phase begins to dominate the powder profile (fig 4.15).

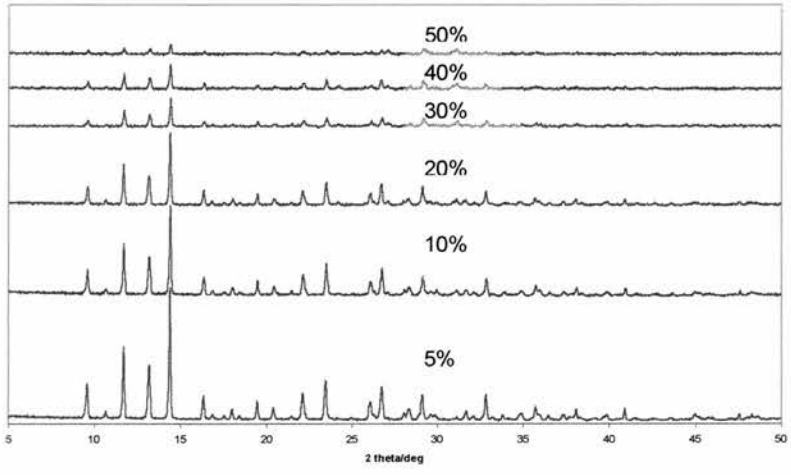

Figure 4.15 *PXRD data for Mn substituted cyclam-GaPO*

Le Bail fits against synchrotron PXRD data reveal similar patterns in the variation of the lattice parameters to those observed for copper (fig. 4.9; previous section). The variation of the lattice parameters for Mn substitution is slightly greater than for Cu, this is thought to be due to the larger size of the Mn^{2+} ion compared to Cu^{2+} (0.97Å and 0.87Å respectively).[11] It was not possible to carry out full Rietveld refinements for the 20% manganese sample however due to a slight impurity in the phase.

Solid state ESR measurements for the Mn substituted phase did show a signal, however, unlike that of the copper substituted material it is a single peak (g = 2.01) and the hyperfine structure cannot be resolved. This only confirms that manganese is present in the sample (fig 4.16).

Magnetic measurements on this material showed once more the predictable paramagnetic behaviour. The signal observed however was much stronger than for copper and did not exhibit any unusual behaviour (fig. 4.17).

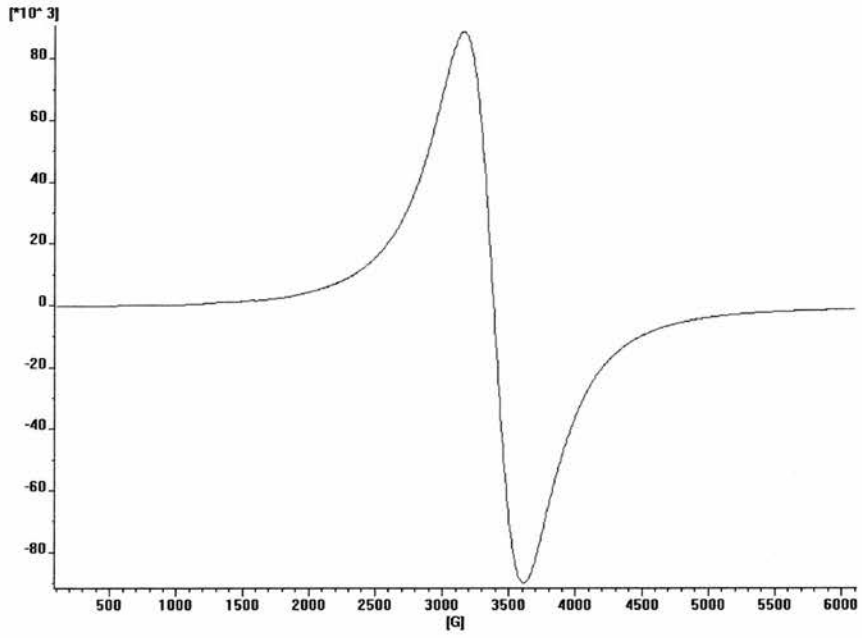

Figure 4.16 *ESR spectrum of cyclam-GaPO containing Mn*

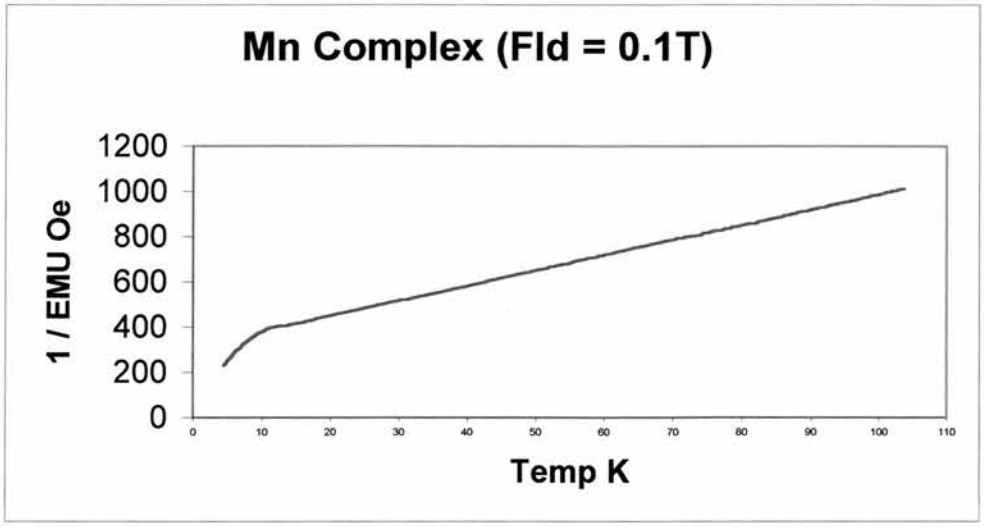

Figure 4.17 *The paramagnetic behaviour of Mn substituted cyclam-GaPO. Plot of $1/\chi$ against temperature*

4.3.3.3 Cobalt substitution

When cobalt is added to the synthesis gel, the product is a pale blue material. This colour is characteristic of Co^{2+} in tetrahedral coordination,[8] which implies that the cobalt occupies the tetrahedral sites in the gallium phosphate layers rather than the octahedral complex site. The cyclam-GaPO phase is strongly evident at levels of substitution up to 30%, however, at higher substitution levels the intensity of the peaks rapidly decreases indicating a more amorphous character in the bulk material with cyclam-GaPO no longer the dominant product (fig 4.18).

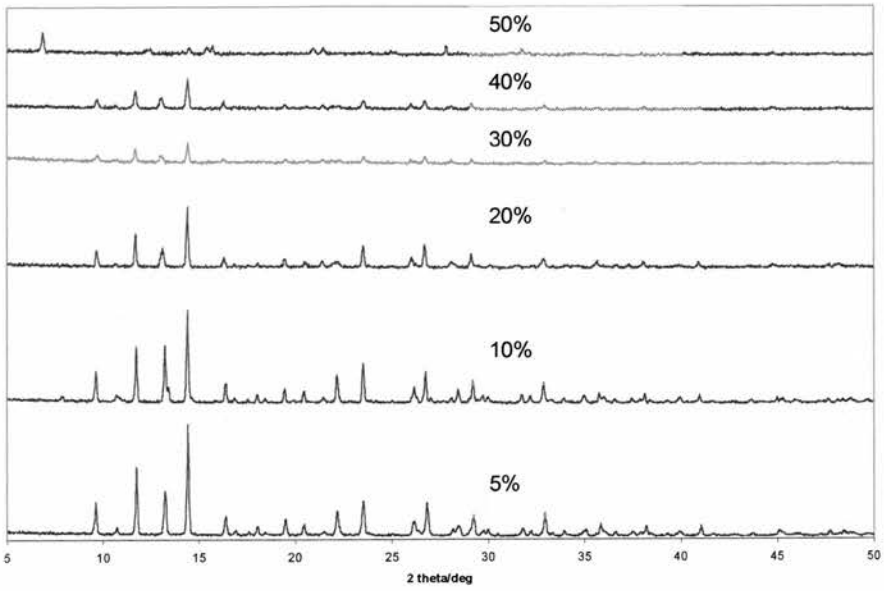

Figure 4.18 *PXRD data for Co substituted cyclam-GaPO, note that a second phase is formed preferentially at 50% substitution*

This raises the question of whether or not cobalt is indeed incorporated in the cyclam-GaPO structure, as we believe to be the case. The theory is supported by Le Bail analysis of the PXRD data, which shows changes in lattice parameters for Co substituted materials and also by the strong blue colour observed in the products even at low levels of Co substitution (for which the product remains highly crystalline and exhibits no impurities). However, it should be noted that the changes in lattice parameters follow the same pattern for Co substitution as for Cu and Mn, although we believe the substitution to be on a different site (fig. 4.19). At 50% substitution no cyclam-GaPO is present in the PXRD pattern of the product, an unidentified crystalline phase.

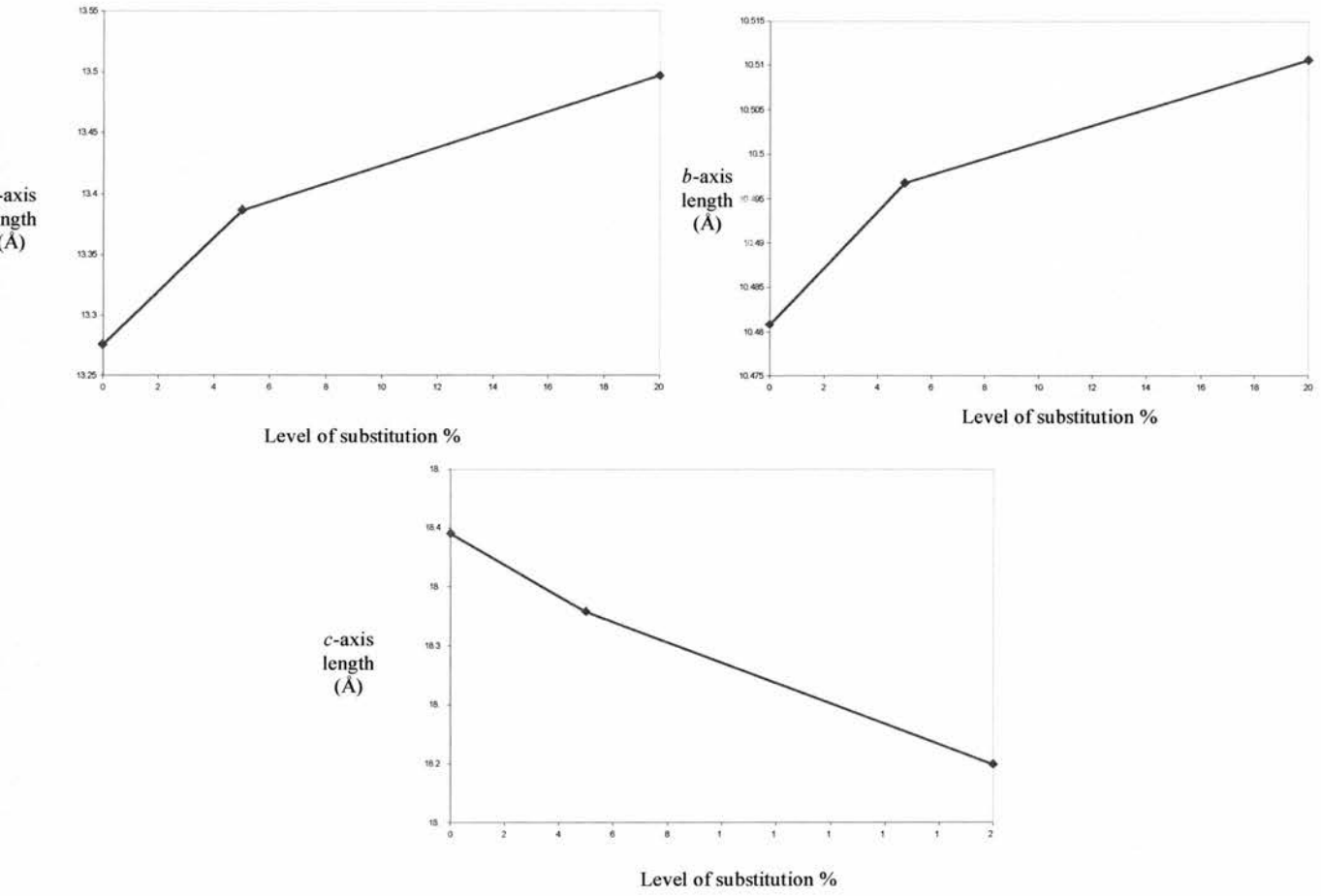

Figure 4.19 *Unit cell axis variation for Co substituted cyclam-GaPO. As for Cu and Mn substitution the a and b axes (top, left and right) increase in length with increasing Co content while the c axis is shortened (bottom graph).*

4.3.3.4 Nickel Substitution

When $NiCl_2$ was added to the synthesis mixture for cyclam-GaPO the product was an off white powder. Powder XRD results showed no change in peak positions from the pure gallium material, suggesting that nickel had not been incorporated into the structure. There was also a significant crystalline impurity. Le Bail analysis of the patterns was unreliable due to the impurity phase but generally showed no systematic trends in lattice parameter variation. It may therefore be concluded that Nickel cannot be

incorporated into the cyclam-GaPO structure. This is not really a surprise as the preferred coordination geometry of Ni^{2+} is square planar,[8] making it unlikely to fit easily into any of the sites in the structure. In addition to this cyclam coordinates nickel very strongly, meaning that the cyclam-GaPO structure would be less likely to form, explaining the high level of crystalline impurities.

4.4 Other Macrocycles

The use of several other polyaza-macrocycles as templates for gallophosphate materials has been investigated with little success. A large hexaaza-macrocycle, Di-meta-pthalyl-[24]-tetraane N_6,[12] was also thought to have given an interesting phase, however, when crystals of the material were eventually prepared (by using a mixture of ethylene glycol and water as the solvent) the structure turned out to be that of the ligand coordinating Ga^{3+} with solvent.

The macrocycle *meso*-5, 5, 7, 12, 12, 14-hexamethyl-1, 4, 8, 11-tetraazacyclotetradecane (tet-A)[13] has also been used in GaPO preparations. This however, did not lead to the inclusion of the macrocycle, instead gallophosphates containing the small template molecules were obtained (see next chapter). It may be that tet-A is too large to fit into a cyclam-GaPO type structure and its nitrogen atoms too sterically hindered to act in the manner of a conventional SDA. Cyclen (1,4,7,10-tetraazacyclooctane, Aldrich) has been used in the preparation of GaPOs but only poorly crystalline materials have resulted.

By further experimentation with different synthesis conditions, these macrocycles may be useable as templates. The importance of template-framework charge balancing in

open framework systems has been emphasised recently and it may be that by methods such as pH modification, altering the fluoride ion concentration or framework ion substitution the problems can be overcome.

References

1. F. Dougnier, J. Patarin, J.L. Guth and D. Anglerot, *Zeolites*, 1992, **12**, 160.
2. (a)P. Reinert, J. Patarin and B. Marler, *Europ. J. Solid State Inorg. Chem.*, 1998, **35**, 389: (b) P.A. Wright, M.J. Maple, A.M.Z. Slawin, V. Patinec, R.A. Aitken, S. Welsh and P.A. Cox, *J. Chem. Soc., Dalton Trans.*, 2000, 1243; (c) F. Serpaggi, T. Loiseau, F. Taulelle and G. Férey, *Microporous And Mesoporous Mater.*, 1998, **20**, 197; (d) T.A. Khan and J.A. Hriljac, *Inorg. Chim. Acta*, 1999, **294**, 179.
3. M. Estermann, L.B. McCusker, C. Baerlocher, A. Merrouche and H. Kessler, *Nature*, 1991, **352**, 320.
4. G. Férey, *C. R. Acad. Sci. Ser. C.*, 1998, **1**, 1.
5. X. Bu, P. Feng and G.D. Stucky, *Science*, 1997, **278**, 2080.
6. G.A. Somorjai, *Introduction to Surface Science and Catalysis,* John Wiley and Sons, New York, 1994, Ch. 3.
7. P.A. Daugherty, J. Glerup, P.A. Goodson, D.J. Hodgson and K. Michelsen, *Acta Chem. Scand.*, 1991, **45**, 244.
8. N. N. Greenwood and A. Earnshaw, *Chemistry of the Elements*, Butterworth-Heinemann, Oxford, 1997.
9. Bruker Analytical, 1994-1996.
10. N.R.J. Poolton J.J. Davies, J.E. Nicholls and B.J. Fitzpatrick, *J Phys C Solid State.*, 1987, **20**, 3553.
11. Web Elements, http://www.webelements.com/, 1993-2000, University of Sheffield.
12. R. Menif, A.E. Martell, P.J. Squattirio and A. Clearfield, *Inorg.Chem.*, 1990, **29**, 4723.

13. R.W. Hay, G.A. Lawrence and N.F. Curtis, *J. Chem. Soc., Perkin Trans. I,* 1975, 591.

CHAPTER 5

GALLOPHOSPHATES WITH SMALL MOLECULE TEMPLATES

5.1 Introduction

It has long been known that the conditions of solvothermal synthesis for open framework materials are crucial to the final product.[1] The first part of this chapter describes a systematic study of the synthesis of several different gallophosphate phases with pyridine as template. The pyridine-GaPO system proves to be ideal for this type of study being of simple initial composition and frequently giving products of suitable crystallinity for single crystal XRD study. The structures of four pyridine-GaPO phases have been determined by laboratory and synchrotron XRD techniques. The second part of the chapter concerns other phases templated by small molecules and their relationships to the pyridine-GaPO structures. Most of these are known structures formed as accidental products during the pyridine study due to the use of trimethylamine as a pH modifier while one is a new layered material, the structure of which was solved from microcrystal XRD on an extremely small crystal.

5.2 A Study of the Synthesis of Pyridine-GaPOs

5.2.1 Synthesis

The method of the study was to vary certain factors in the synthesis and analyse the products obtained. The variables used were:

- pH
- Temperature
- Pyridine to water ratio in solvent
- Gallium to phosphorus ratio
- Heating time

The preparations were generally carried out in sets of four with one of the variables being altered and the rest set for all four autoclaves. In a typical preparation phosphoric acid (0.2g, 85% weight solution, Aldrich) was diluted with distilled water (2ml) and pyridine (8ml, 98%, Fisher). To this solution gallium sulfate (0.5g, 99.8%, Aldrich) was added, followed by hydrofluoric acid (0.2ml, 70% solution in pyridine, Aldrich) with stirring. After the addition of a pH modifier (TMA or hydrochloric acid) the mixture was stirred for approximately 20 minutes to allow homogenisation and transferred to a Teflon lined stainless steel autoclave. The pH of the mixtures was measured using either a pH electrode or short range indicator paper. Autoclaves were heated at between 140° and 190°C in a force draft oven and the products recovered by suction filtration. The products were identified by powder XRD. A full list of the reactions carried out and their major products is given in tables 5.1 (acidic pH modifier) and 5.2 (basic pH modifier).

Table 5.1 *Products of pyridine-GaPO preparations with HCL as pH modifier*

Ga: P: HCl: pyridine: water: HF	pH	T/C	Time/days	Product phase
2: 2: 1300: 10: 10: 1	4	150	5	gallium sulfate
2: 2: 1300: 10: 10: 1	4	180	4	PFG1
2: 2: 1950: 12.5: 0: 1	4	160	3	PFG2
2: 2: 1700: 10: 10:1	4	150	3	Unknown
2: 2: 870: 12.5: 0: 1	4	160	3	PFG2
2: 2: 870: 10: 10:0	4	180	3	gallium sulfate
2: 2: 870: 12.5: 0: 0	4	180	4	PG4
2: 2: 870: 10: 10:0	4	150	3	PG4
2: 2: 1700: 10: 10:0	4	150	3	PG4
2: 2: 750: 8: 20: 1	5	150	3	PFG1
2: 2: 1700: 10: 10: 1	4	150	3	PFG1

Table 5.2 *Products of pyridine-GaPO preparations with TMA as pH modifier*

Ga: P: TMA: pyridine: water: HF	pH	T/C	Time/days	Product phase
2: 2: 0: 10: 10: 1	5.8	150	3	PFG1
2: 2: 0: 10: 10: 1	5.8	150	4	PFG3
2: 2: 0: 10: 10: 1	5.8	150	5	PFG2
2: 2: 0: 10: 10: 1	5.8	150	6	PFG1/3
2: 2: 0: 10: 10: 1	5.8	150	14	PFG1
2: 2: 0: 10: 10: 1	5.8	180	3	PFG3
2: 2: 0: 10: 10: 1	5.8	180	4	PFG1
2: 2: 0: 10: 10: 1	5.8	170	3	PFG2
2: 2: 0: 10: 10: 0	5.8	150	3	PG4
2: 2: 0: 12.5: 0: 1	6	160	3	PFG3, 1
2: 2: 0: 12.5: 0: 1	6	180	4	PFG2
2: 2: 0: 0: 50: 1	1.5	180	3 or 4	Berlinite
2: 2: 1: 10: 10: 1	8.4	150	5	PFG1
2: 2: 1: 10: 10: 0	8.4	150	3	Unknown
2: 4: 0: 10: 10: 1	5.8	150	3	PFG2
2: 8: 0: 10: 10: 1	5.8	150	3	PFG2
2: 4: 0: 10: 10: 1	5.8	170	3	PFG2
2: 2: 0: 6: 25: 1	5	150	3	PFG1
2: 2: 0: 4: 40: 1	5	180	4	Berlinite
2: 2: 0: 6: 25: 1	5	180	4	PFG2
2: 2: 0: 8: 20: 1	6	180	4	PFG2
2: 2: 0: 4: 40: 1	5	150	3	PFG1
2: 2: 0: 8: 20: 1	6	150	3	PG4
2: 2: 1.5: 12.5: 0: 1	6	150/180	3 or 4	GaPO-A21
2: 2: 1.5: 10: 10: 0	9.4	150	3	Unknown
2: 2: 0: 4: 40: 1	6	150	3	PFG1
2: 2: 2.5: 4: 40: 1	8.4	150	3	PFG1
2: 2: 2.5: 10:10 1	9.7	170	3	GaPO-A21
2: 2: 2.5: 12.5: 0: 1	8.7	170	3	PFG2
2: 2: 0: 12.5: 0: 1	6	150	14	amorphous
2: 2: 0.5: 10: 10: 1	9.1	150	5	PFG2
2: 2: 1: 10: 10: 1	9.4	150/180	5 or 4	PFG2
2: 2: 1: 12.5: 0: 1	8.3	160	3	PFG2
2: 2: 1.5: 12.5: 0: 1	8.7	160	3	PFG2
2: 2: 0.5: 10: 10: 1	8.4	150	3	GaPO-NH_3
2: 2: 1: 10: 10: 1	9.1	150	3	PFG1
2: 2: 2: 12.5: 0: 1	8.3	160	3	PFG2
2: 2: 2.5: 12.5: 0: 1	8.7	160	3	PFG2
2: 2: 2: 10: 10: 1	9.4	180	3	PFG2
2: 2: 2.5: 10: 10: 1	9.7	180	3	PFG2
2: 2: 2: 12.5: 0: 1	8.3	180	3	GaPO-A21
2: 2: 2.5: 12.5: 0: 1	8.7	180	3	PFG2

5.2.2 Pyridine-GaPO structures

Four gallophosphate structures have been determined in which pyridine acts as a structure directing agent (SDA). Of these one has previously been reported[2] and one

is analogous to the UT-6 AlPO structure.[3] In order to give full consideration to the structures crystallographic data for all four are included here.

5.2.2.1 Pyridine,F-GaPO-1

The structure of this material was solved from microcrystal diffraction data collected on station 9.8 of the SRS. Details of the data collection and structure solution are given in table 5.3.

Table 5.3 *structure solution and refinement data for [pyr,F]-GaPO-1*

Identification code	[pyr,F]-GaPO-1
Empirical formula	$(GaPO_4)_3F.C_5NH_6.0.5H_2O$
Formula weight	601.18
Temperature	150(2) K
Wavelength	0.68490 Å
Crystal system, space group	Triclinic, $P\bar{1}$
Unit cell dimensions	a = 11.391(4) Å alpha = 71.04(3)° b = 12.414(3) Å beta = 68.39(2)° c = 12.846(4) Å gamma = 66.88(2)°
Volume	1518.3(8) $Å^3$
Z, Calculated density	2, 2.630 Mg/m^3
Absorption coefficient	5.682 mm^{-1}
F(000)	1160
Crystal size	0.02 x 0.02 x 0.008 mm
Theta range for data collection	1.95° to 29.25°
Limiting indices	$-15 \leq h \leq 15, -17 \leq k \leq 17, -17 \leq l \leq 18$
Reflections collected / unique	14097 / 7704 [R(int) = 0.0290]
Completeness to theta	29.25, 83.3 %
Max. and min. transmission	0.6592 and 0.3961
Refinement method	Full-matrix least-squares on F^2
Data / restraints / parameters	7704 / 0 / 469
Goodness-of-fit on F^2	1.207
Final R indices [I>2sigma(I)]	R1 = 0.0454, wR^2 = 0.1272
R indices (all data)	R1 = 0.0481, wR^2 = 0.1288
Largest diff. peak and hole	1.766 and -1.364 $e.Å^{-3}$

The asymmetric unit of the structure contains six Ga atoms four tetrahedrally coordinated to four oxygen atoms and two octahedrally coordinated to four oxygen

and two fluorine atoms. Six phosphorous atoms are all tetrahedrally coordinated. The unit is shown in figure 5.1.

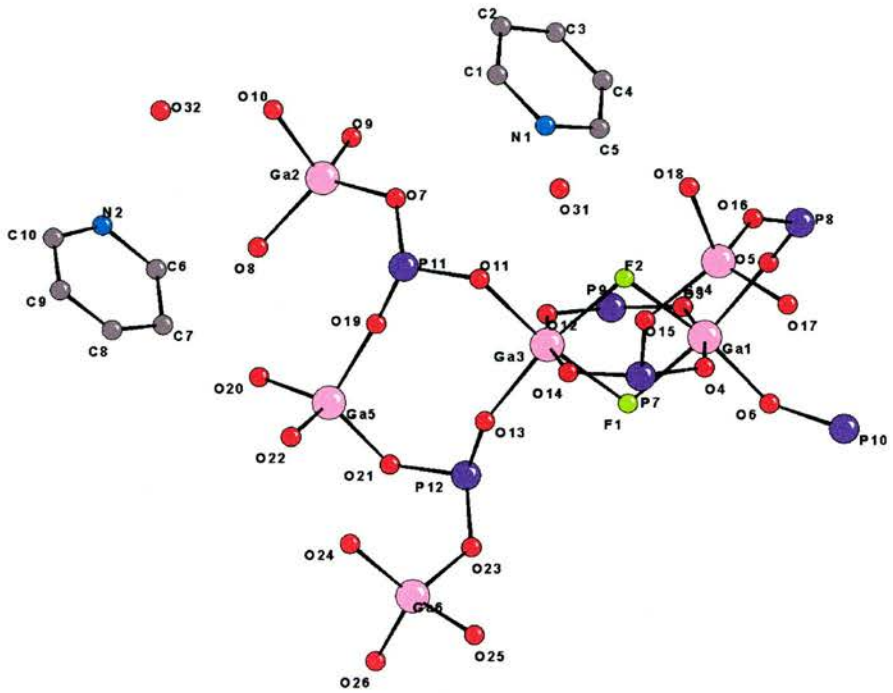

Figure 5.1 *The asymmetric unit of [pyr,F]-GaPO-1*

The main unit from which the [pyr,F]-GaPO-1 structure is composed is a double six ring (D6R) unit (fig. 5.2) with two opposite corners of the unit being occupied by octahedral gallium atoms.

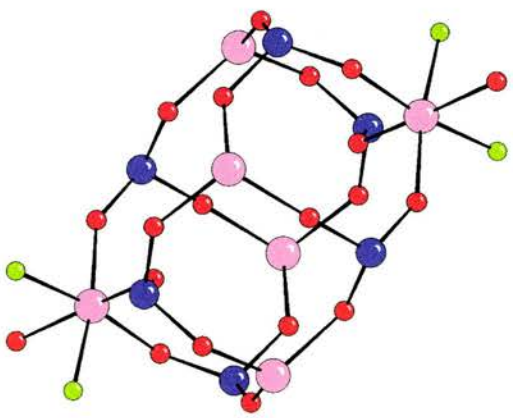

Figure 5.2 *The D6R unit of [pyr,F]-GaPO-1. Colour scheme as for fig. 5.1*

The fluorine atoms of the octahedral gallium units form a link between the D6Rs and they are also linked by single four rings, giving an extended structure of eight ring channels in the (101) direction (fig. 5.3).

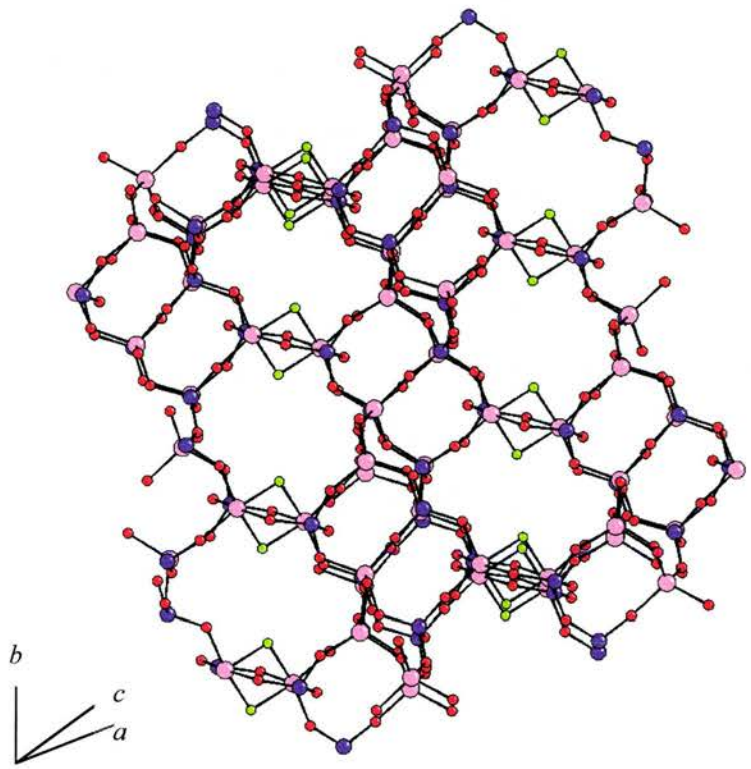

Figure 5.3 *The framework structure of [pyr,F]-GaPO-1 viewed in the (101) direction. Note that there are two slightly different shapes of eight-ring window. The non-framework atoms are omitted for clarity*

When viewed in the $(11\bar{1})$ direction the structure presents a second set of eight ring windows. These channels are occupied by the pyridine template molecules (figure 5.4). In addition to the pyridine, the voids in the structure are occupied by water molecules which are disordered through the structure (50% crystallographic site occupancy). The template-framework distances suggest that hydrogen bonding may

exist between the pyridine N-H groups and the framework oxygen atoms (N(1)-O(3) = 2.837Å, N(2)-O(14) = 2.875Å), however, some of the C-O distances are similarly short, therefore we cannot imply too much from these values.

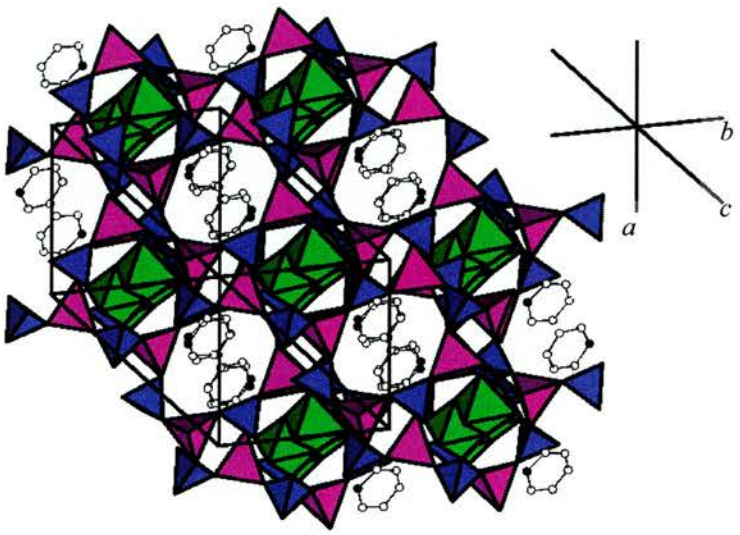

Figure 5.4 *The second pore system of [pyr,F]-GaPO-1 perpendicular to the zeolite like layers. Projection in the* $(11\bar{1})$ *direction.* GaO_4 *tetrahedra purple,* PO_4 *blue,* GaO_4F_2 *octahedra green; carbon white spheres, nitrogen black*

The distance between the two pyridine rings and their associated water molecules are 2.818Å and 2.894Å respectively. The ^{31}P NMR spectrum of [pyr,F]-GaPO-1 consists of three sharp resonances at δ = –1.2, -13.7 and –20.5ppm in the ratio 1: 1: 1 suggesting that the six crystallographic sites are separated into three pairs of indistinguishable NMR environments (fig. 5.5). On closer inspection of the asymmetric unit a non-crystallographic plane of symmetry is observed which supports this hypothesis. The ^{19}F spectrum (fig. 5.6) contains a single resonance at δ = –101.9ppm, again meaning that the two crystallographic sites are equivalent to NMR.

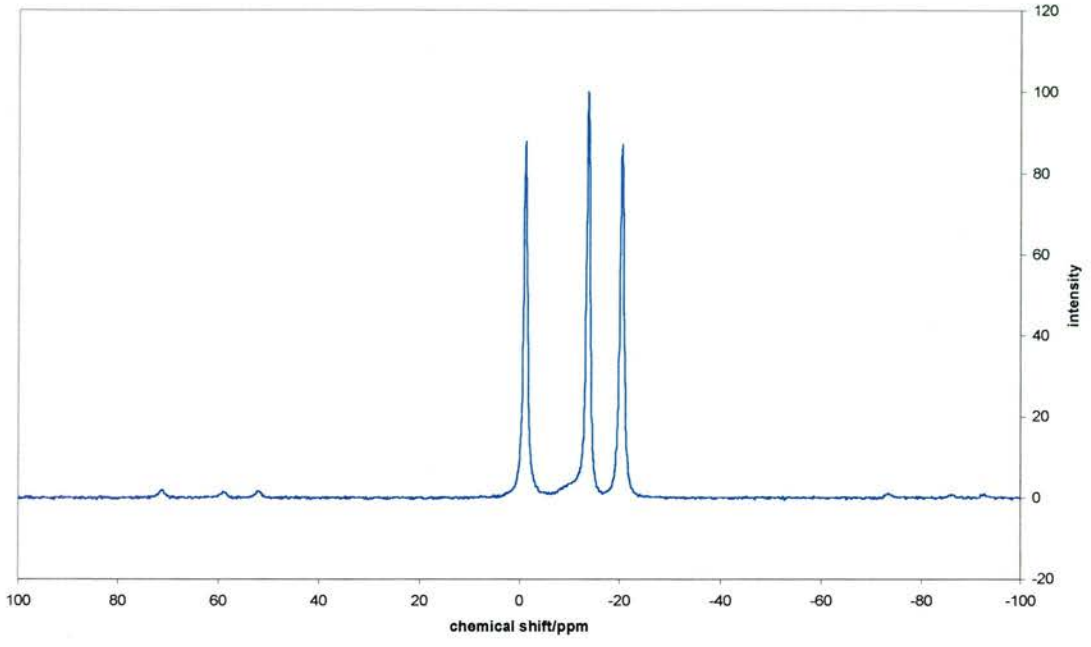

Figure 5.5 *^{31}P MASNMR spectrum of [pyr,F]-GaPO-1*

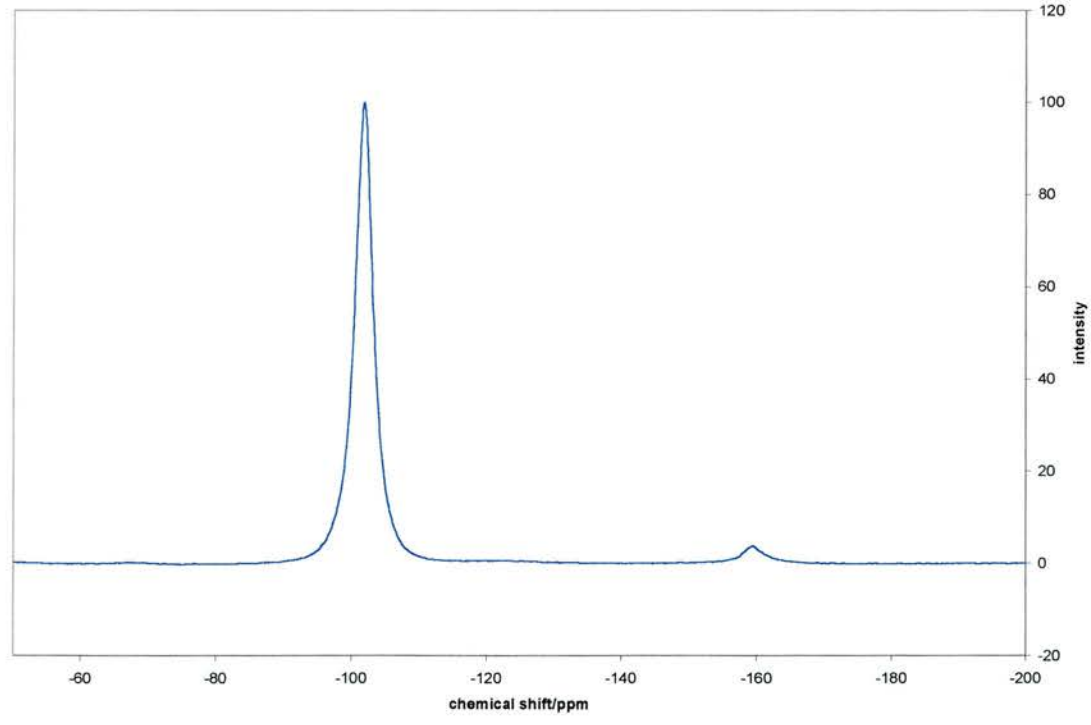

Figure 5.6 *^{19}F MASNMR spectrum of [pyr,F]-GaPO-1*

Thermal analysis of a sample of [pyr,F]-GaPO-1 demonstrates the strong binding of the water molecule. A mass loss corresponding to the loss of water is observed at around 250°C (observed 1.2%; calculated 1.5%). A second mass loss corresponding to loss of pyridine occurs between 330°C and 360°C (observed 12.94%; calculated 13.3%). Powder XRD after TGA showed that the structure had completely broken down on removal of the template. Atomic coordinates, bond lengths and angles and thermal displacement parameters are given in tables 5.4 to 5.6.

Table 5.4 *Atomic coordinates (x 10^4) and equivalent isotropic displacement parameters ($Å^2$ x 10^3) for pyr-GaPO-1. U(eq) is defined as one third of the trace of the orthogonalized U_{ij} tensor*

	x	y	z	U(eq)
Ga(1)	3957(1)	7079(1)	2463(1)	6(1)
Ga(2)	-1986(1)	12787(1)	636(1)	6(1)
Ga(3)	1063(1)	8259(1)	2566(1)	5(1)
Ga(4)	3161(1)	7775(1)	5805(1)	6(1)
Ga(5)	-2680(1)	9292(1)	1661(1)	5(1)
Ga(6)	-2152(1)	5545(1)	3352(1)	6(1)
P(7)	1875(1)	6804(1)	4827(1)	6(1)
P(8)	5542(1)	7894(1)	3500(1)	5(1)
P(9)	3135(1)	8510(1)	204(1)	6(1)
P(10)	6369(1)	4570(1)	2300(1)	5(1)
P(11)	-1347(1)	10614(1)	2483(1)	5(1)
P(12)	-352(1)	7065(1)	1702(1)	6(1)
F(1)	2490(2)	6744(2)	2311(2)	9(1)
F(2)	2527(2)	8597(2)	2736(2)	9(1)
O(3)	4201(3)	7868(3)	850(2)	9(1)
O(4)	3308(3)	6477(3)	4093(2)	10(1)
O(5)	5225(3)	7652(3)	2569(2)	10(1)
O(6)	5117(3)	5585(3)	2143(3)	12(1)
O(7)	-1071(3)	11779(3)	1683(2)	10(1)
O(8)	-3263(3)	12300(3)	561(2)	9(1)
O(9)	-885(3)	13277(3)	-721(2)	11(1)
O(10)	-2926(3)	14163(3)	1156(3)	16(1)
O(11)	-142(3)	9770(2)	2888(2)	8(1)
O(12)	1705(3)	8871(3)	945(2)	9(1)
O(13)	-182(3)	7639(3)	2488(2)	9(1)
O(14)	808(3)	7519(3)	4193(2)	9(1)
O(15)	1757(3)	7524(3)	5668(2)	11(1)
O(16)	4338(3)	8254(3)	4503(2)	11(1)
O(17)	3995(3)	6469(3)	6740(3)	13(1)
O(18)	2531(3)	9060(3)	6479(3)	13(1)
O(19)	-1712(3)	10056(3)	1803(3)	12(1)
O(20)	-3510(3)	10356(2)	598(2)	9(1)
O(21)	-1535(3)	7907(2)	1210(3)	10(1)
O(22)	-3915(3)	8967(3)	3001(3)	14(1)

Table 5.4 continued

	x	*y*	*z*	U(eq)
O(23)	-641(3)	5879(2)	2384(2)	10(1)
O(24)	-3403(3)	6787(3)	3965(3)	13(1)
O(25)	-1505(3)	4346(3)	4455(2)	11(1)
O(26)	-2655(3)	4960(3)	2530(3)	17(1)
C(1)	889(6)	12741(8)	2046(6)	44(2)
N(1)	1584(9)	11569(8)	2239(7)	72(3)
C(5)	2829(10)	11156(6)	1468(9)	55(2)
C(2)	1393(6)	13521(5)	1097(6)	37(1)
C(4)	3298(6)	11928(7)	596(5)	41(2)
C(3)	2617(7)	13048(7)	388(5)	48(2)
C(7)	-6294(7)	11620(6)	3807(7)	41(2)
C(9)	-8338(7)	12911(10)	4537(6)	59(3)
C(6)	-5991(7)	12585(11)	2932(6)	59(3)
C(8)	-7507(8)	11885(9)	4599(6)	55(2)
N(2)	-6873(12)	13684(9)	2926(9)	95(4)
C(10)	-8098(10)	13814(9)	3807(11)	72(3)
O(31)	894(10)	10300(7)	4524(7)	34(2)
O(32)	-4336(13)	15253(11)	-594(10)	59(3)

Table 5.5 *Selected Bond lengths (Å) and angles (°) for [pyr,F]-GaPO-1*

Ga(1)-O(6)	1.878(3)	O(3)-Ga(1)-F(1)	85.23(11)
Ga(1)-O(5)	1.904(3)	O(6)-Ga(1)-F(2)	170.89(12)
Ga(1)-O(4)	1.942(3)	O(5)-Ga(1)-F(2)	91.27(12)
Ga(1)-O(3)	1.949(3)	O(4)-Ga(1)-F(2)	85.45(11)
Ga(1)-F(1)	1.960(2)	O(3)-Ga(1)-F(2)	84.56(11)
Ga(1)-F(2)	1.982(2)	F(1)-Ga(1)-F(2)	80.61(10)
Ga(2)-O(9)	1.811(3)	O(9)-Ga(2)-O(10)	102.75(14)
Ga(2)-O(10)	1.813(3)	O(9)-Ga(2)-O(8)	116.19(14)
Ga(2)-O(8)	1.823(3)	O(10)-Ga(2)-O(8)	103.38(15)
Ga(2)-O(7)	1.838(3)	O(9)-Ga(2)-O(7)	111.90(14)
P(7)-O(4)	1.521(3)	O(10)-Ga(2)-O(7)	106.17(14)
P(7)-O(14)	1.529(3)	O(8)-Ga(2)-O(7)	114.73(13)
P(7)-O(25)#1	1.548(3)	O(4)-P(7)-O(14)	116.73(16)
P(7)-O(15)	1.553(3)	O(4)-P(7)-O(25)#1	110.10(17)
C(1)-N(1)	1.346(12)	O(14)-P(7)-O(25)#1	105.04(17)
C(1)-C(2)	1.380(10)	O(4)-P(7)-O(15)	107.87(17)
N(1)-C(5)	1.407(13)	O(14)-P(7)-O(15)	108.81(17)
C(5)-C(4)	1.312(12)	O(25)#1-P(7)-O(15)	107.99(17)
C(2)-C(3)	1.374(9)	Ga(1)-F(1)-Ga(3)	99.69(11)
C(4)-C(3)	1.293(10)	P(7)-O(4)-Ga(1)	126.81(17)
		P(8)-O(5)-Ga(1)	137.20(18)
O(6)-Ga(1)-O(5)	97.69(14)	P(10)-O(6)-Ga(1)	146.6(2)
O(6)-Ga(1)-O(4)	95.17(13)	P(11)-O(7)-Ga(2)	124.63(18)
O(5)-Ga(1)-O(4)	96.48(13)	P(10)#8-O(26)-Ga(6)	153.7(2)
O(6)-Ga(1)-O(3)	93.53(13)	N(1)-C(1)-C(2)	120.1(6)
O(5)-Ga(1)-O(3)	91.20(12)	C(1)-N(1)-C(5)	119.1(6)
O(4)-Ga(1)-O(3)	167.52(12)	C(4)-C(5)-N(1)	119.2(6)
O(6)-Ga(1)-F(1)	90.36(12)	C(3)-C(2)-C(1)	117.2(6)
O(5)-Ga(1)-F(1)	171.39(11)	C(3)-C(4)-C(5)	121.9(7)
O(4)-Ga(1)-F(1)	85.79(11)	C(4)-C(3)-C(2)	122.4(6)

Table 5.6 *Anisotropic displacement parameters ($Å^2$ x 10^3) for [pyr,F]-GaPO-1. The anisotropic displacement factor exponent takes the form:*
$-2\pi^2 [h^2 a^{*2} U_{11} + ... + 2 h k a^* b^* U_{12}]$

	U_{11}	U_{22}	U_{33}	U_{23}	U_{13}	U_{12}
Ga(1)	4(1)	7(1)	3(1)	-1(1)	-1(1)	1(1)
Ga(2)	7(1)	5(1)	3(1)	-1(1)	0(1)	-1(1)
Ga(3)	4(1)	6(1)	3(1)	-1(1)	-1(1)	1(1)
Ga(4)	6(1)	5(1)	4(1)	-1(1)	1(1)	-1(1)
Ga(5)	6(1)	5(1)	3(1)	-1(1)	-1(1)	-1(1)
Ga(6)	7(1)	5(1)	5(1)	0(1)	-2(1)	-2(1)
P(7)	5(1)	7(1)	3(1)	1(1)	-1(1)	-1(1)
P(8)	6(1)	5(1)	4(1)	-1(1)	1(1)	-1(1)
P(9)	5(1)	8(1)	3(1)	0(1)	-1(1)	-1(1)
P(10)	6(1)	4(1)	5(1)	-2(1)	-2(1)	1(1)
P(11)	6(1)	4(1)	6(1)	-2(1)	-2(1)	0(1)
P(12)	6(1)	5(1)	4(1)	-2(1)	1(1)	-1(1)
F(1)	8(1)	9(1)	8(1)	-3(1)	-2(1)	0(1)
F(2)	6(1)	10(1)	7(1)	-3(1)	-2(1)	0(1)
O(3)	7(1)	11(1)	4(1)	0(1)	-1(1)	-1(1)
O(4)	5(1)	14(1)	4(1)	0(1)	-1(1)	1(1)
O(5)	7(1)	16(1)	7(1)	-4(1)	-1(1)	-4(1)
O(6)	10(1)	10(1)	10(1)	-2(1)	-3(1)	2(1)
O(7)	12(1)	9(1)	10(1)	2(1)	-5(1)	-5(1)
O(8)	8(1)	10(1)	8(1)	-4(1)	0(1)	-3(1)
O(9)	10(1)	10(1)	7(1)	-2(1)	4(1)	-3(1)
O(10)	22(2)	10(1)	9(1)	-7(1)	0(1)	2(1)
O(11)	9(1)	7(1)	9(1)	-2(1)	-5(1)	2(1)
O(12)	6(1)	12(1)	3(1)	2(1)	-1(1)	0(1)
O(13)	9(1)	11(1)	8(1)	-4(1)	-1(1)	-2(1)
O(14)	5(1)	14(1)	4(1)	1(1)	-2(1)	0(1)
O(15)	7(1)	16(1)	9(1)	-8(1)	-1(1)	-1(1)
O(16)	12(1)	10(1)	6(1)	-3(1)	4(1)	-4(1)
O(17)	12(1)	12(1)	10(1)	4(1)	-3(1)	-4(1)
O(18)	10(1)	11(1)	14(1)	-9(1)	4(1)	-1(1)
O(19)	16(1)	9(1)	12(1)	-2(1)	-6(1)	-5(1)
O(20)	11(1)	8(1)	8(1)	2(1)	-5(1)	-4(1)
O(21)	9(1)	8(1)	12(1)	-6(1)	-6(1)	3(1)
O(22)	18(1)	12(1)	7(1)	-4(1)	7(1)	-9(1)
O(23)	8(1)	6(1)	11(1)	-3(1)	4(1)	-2(1)
O(24)	11(1)	13(1)	9(1)	-4(1)	-4(1)	5(1)
O(25)	11(1)	9(1)	9(1)	5(1)	-4(1)	-4(1)
O(26)	18(2)	15(1)	24(2)	-6(1)	-13(1)	-3(1)
C(1)	23(3)	80(5)	33(3)	-25(3)	7(2)	-23(3)
N(1)	106(7)	87(6)	58(4)	44(4)	-51(5)	-85(6)
C(5)	77(6)	20(3)	92(7)	-9(3)	-64(5)	-4(3)
C(2)	35(3)	17(2)	46(4)	-8(2)	-9(3)	2(2)
C(4)	28(3)	55(4)	25(3)	-25(3)	-8(2)	18(3)
C(3)	45(4)	50(4)	20(3)	13(3)	3(3)	-15(3)
C(7)	33(3)	35(3)	64(5)	-29(3)	-25(3)	5(3)
C(9)	23(3)	105(7)	26(3)	-28(4)	-9(2)	16(4)
C(6)	25(3)	130(9)	30(3)	-25(4)	9(3)	-40(4)
C(8)	42(4)	93(7)	27(3)	22(4)	-17(3)	-38(4)
N(2)	145(9)	86(6)	107(7)	66(6)	-102(7)	-97(7)
C(10)	66(6)	55(5)	116(9)	-54(6)	-65(6)	25(5)
O(31)	50(5)	24(4)	22(4)	-6(3)	-10(4)	-6(4)
O(32)	66(8)	66(8)	44(6)	12(5)	-30(5)	-23(6)

5.2.2.2 Pyridine, F-GaPO-2

This material is isostructural with the AlPO UT-6,[3] its structure is also very similar to that of [pyr,F]-GaPO-1. The structure was determined from laboratory single crystal XRD data. Full details of the data collection and structure solution are given in table 5.6.

Table 5.6 *Structure solution and refinement data for [pyr,F]-GaPO-2*

Identification code	[pyr,F]-GaPO-2
Empirical formula	$C_5 H_6 F Ga_3 N O_{12.50} P_3$
Formula weight	601.18
Temperature	293(2) K
Wavelength	0.71073 Å
Crystal system, space group	Triclinic, $P\bar{1}$
Unit cell dimensions	a = 9.265(5) Å alpha = 94.36(6)° b = 9.397(8) Å beta = 90.64(5)° c = 9.238(5) Å gamma = 103.67(5)°
Volume	778.9(9) $Å^3$
Z, Calculated density	2, 2.563 Mg/m^3
Absorption coefficient	5.538 mm^{-1}
F(000)	580
Crystal size	0.05 x 0.05 x 0.05 mm
Theta range for data collection	2.78° to 25.02°
Limiting indices	$0 \le h \le 10, -11 \le k \le 10, -10 \le l \le 10$
Reflections collected / unique	2730 / 2730 [R(int) = 0.0000]
Completeness to theta	25.02 99.5 %
Max. and min. transmission	0.7692 and 0.7692
Refinement method	Full-matrix least-squares on F^2
Data / restraints / parameters	2730 / 0 / 235
Goodness-of-fit on F^2	1.020
Final R indices [I>2sigma(I)]	R1 = 0.0276, wR^2 = 0.0788
R indices (all data)	R1 = 0.0313, wR^2 = 0.0809
Largest diff. Peak and hole	0.548 and –0.756 $e.A^{-3}$

The asymmetric unit of [pyr,F]-GaPO-2 (fig. 5.7) consists of three gallium and three phosphorus atoms with all but one being tetrahedrally coordinated. One corner gallium is octahedrally coordinated to four oxygen and two fluorine atoms.

Two of these asymmetric units are linked to form the same SBU observed in [pyr,F]-GaPO-1 and the units are linked in the same way through the double octahedral gallium unit.

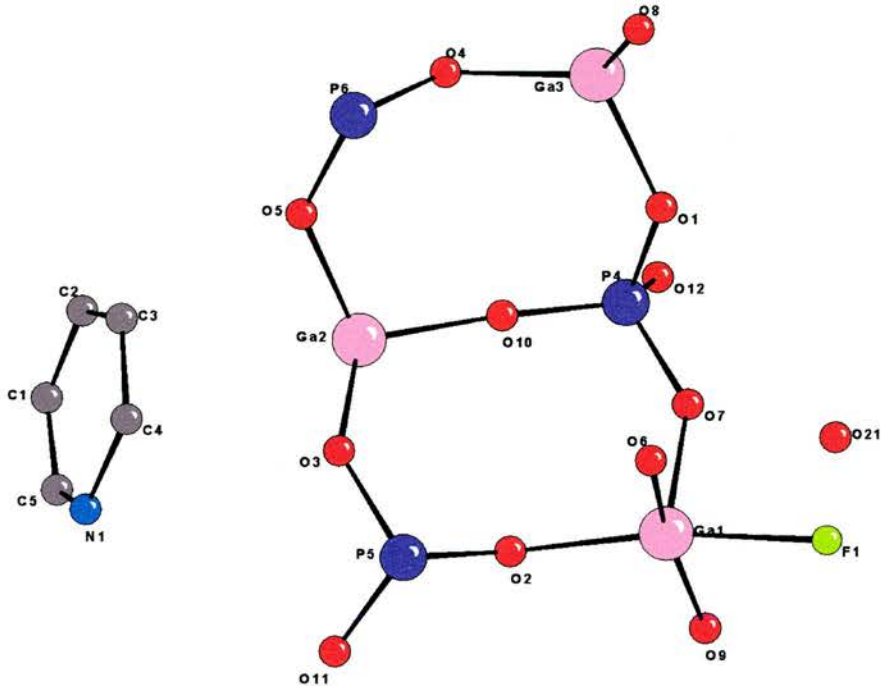

Figure 5.7 *The asymmetric unit of [pyr,F]-GaPO-2*

When viewed in the (011) direction the structure is very similar to that of [pyr,F]-GaPO-1, indeed the two are topologically identical, however, a close inspection reveals that the structure of [pyr,F]-GaPO-2 contains only one type of eight ring window (fig 5.8) while [pyr,F]-GaPO-1 contains two, one of a nearly circular shape and the other more oval(fig 5.3, above). The reason for this slight twisting of the structure of [pyr,F]-GaPO-1 (which leads to the larger unit cell and doubled asymmetric unit observed) is unclear and will be further discussed below. The shortest template-framework distance is 2.877Å between N(1) and O(9), very similar to the distances observed for [pyr,F]-GaPO-1, emphasising the structural similarities.

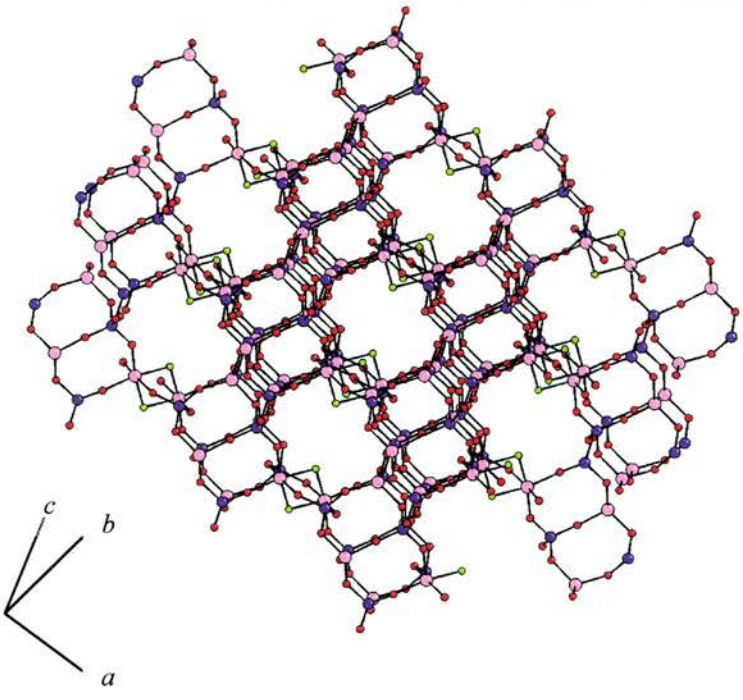

Figure 5.8 *Projection of the [pyr,F]-GaPO-2 structure in the (011) direction, showing that there is only one type of eight ring window shape. Colour scheme as for fig. 5.7*

The pyridine to water distance however is notably longer (3.006Å) indicating the possibility of a slightly different template grouping. Again, disordered water molecules are present in the void spaces. 31P MASNMR reinforces the similarity of this structure to [pyr,F]-GaPO-1, with three phosphorus environments (δ as for [pyr,F]-GaPO-1), the 19F spectrum is also identical to that of [pyr,F]-GaPO-1.

Thermal analysis of the material gave the approximately the same result as for pyridine-GaPO-1, unsurprisingly as the materials have the same empirical formula. Crystallographic data for the structure are given in tables 5.7 to 5.9.

Table 5.7 *Atomic coordinates (x 10^4) and equivalent isotropic displacement parameters ($Å^2$ x 10^3) for [Pyr,F]-GaPO-2. U(eq) is defined as one third of the trace of the orthogonalized U_{ij} tensor*

	x	y	z	U(eq)
Ga(1)	1391(1)	860(1)	4356(1)	12(1)
Ga(2)	6089(1)	3414(1)	3923(1)	12(1)
Ga(3)	6250(1)	-786(1)	1572(1)	13(1)
P(4)	3772(1)	902(1)	1853(1)	12(1)
P(5)	3796(1)	3295(1)	6266(1)	12(1)
P(6)	8322(1)	1499(1)	3566(1)	13(1)
F(1)	-201(2)	-906(2)	3875(2)	16(1)
O(1)	4394(3)	-469(3)	1776(4)	30(1)
O(2)	2712(3)	2667(3)	5023(3)	18(1)
O(3)	5396(3)	3462(3)	5747(3)	23(1)
O(4)	7686(3)	884(3)	2025(3)	20(1)
O(5)	7891(3)	2975(3)	3915(3)	19(1)
O(6)	2367(3)	-403(3)	5361(3)	18(1)
O(7)	2276(3)	597(3)	2551(3)	19(1)
O(8)	6427(3)	-2405(3)	2413(3)	19(1)
O(9)	16(3)	1882(3)	3533(3)	16(1)
O(10)	4877(3)	2185(4)	2622(4)	35(1)
O(11)	3589(4)	4812(3)	6819(3)	24(1)
O(12)	3543(4)	1329(4)	320(3)	32(1)
C(1)	8795(9)	5342(14)	7574(11)	89(3)
C(2)	9200(11)	4161(17)	7428(10)	106(4)
C(3)	8862(11)	3151(9)	8369(16)	97(3)
N(1)	7559(9)	4692(12)	9607(9)	118(3)
C(5)	8011(11)	5605(10)	8485(14)	98(3)
C(4)	8060(13)	3366(10)	9475(11)	100(4)
O(21)	-181(12)	-896(12)	258(11)	79(3)

Table 5.8 *Selected bond lengths (Å) and angles (°) for [pyr,F]-GaPO-2*

Ga(1)-O(7)	1.892(3)	O(7)-Ga(1)-O(2)	97.29(13)
Ga(1)-O(2)	1.898(3)	O(7)-Ga(1)-O(6)	95.55(13)
Ga(1)-O(6)	1.935(3)	O(2)-Ga(1)-O(6)	96.88(13)
Ga(1)-O(9)	1.947(3)	O(7)-Ga(1)-O(9)	92.84(12)
Ga(1)-F(1)	1.960(3)	O(2)-Ga(1)-O(9)	91.40(13)
Ga(1)-F(1)#1	1.985(2)	O(6)-Ga(1)-O(9)	167.36(11)
Ga(1)-Ga(1)#1	3.010(2)	O(7)-Ga(1)-F(1)	90.99(12)
Ga(2)-O(10)	1.785(3)	O(2)-Ga(1)-F(1)	170.88(10)
Ga(2)-O(5)	1.811(3)	O(6)-Ga(1)-F(1)	86.06(12)
Ga(2)-O(3)	1.811(3)	O(9)-Ga(1)-F(1)	84.35(12)
Ga(2)-O(11)#2	1.811(3)	O(10)-Ga(2)-O(5)	109.13(14)
P(4)-O(7)	1.510(3)	O(10)-Ga(2)-O(3)	114.80(15)
P(4)-O(10)	1.509(3)	O(5)-Ga(2)-O(3)	110.74(13)
P(4)-O(12)	1.527(3)	O(10)-Ga(2)-O(11)#2	104.78(17)
P(4)-O(1)	1.528(3)	O(5)-Ga(2)-O(11)#2	104.47(14)
P(6)-O(4)	1.550(3)	O(3)-Ga(2)-O(11)#2	112.27(14)
C(1)-C(5)	1.168(13)	O(8)-Ga(3)-O(12)#3	101.19(15)
C(1)-C(2)	1.252(14)	O(7)-P(4)-O(10)	112.76(17)
C(2)-C(3)	1.321(15)	O(7)-P(4)-O(12)	107.36(18)
C(3)-C(4)	1.302(14)	O(10)-P(4)-O(12)	106.4(2)
N(1)-C(5)	1.400(13)	O(7)-P(4)-O(1)	110.32(17)
N(1)-C(4)	1.427(13)	O(10)-P(4)-O(1)	110.15(19)
		O(12)-P(4)-O(1)	109.70(19)

Table 5.8 continued		C(5)-C(1)-C(2)	123.4(9)
Ga(1)-F(1)-Ga(1)#1	99.46(11)	C(1)-C(2)-C(3)	122.2(9)
P(4)-O(1)-Ga(3)	133.99(19)	C(4)-C(3)-C(2)	119.5(9)
P(5)-O(2)-Ga(1)	139.28(18)	C(5)-N(1)-C(4)	113.7(8)
P(6)-O(4)-Ga(3)	126.44(18)	C(1)-C(5)-N(1)	122.9(9)
P(5)#4-O(8)-Ga(3)	148.60(18)	C(3)-C(4)-N(1)	117.9(8)

Table 5.9 *Anisotropic displacement parameters ($Å^2$ x 10^3) for Pyridine-GaPO-3. The anisotropic displacement factor exponent takes the form:*
$-2\pi^2 [h^2 a^{*2} U_{11} + ... + 2 h k a^* b^* U_{12}]$

	U_{11}	U_{22}	U_{33}	U_{23}	U_{13}	U_{12}
Ga(1)	9(1)	13(1)	14(1)	4(1)	4(1)	3(1)
Ga(2)	12(1)	11(1)	16(1)	1(1)	3(1)	5(1)
Ga(3)	14(1)	12(1)	13(1)	4(1)	3(1)	5(1)
P(4)	12(1)	14(1)	11(1)	0(1)	4(1)	4(1)
P(5)	14(1)	10(1)	12(1)	2(1)	4(1)	4(1)
P(6)	11(1)	13(1)	18(1)	4(1)	4(1)	5(1)
F(1)	15(1)	17(1)	15(1)	1(1)	5(1)	4(1)
O(1)	19(2)	20(2)	53(2)	8(1)	10(1)	10(1)
O(2)	15(1)	18(1)	18(1)	4(1)	-2(1)	-2(1)
O(3)	15(1)	39(2)	15(1)	4(1)	4(1)	8(1)
O(4)	17(1)	21(1)	20(1)	5(1)	-1(1)	0(1)
O(5)	13(1)	13(1)	33(2)	1(1)	3(1)	6(1)
O(6)	13(1)	20(1)	23(1)	11(1)	6(1)	6(1)
O(7)	13(1)	26(1)	19(1)	2(1)	7(1)	6(1)
O(8)	28(2)	16(1)	16(1)	6(1)	6(1)	7(1)
O(9)	9(1)	17(1)	24(1)	8(1)	3(1)	5(1)
O(10)	18(2)	39(2)	42(2)	-21(2)	0(1)	1(1)
O(11)	41(2)	13(1)	19(2)	1(1)	6(1)	11(1)
O(12)	48(2)	39(2)	13(1)	9(1)	9(1)	15(2)
C(1)	48(5)	141(9)	85(6)	77(7)	13(4)	14(5)
C(2)	64(6)	169(11)	61(5)	-41(7)	15(4)	-7(7)
C(3)	84(7)	45(4)	153(10)	-36(6)	-9(7)	14(4)
N(1)	97(6)	163(9)	78(5)	-24(6)	33(5)	8(6)
C(5)	77(6)	77(6)	155(10)	55(6)	5(7)	35(5)
C(4)	124(9)	58(5)	91(7)	45(5)	-30(6)	-40(5)
O(21)	63(6)	105(8)	72(7)	-3(6)	1(5)	32(6)

5.2.2.3 Pyridine, F-GaPO-3

This is the phase previously reported by Wiegel.[2] The structure was solved from single crystal XRD data collected in the laboratory, details of the structure solution and data collection are given in table 5.10 below.

The cage from which this structure is built is shown quite clearly in the asymmetric unit (fig. 5.9). It consists of four five coordinate gallium atoms and four tetrahedrally coordinated phosphorus atoms. The five coordinate gallium atoms are

linked in pairs by two bridging fluorine atoms and there are two terminal –OH groups, one attached to P(4) and the other to Ga(3).

Table 5.10 *Structure solution and refinement data for [pyr,F]-GaPO-3*

Identification code	[pyr,F]-GaPO-3
Empirical formula	$(GaPO_4)_3(OH)(GaPO_3OH)$ 2F.2(C_5NH_6)
Formula weight	874.95
Temperature	293(2) K
Wavelength	0.71073 Å
Crystal system, space group	Monoclinic, $P2_1/n$
Unit cell dimensions	a = 12.157(3) Å alpha = 90°
	b = 14.202(3) Å beta = 91.848(2)°
	c = 13.065(5) Å gamma = 90°
Volume	2254.6(11) $Å^3$
Z, Calculated density	3, 2.578 Mg/m^3
Absorption coefficient	5.120 mm^{-1}
F(000)	1704
Crystal size	0.02 x 0.02 x 0.02 mm
Theta range for data collection	2.67° to 25.01°
Limiting indices	$0 \leq h \leq 14$, $0 \leq k \leq 16$, $-15 \leq l \leq 15$
Reflections collected / unique	3964 / 3964 [R(int) = 0.0000]
Completeness to theta	25.01 99.5 %
Max. and min. transmission	0.9045 and 0.9045
Refinement method	Full-matrix least-squares on F^2
Data / restraints / parameters	3964 / 0 / 347
Goodness-of-fit on F^2	1.123
Final R indices [I>2sigma(I)]	R1 = 0.0485, wR^2 = 0.1437
R indices (all data)	R1 = 0.0776, wR^2 = 0.1593
Largest diff. peak and hole	1.350 and -1.218 $e.Å^{-3}$

^{19}F NMR data presented by Wiegel suggest that the bridging fluorine atoms and the terminal –OH groups are not distributed as shown, with one of the gallium bridging sites being occupied by OH and one of the terminal sites by fluorine. The XRD data from this sample seems to fit more effectively to a model in which the OH and F positions are as shown. However, OH and F are isoelectronic and therefore difficult to distinguish by XRD, the assignment in this case is due to a small amount

of residual electron density ~1.2Å from the terminal O/F of Ga(3). No additional electron density is observed around the bridging site, which is therefore assigned as F.

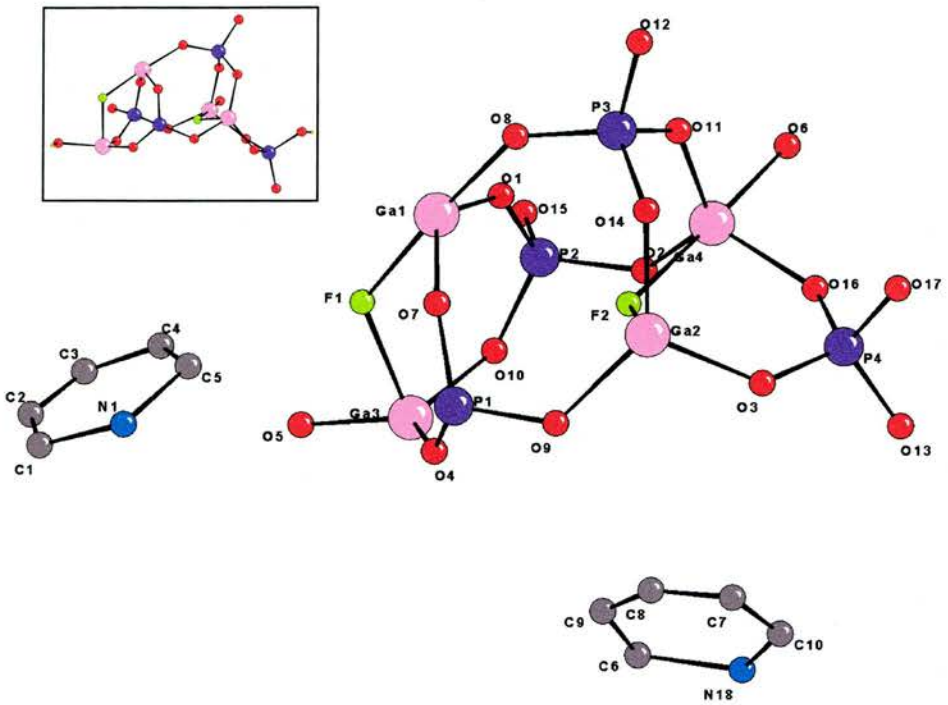

Figure 5.9 *The asymmetric unit of [pyr,F]-GaPO-3, an alternative view of the SBU cage is shown in the inset*

The structure of [pyr,F]-GaPO-3 is composed of these units linked by four rings. When viewed along the (100) axis two sets of 8-ring channels are visible (fig. 5.10), with the pyridine molecules inside the channels. Viewing the structure along the (010) axis another set of eight ring channels is visible (fig. 5.11). In these channels, four of the atoms forming the ring carry terminal -OH groups. The distance between the oxygen atoms (2.514Å) suggests that hydrogen bonding across the channels may stabilise the structure.

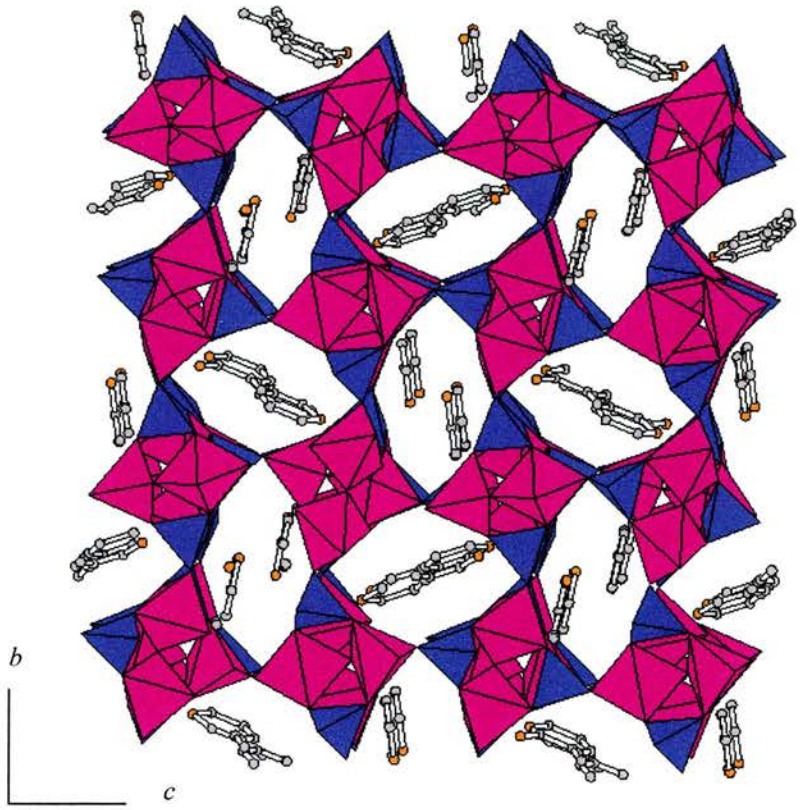

Figure 5.10 *The structure of [pyr,F]-GaPO-3 viewed along the (100) axis.The two sets of 8-ring channels are clearly visible. Blue polyhedra are PO_4 purple polyhedra GaO_4F*

The shortness of this O-O distance suggests that the channels may contain an unusual type of hydrogen bond similar to that observed in the material $[(C_{10}H_9N_2)^+]_2.[(C_{10}H_4O_8)^{2-}]$ by Wheatly *et.al.*[4] in which a single hydrogen is shared between the two oxygen atoms. Hydrogen could also be shared between –OH and F if the terminal atom of Ga(3) is fluorine. There is no interaction between the terminal groups and the pyridine molecules, which, as for the above structures, have some N to O distances which suggest possible hydrogen bonds (N(2)-O(9) = 2.942(12)Å, N(1)-O(15) = 2.939(13)Å). As for the other two structures the carbon to framework distances are in some cases only slightly longer than the N to framework distances, therefore the presence of hydrogen bonds is not confirmed.

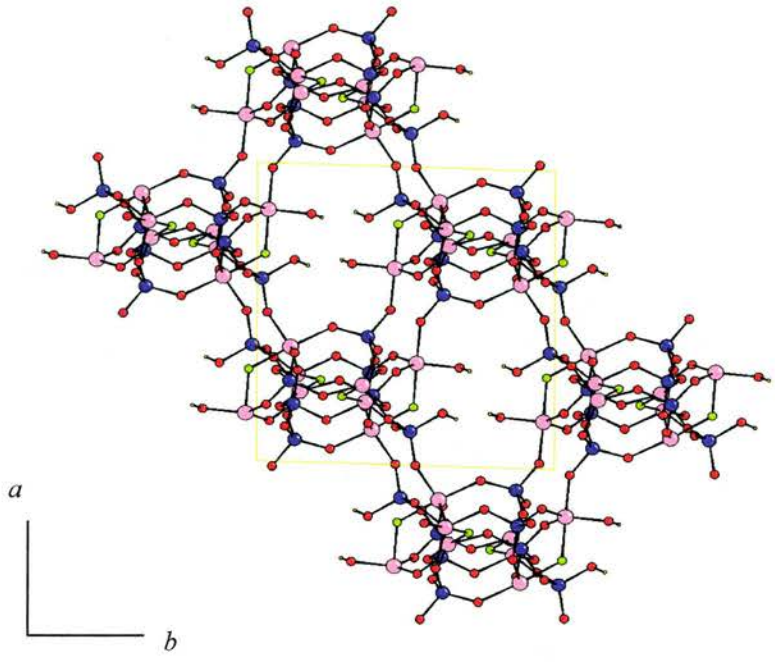

Figure 5.11 *The second pore system of [pyr,F]-GaPO-3 viewed along the (010) axis. The possible hydrogen bonds are between the oxygen atoms projecting into the pores. The template is omitted for clarity*

Thermal analysis shows a gradual mass loss between 200° and 400°C which is thought to correspond to the loss of pyridine from the structure (observed 14.8%, calculated 18.5%). A second mass loss at around 550°C may be due to the loss of the free OH groups (observed 2.2%, calculated 1.8%). Powder XRD after TGA showed that the structure had completely broken down on removal of the organic part. Atomic coordinates, bond lengths and angles and anisotropic thermal displacement parameters for this structure are given in tables 5.11 to 5.13.

Table 5.11 *Atomic coordinates (x 10^4) and equivalent isotropic displacement parameters ($Å^2$ x 10^3) for [Pyr,F]-GaPO-3. U(eq) is defined as one third of the trace of the orthogonalized U_{ij} tensor*

	x	y	z	U(eq)
Ga(1)	1126(1)	7735(1)	3853(1)	11(1)
Ga(2)	3550(1)	6210(1)	2632(1)	11(1)
Ga(3)	-374(1)	7341(1)	1581(1)	11(1)
Ga(4)	3647(1)	8652(1)	2067(1)	11(1)
P(1)	1098(2)	5791(1)	2715(2)	11(1)
P(2)	1219(2)	9073(1)	1936(2)	11(1)
P(3)	3728(2)	7801(1)	4259(2)	11(1)
P(4)	5161(2)	7090(1)	1116(2)	13(1)
F(1)	-269(4)	7632(3)	3060(3)	13(1)
F(2)	2863(4)	7407(3)	2230(3)	15(1)
O(1)	1369(4)	8811(3)	3083(4)	13(1)
O(2)	2338(4)	9020(4)	1426(4)	14(1)
O(3)	4441(5)	6307(4)	1513(4)	19(1)
O(4)	313(5)	6211(3)	1887(4)	16(1)
O(5)	-1816(5)	7609(4)	1689(4)	15(1)
O(6)	4350(4)	9845(3)	1939(4)	14(1)
O(7)	1255(4)	6445(4)	3644(4)	16(1)
O(8)	2537(5)	7808(4)	4544(4)	15(1)
O(9)	2223(4)	5633(4)	2235(4)	14(1)
O(10)	414(5)	8435(4)	1348(4)	16(1)
O(11)	3968(5)	8577(4)	3461(4)	17(1)
O(12)	4488(4)	8009(4)	5181(4)	15(1)
O(13)	5341(5)	6926(4)	-13(4)	17(1)
O(14)	4061(5)	6823(4)	3820(4)	16(1)
O(15)	773(5)	10080(4)	1840(4)	16(1)
O(16)	4685(5)	8066(4)	1270(5)	27(2)
O(17)	6254(5)	6981(5)	1765(5)	38(2)
C(9)	1551(14)	5417(12)	-242(14)	76(5)
C(5)	-1578(11)	5728(19)	4253(10)	94(8)
C(4)	-2167(16)	6456(14)	4086(10)	82(6)
C(8)	2409(16)	5124(9)	73(9)	54(4)
C(10)	3410(11)	5374(10)	-1152(15)	64(4)
N(1)	-2190(30)	4810(14)	4403(9)	171(12)
C(7)	3293(19)	5091(9)	-296(16)	92(7)
N(18)	2500(20)	5756(8)	-1768(8)	130(9)
C(6)	1430(15)	5761(10)	-1198(16)	88(6)
C(2)	-3729(9)	5773(10)	4162(8)	44(3)
C(3)	-3191(14)	6420(11)	4051(10)	67(4)
C(1)	-3374(19)	4960(13)	4323(10)	96(7)

Table 5.12 *Selected bond lengths (Å) and angles (°) for [pyr,F]-GaPO-3*

Ga(1)-O(13)#1	1.851(5)	O(13)#1-Ga(1)-F(1)	89.0(2)
Ga(1)-O(1)	1.858(5)	O(1)-Ga(1)-F(1)	85.7(2)
Ga(1)-O(7)	1.860(5)	O(7)-Ga(1)-F(1)	85.7(2)
Ga(1)-O(8)	1.915(6)	O(8)-Ga(1)-F(1)	176.1(2)
Ga(1)-F(1)	1.965(5)	O(6)#2-P(1)-O(7)	109.6(3)
P(1)-O(6)#2	1.523(5)	O(6)#2-P(1)-O(4)	109.3(3)
P(1)-O(7)	1.535(6)	O(7)-P(1)-O(4)	112.3(3)
P(1)-O(4)	1.540(6)	O(6)#2-P(1)-O(9)	108.8(3)
P(1)-O(9)	1.540(6)	O(7)-P(1)-O(9)	108.7(3)
C(5)-C(4)	1.27(2)	O(4)-P(1)-O(9)	108.0(3)
C(5)-N(1)	1.52(3)	Ga(1)-F(1)-Ga(3)	123.9(2)
C(4)-C(3)	1.25(2)	Ga(2)-F(2)-Ga(4)	126.1(2)
N(1)-C(1)	1.46(3)	P(2)-O(1)-Ga(1)	134.9(3)
C(2)-C(3)	1.141(19)	P(2)-O(2)-Ga(4)	125.3(3)
C(2)-C(1)	1.25(2)	P(4)-O(3)-Ga(2)	133.1(4)
		P(1)-O(4)-Ga(3)	139.0(3)
O(13)#1-Ga(1)-O(1)	108.4(2)	C(4)-C(5)-N(1)	116.6(14)
O(13)#1-Ga(1)-O(7)	114.9(2)	C(3)-C(4)-C(5)	122.0(17)
O(1)-Ga(1)-O(7)	135.6(2)	C(1)-N(1)-C(5)	110.5(11)
O(13)#1-Ga(1)-O(8)	94.9(2)	C(3)-C(2)-C(1)	124.8(15)
O(1)-Ga(1)-O(8)	93.2(2)	C(2)-C(3)-C(4)	127.3(17)
O(7)-Ga(1)-O(8)	92.5(2)	C(2)-C(1)-N(1)	118.9(14)

Table 5.13 *Anisotropic displacement parameters ($Å^2$ x 10^3) for [pyr,F]-GaPO-3. The anisotropic displacement factor exponent takes the form:*
$-2\pi^2 [h^2 a^{*2} U_{11} + ... + 2 h k a^* b^* U_{12}]$

	U_{11}	U_{22}	U_{33}	U_{23}	U_{13}	U_{12}
Ga(1)	11(1)	12(1)	9(1)	0(1)	2(1)	0(1)
Ga(2)	11(1)	11(1)	11(1)	0(1)	3(1)	0(1)
Ga(3)	10(1)	13(1)	11(1)	0(1)	0(1)	-1(1)
Ga(4)	12(1)	11(1)	11(1)	1(1)	2(1)	0(1)
P(1)	13(1)	10(1)	11(1)	1(1)	0(1)	0(1)
P(2)	12(1)	10(1)	13(1)	0(1)	2(1)	1(1)
P(3)	12(1)	13(1)	9(1)	0(1)	-2(1)	1(1)
P(4)	11(1)	17(1)	11(1)	0(1)	4(1)	0(1)
F(1)	9(2)	18(2)	13(2)	0(2)	1(2)	1(2)
F(2)	17(2)	13(2)	14(2)	4(2)	0(2)	-1(2)
O(1)	15(3)	9(3)	15(3)	3(2)	2(2)	1(2)
O(2)	10(3)	17(3)	16(3)	7(2)	1(2)	3(2)
O(3)	20(3)	19(3)	17(3)	6(2)	4(2)	6(2)
O(4)	19(3)	13(3)	14(3)	2(2)	-5(2)	3(2)
O(6)	11(3)	11(3)	20(3)	1(2)	8(2)	1(2)
O(7)	16(3)	13(3)	19(3)	1(2)	-4(2)	0(2)
O(8)	14(3)	19(3)	11(3)	-2(2)	-3(2)	-3(2)
O(9)	14(3)	16(3)	12(3)	-2(2)	-1(2)	-2(2)
O(10)	21(3)	14(3)	13(3)	0(2)	0(2)	-4(2)
O(11)	22(3)	14(3)	15(3)	-1(2)	0(2)	-8(2)
O(12)	15(3)	17(3)	13(3)	0(2)	-2(2)	0(2)
O(13)	22(3)	19(3)	10(3)	1(2)	9(2)	0(2)
O(14)	24(3)	11(3)	15(3)	2(2)	0(2)	7(2)
O(15)	15(3)	13(3)	18(3)	0(2)	-4(2)	-1(2)
O(16)	32(4)	15(3)	34(4)	2(3)	24(3)	-1(3)
O(17)	21(4)	63(5)	30(4)	5(3)	-5(3)	-14(3)
C(9)	54(10)	89(12)	88(13)	-34(10)	40(9)	-13(9)

Table 5.13 Cont'd

	U_{11}	U_{22}	U_{33}	U_{23}	U_{13}	U_{12}
C(5)	21(7)	230(20)	32(8)	-61(12)	-7(6)	30(11)
C(4)	90(13)	124(15)	35(7)	1(8)	25(9)	-63(12)
C(8)	98(13)	39(7)	26(6)	-2(5)	25(8)	-17(8)
C(10)	33(7)	59(9)	100(13)	-15(9)	-3(8)	1(6)
N(1)	360(30)	120(14)	25(6)	-39(8)	-53(13)	168(18)
C(7)	150(20)	25(7)	99(15)	-5(8)	-65(14)	2(9)
N(18)	320(30)	42(7)	24(6)	5(5)	10(11)	-49(12)
C(6)	97(13)	48(8)	113(14)	-33(9)	-82(11)	39(9)
C(2)	30(6)	76(9)	27(6)	18(6)	-7(5)	-26(6)
C(3)	91(12)	72(10)	37(7)	17(7)	7(8)	32(10)
C(1)	170(20)	81(12)	32(7)	-9(8)	3(10)	-93(13)

5.2.2.4 Pyridine-GaPO-4

This is the only pyridine-GaPO structure to have been prepared without the presence of fluorine. A similar structure, MU-1 synthesised in the presence of fluorine with bis(cyclopentadienyl)cobalt(III) cations as the SDA has been reported by Patarin.[5] In addition to this an iron phosphate structure containing a similar D4R unit has been prepared by De Bord and co workers.[6]

The solution of this structure has been problematic due to a form of twinning in the crystals. The structure was initially solved using a small tetragonal unit cell (a = 13.0160 Å, b = 7.3560Å) in the spacegroup $I\bar{4}2m$, however, the fit obtained on structure solution was poor ($R_{all\ data}$ = 8.18%) and further examination of the data showed some weak reflections which suggested a larger unit cell. Data was subsequently collected on station 9.8 of the SRS and the larger unit cell (a = 18.3247Å, c = 14.6191; spacegroup $I\bar{4}c2$) was observed, still with tetragonal symmetry. The structure proved to be the same as that determined from the original lab data with some disorder, which appeared to be due to a twinning of the original cell. Unfortunately no twin law could be determined and the structure was solved in the smaller cell to avoid the disorder. Details of the data collection and structure solution (laboratory data) are given in table 5.14.

Table 5.14 *Structure solution and refinement data for pyr-GaPO-4*

Identification code	Pyr-GaPO-4
Empirical formula	$(GaPO_4)(OH)(GaPO_3OH).0.5O.0.5(C_5H_6N)$
Formula weight	818.87
Temperature	293(2)K
Wavelength	0.71073Å
Crystal system, space group	Tetragonal, $I\bar{4}2m$
Unit cell dimensions	a = 13.016(3) Å α = 90°
	b = 13.016(3) Å β = 90°
	c = 7.356(4) Å γ = 90°
Volume	1246.2(8) $Å^3$
Z, Calculated density	2, 2.182 Mgm^{-3}
Absorption coefficient	4.622 mm^{-1}
F(000)	790
Crystal size	0.01 x 0.01 x 0.01 mm
Theta range for data collection	2.21° to 23.56°
Limiting indices	$0 \leq h \leq 14$, $0 \leq k \leq 14$, $0 \leq l \leq 8$
Reflections collected / unique	562 / 302 [R(int) = 0.0463]
Completeness to theta	23.56, 100.0 %
Max. and min. transmission	0.9552 and 0.9552
Refinement method	Full-matrix least-squares on F^2
Data / restraints / parameters	302 / 0 / 52
Goodness-of-fit on F^2	1.121
Final R indices [I>2sigma(I)]	R1 = 0.0818, wR^2 = 0.2082
R indices (all data)	R1 = 0.0909, wR^2 = 0.2212
Absolute structure parameter	0.43(14)
Largest diff. peak and hole	0.758 and -1.624 $e.Å^{-3}$

The asymmetric unit of pyr-GaPO-4 consists of two five coordinate gallium and two four coordinate phosphorus atoms (fig 5.12). Each of these has one terminal -OH group. The asymmetric unit does not contain any complete pyridine molecules, making it impossible to assign the nitrogen positions due to the symmetry of the spacegroup.

The overall structure of pyridine-GaPO-4 is simply a cubic gallium phosphate cage with –OH groups at each corner and an additional oxygen atom at the centre, bonded to all four gallium corners (fig. 5.13). The cubes are packed in a way that appears similar to the ACO zeolite structure, but without the covalent bonds linking

the D4R cubes. It is thought that hydrogen bonding may exist between the –OH groups on the cage corners (approximate O to O distance between cages 2.6Å).

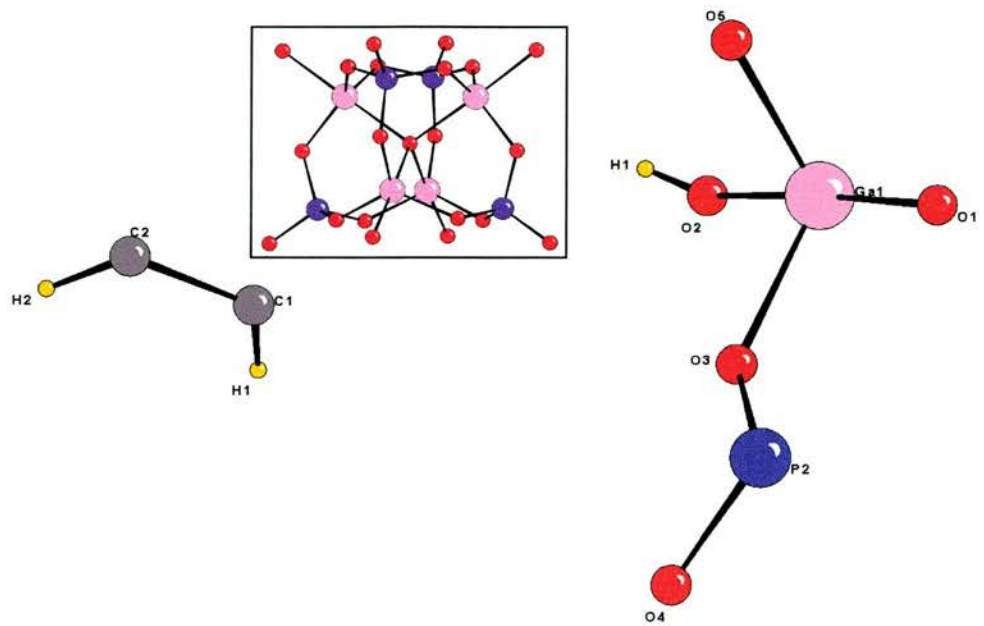

Figure 5.12 *The Asymmetric unit of [pyr,O]-GaPO-4. Inset;* ***figure 5.13****The cubic D4R unit of [pyr,O]-GaPO-4*

The pyridine molecules reside in areas of the structure where they have no effect on the possible hydrogen bonding system and have no close interactions with the cubes (fig. 5.14).

The central oxygen atom is interesting and novel in this type of material. In MU-1 the central position in the cages was occupied by fluorine with this observation being confirmed by ^{19}F MASNMR data. For pyridine-GaPO-4 the ^{19}F MASNMR spectrum has no signals, confirming that the central atom must be oxygen. Further experiments are in progress to determine the oxygen species at the centre of the cube.

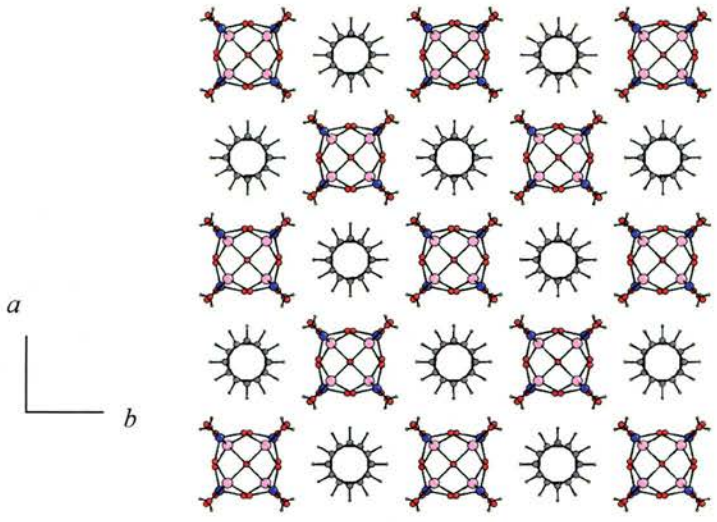

Figure 5.14 *Projection of the overall structure of [pyr,O]-GaPO-4 along the (001) axis. Colour scheme as for fig. 5.12. The similarity to the ACO zeolite structure is clear*

The ^{31}P MASNMR spectrum of [pyr,O]-GaPO-4 has a single resonance at δ = 3.9ppm (fig. 5.15), this is different from the peak observed for the fluoride containing cage, however it should be noted that a peak at this shift is present as a minor impurity alongside the main peak (δ = -4ppm).[5]

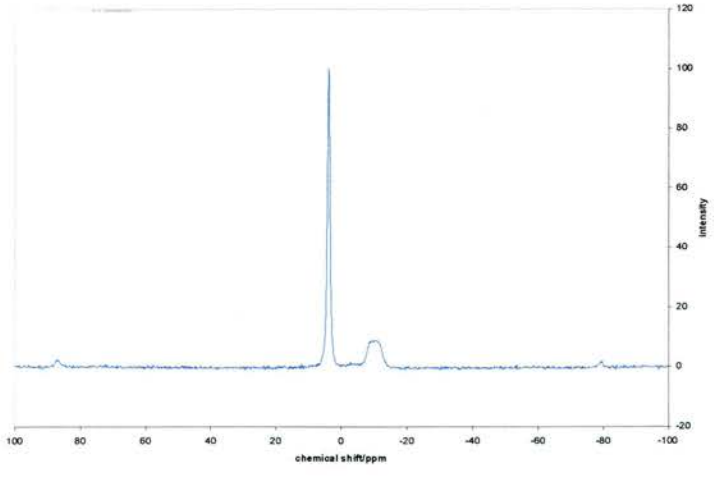

Figure 5.15 *^{31}P MASNMR spectrum of [pyr,O]-GaPO-4*

The location of the protons in this structure is of interest. For the fluoride containing D4R units of the layered material ULM-18 NMR and computer modelling studies have shown that there is a proton associated with the central fluoride. This leads to an intriguing series of possibilities for the location of protons. ^{15}N MASNMR gives a spectrum with a single resonance at $\delta = -182$ppm, confirming that all of the pyridine molecules are protonated at the nitrogen atom (as might be expected from the pH at which the preparation was carried out). The pyr-GaPO-4 cages must therefore have a charge of –2 to balance that of the pyridinium ions. This can be fulfilled in three ways, eight protons on the corner groups of the cage with O^{2-} in the middle, seven protonated corners and a central OH- or six protonated corners and OH_2 at the cage centre. As previously mentioned it is difficult to distinguish F and OH in crystal structures and they will often occupy the same sites. This leads us to believe that as the structure is so similar to MU-1 the most likely central species is either OH or OH_2. Suggestions by Taulelle that protons inside the D4R units play an important role in their formation also lend credence to this theory,[7] however, further experiments are needed to determine the true proton distribution.

Pyr-GaPO-4 is soluble in basic media (KOH). The ^{31}P NMR spectrum of the solution consists of a single peak shifted only slightly downfield from that of the solid material, indicating that the D4R units are probably still intact. On thermal analysis however the structure breaks down easily at around 200°C, with a dense GaPO phase resulting. Full crystallographic data for pyridine-GaPO-4 are given in tables 5.15 to 5.18.

Table 5.15 *Atomic coordinates (x 10^4) and equivalent isotropic displacement parameters ($Å^2$ x 10^3) for [Pyr,O]-GaPO-4. U(eq) is defined as one third of the trace of the orthogonalized U_{ij} tensor*

	x	y	z	U(eq)
Ga(1)	925(1)	925(1)	1640(4)	55(1)
P(2)	1293(4)	1293(4)	-2362(9)	70(3)
O(1)	0	0	0	25(6)
O(2)	1799(14)	1799(14)	3040(40)	140(20)
O(3)	1509(12)	1509(12)	-380(20)	115(11)
O(4)	1946(11)	1946(11)	-3550(30)	124(15)
O(5)	-134(17)	1532(14)	2690(30)	93(6)
C(1)	1060(30)	5000	0	87(11)
C(2)	506(17)	5876(17)	0(50)	86(7)

Table 5.16 *Bond lengths (Å) and angles (°) for [pyr,O]-GaPO-4*

Ga(1)-O(5)	1.77(2)	O(5)-Ga(1)-O(1)	93.5(6)
Ga(1)-O(3)	1.84(2)	O(3)-Ga(1)-O(1)	90.5(6)
Ga(1)-O(2)	1.91(3)	O(2)-Ga(1)-O(1)	177.1(8)
Ga(1)-O(1)	2.086(3)	O(4)-P(2)-O(3)	110.6(13)
P(2)-O(4)	1.48(2)	O(4)-P(2)-O(5)#2	110.4(8)
P(2)-O(3)	1.511(18)	O(3)-P(2)-O(5)#2	107.1(9)
P(2)-O(5)#2	1.56(2)	O(4)-P(2)-O(5)#3	110.3(8)
C(1)-C(2)	1.35(3)	O(3)-P(2)-O(5)#3	107.0(9)
C(2)-C(2)#3	1.32(4)	Ga(1)#4-O(1)-Ga(1)#3	109.54(8)
		Ga(1)#3-O(1)-Ga(1)#5	109.33(16)
O(5)#1-Ga(1)-O(5)	120.4(14)	P(2)-O(3)-Ga(1)	128.8(14)
O(5)-Ga(1)-O(3)	119.5(7)	P(2)#3-O(5)-Ga(1)	126.6(10)
O(5)-Ga(1)-O(2)	87.8(7)	C(2)#6-C(1)-C(2)	115(4)
O(3)-Ga(1)-O(2)	86.6(10)	C(2)#3-C(2)-C(1)	122.3(18)

Table 5.17 *Anisotropic displacement parameters ($Å^2$ x 10^3) for [pyr,O]-GaPO-4. The anisotropic displacement factor exponent takes the form:*
$-2\pi^2 [h^2 a^{*2} U_{11} + ... + 2 h k a^* b^* U_{12}]$

	U_{11}	U_{22}	U_{33}	U_{23}	U_{13}	U_{12}
Ga(1)	68(2)	68(2)	30(2)	0(1)	0(1)	-30(2)
P(2)	96(5)	96(5)	17(3)	0(2)	0(2)	-70(5)
O(1)	23(8)	23(8)	29(15)	0	0	0
O(2)	200(30)	200(30)	28(14)	-14(7)	-14(7)	-180(40)
O(3)	165(16)	165(16)	14(10)	-13(6)	-13(6)	-130(20)
O(4)	170(20)	170(20)	33(10)	15(8)	15(8)	-140(30)
O(5)	88(12)	110(12)	80(12)	-69(11)	-13(11)	14(12)

5.2.3 Synthetic Studies 1: Fluoride media

By varying the pH, gel composition, temperature and heating time used in the synthesis of pyridine,F-GaPO phases it has been possible to control to some extent the

final product. All of the three fluorine-containing phases described above may be obtained and in addition to this three other phases have been obtained, firstly the GaPO analogue of AlPO-21[8] which is templated by trimethylamine (GaPO-A21), second ULM-3,[9] also templated by TMA and third an ammonium templated phase containing 3-coordinate fluorine (GaPO-NH_4) previously reported by Xu *et.al.*.[10] The conditions of the syntheses and resulting phases are given in table 5.19, below the effects of altering some important parameters are discussed in turn.

5.2.3.1 pH variation

The pH of the initial synthesis gel (prior to solvothermal treatment) was measured for all preparations using either a pH electrode or short range indicator paper. The results, excluding preparations in which GaPO-A21, ULM-3, Berlinite and GaPO-NH_4 were the products are shown in figure 5.16.

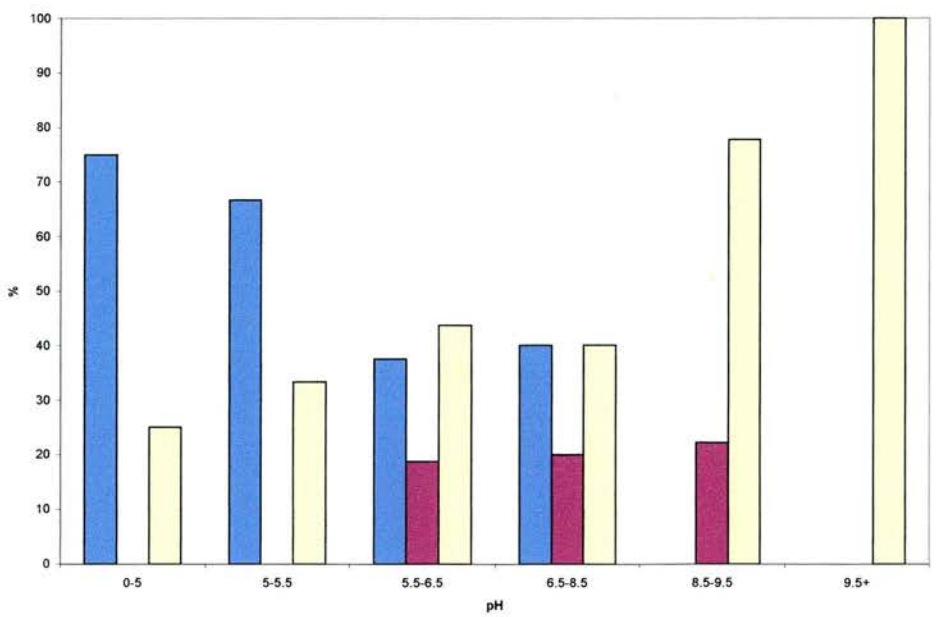

Figure 5.16 *Percentages of [pyr,F]-GaPO phases produced at various pHs. [pyr,F-GaPO-1, blue; [pyr,F]-GaPO-2, yellow; [pyr,F]-GaPO-3 red. The percentage is based only on preparations which resulted in these products.*

The most significant effect of pH variation is on the production of the two D6R based phases; [pyr,F]-GaPO-1 and 2. At low pH (<5.5) the less ordered [pyr,F]-GaPO-1 is favoured with no real selectivity between the two in the middle of the range studied and [pyr,F]-GaPO-2 favoured at higher pH (above 8.5). [pyr,F]-GaPO-3 is only produced in the mid range of pH (5.5-9.5). The reason for this interesting trend in the production of pyr,F-GaPOs 1 and 2 could lie in the mechanism proposed for the formation of UT-6 and other similar AlPO structures by Ozin and co workers.[11] This mechanism is based on the formation of layered structures by twisting, hydrolysis and condensation of monodimesional aluminophosphate chains. It is possible that in the presence of higher concentrations of protons there is a greater level of hydrolysis of the bonds in the parent chain allowing more twisting and thus the formation of two slightly different types of 8-ring window. At higher pH the chains would be less likely to be broken down and would therefore form a more ordered structure. The fact that both structures are obtained at low pH but only [pyr,F]-GaPO-2 is found at high pH suggests that he low pH process is the less predictable and controlled of the two, which supports the hypothesis. The TMA templated phases both seem to be favoured at higher pH, however this is probably simply due to the high concentrations of TMA used to increase the pH of the system to high levels. GaPO-NH_4 may be prepared at a pH of around 6. It should also be noted that the dense GaPO-Berlinite phase is commonly obtained at low pHs in addition to pyr,F-GaPO 1 and 2.

5.2.3.2 Solvent Composition

The solvent composition in this case is defined as the ratio of pyridine to water. Again this seems to have a significant level of control over the synthesis of the D6R based phases with [pyr,F]-GaPO-2 being favoured at low levels of water and

[pyr,F]-GaPO-1 prevailing at high water contents (fig. 5.17). None of the pyridine phases may be prepared from a solvent composition of 100% water, even though pyridine is still present in these systems as the solvent for hydrofluoric acid. [pyr,F]-GaPO-3 is only obtained in solvent mixtures containing less than 50% water. The explanation of [pyr,F]-GaPO-1 being a product of increased hydrolysis and flexibility may be supported by its prevalence at high levels of water.

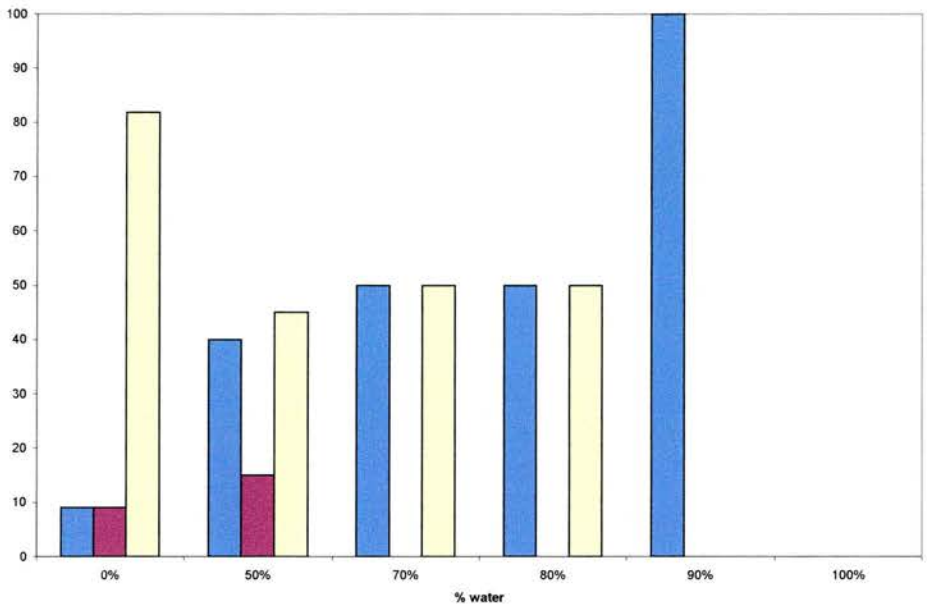

Figure 5.17 *Percentages of [pyr,F]-GaPO phases produced over a range of solvent compositions. Colours as for fig. 5.16*

5.2.3.3 Temperature

When the results of preparations at a range of temperatures are plotted (fig.5.18) no obvious trends emerge. It is possible for any of the phases to crystallise across the range of temperatures from 150 to 180°C, the most common range for the synthesis of this type of material. Some selectivity for [pyr,F]-GaPO-2 is shown at

160 and 170°C, but this is probably due to the fact that it is the most common of the phases overall and also the other synthesis conditions applied.

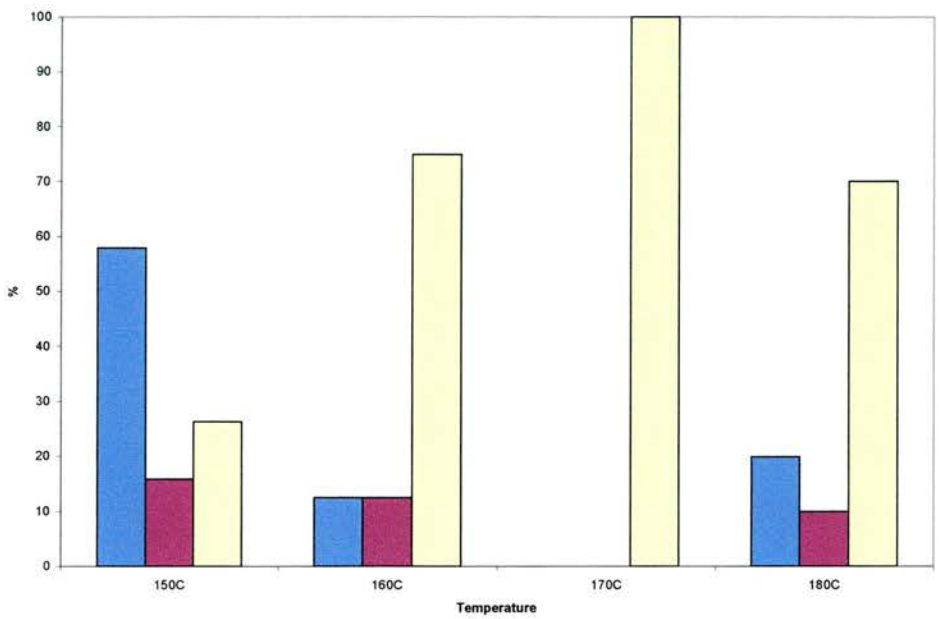

Figure 5.18 *Percentage of [pyr,F]-GaPO phases produced between 150℃ and 180℃. Colours as for last two figures*

5.2.3.4 Time

The time of heating in a solvothermal synthesis is known to be of great importance in several systems. The phenomenon of Ostwald ripening in zeolitic phases is well known,[12] with the phase transforming over the period of heating from a large pore material to a one with smaller pores and eventually to a dense phase. In the synthesis of pyridine templated GaPOs it seems that when short heating times are used any of the three phases could result, along with all of the three non-pyridine phases. When the mixtures are solvothermally treated for 5 days or more [pyr,F]-GaPO-1 and 2 are the only observed products with longer heating times favouring [pyr,F]-GaPO-1 (fig. 5.19). Interestingly the dense berlinite phase does not become

more dominant with greater heating times, at least up to the longest time used in this study (14 days).

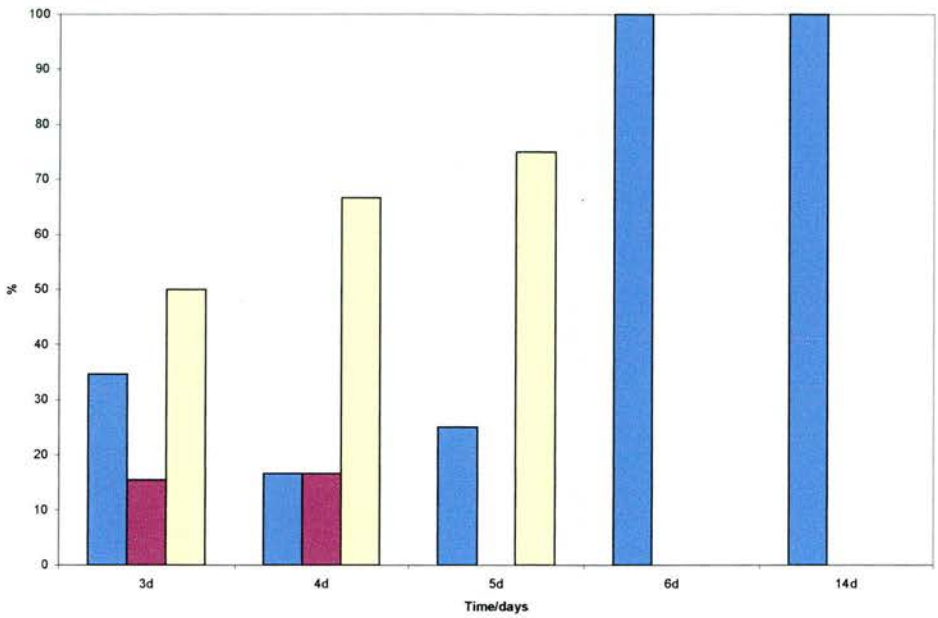

Figure 5.19 *Percentage of [pyr,F]-GaPO phases produced over a range of heating times. Colours as for fig. 5.16*

The increased production of [pyr,F]-GaPO-1 at longer heating times seems to go against the intuitive reasoning of the hydrolysis and condensation argument, however it may be that this structure is slightly energetically favoured over [pyr,F]-GaPO-2. There is some evidence in this type of material for the formation after long heating times of kinetic products, which have a slightly lower energy than the initial products.

5.2.3.5 Gallium to Phosphorus Ratio

The ratio of M to P in open metallophosphate open framework materials and in some cases have a great influence over the product. It is also of importance in

zeolite synthesis, where the Al: Si ratio can control the structure to a large extent.[13] In the case studied here, the reduction of the amount of gallium leads in all cases to production of [pyr,F]-GaPO-1. This might be explained by the increased ratio of protons (from the phosphoric acid) relative to gallium in the synthesis gel.

5.2.4 Synthetic studies 2: synthesis without fluoride

When a pyridine templated gallophosphate synthesis is carried out without the addition of the HF/pyridine solution the uncondensed cube pyr-GaPO-4 structure is the most common product. A second phase, which has yet to be characterised, has also been produced in two cases and under some conditions berlinite results. The stability of the pyr-GaPO-4 structure is somewhat surprising and is thought to be due to the stabilising interactions of the corner –OH groups and the presence of the central oxygen atom. Preparations carried out with conditions and results are shown in table 5.20.

Table 5.20 *Pyridine-GaPO preparations without fluoride*

Ga: P: HCl/TMA: pyridine: water: HF	pH	T/C	Time/days	Product phase
2: 2: 0: 10: 10: 0	5.8	150	3	PG4
2: 2: 1: 10: 10: 0	8.4	150	3	Unknown
2: 2: 1.5: 10: 10: 0	9.4	150	3	Unknown
2: 2: 870: 10: 10:0	4	180	3	Gallium sulfate
2: 2: 870: 12.5: 0: 0	4	180	4	PG4
2: 2: 870: 10: 10:0	4	150	3	PG4
2: 2: 1700: 10: 10:0	4	150	3	PG4

5.3 Another Small Molecule Templated Structure

Another novel structure related to the materials described above has been synthesised in the presence of 4-dimethylaminopyridine (DMAP). The material is layered and the GaPO framework contains an SBU related to the D4R unit, similar to that of [pyr,F]-GaPO-3. This material is also of interest as its complex structure was solved from XRD data collected from an extremely small single crystal.

5.3.1 Synthesis

DMAP-GaPO (formula) was synthesised in a solvothermal preparation using pyridine as the solvent. Gallium sulfate (99%, Aldrich) and DMAP (99%, Aldrich) were slurried in pyridine (99%, Fisher) and to this mixture phosphoric acid (85% weight solution in water, Aldrich) was added with stirring. HF (70% solution in pyridine, Aldrich) was then added to give a gel of approximate composition P_2O_5: Ga_2O_3: 70 pyridine: HF: 6 DMAP. The pH of the gel was adjusted to ~5 with TMA and it was then aged for one hour at room temperature and transferred to a Teflon lined stainless steel autoclave which was heated at 135°C for 72 hours. The product, a small crop of tiny colourless crystals, was recovered by suction filtration, washed with acetone and water and dried at room temperature.

5.3.2 Structure

The crystals obtained were very small indeed (~15x10x3μm), therefore singe crystal XRD data were collected on the high flux SCXRD facility, beamline ID11 of the European Synchrotron Radiation Facility (ESRF) in Grenoble. Details of the data collection and structure solution are given in table 5.21.

Table 5.21 *Structure solution and refinement details for DMAP-GaPO*

Identification code	DMAP-GaPO
Empirical formula	$(GaPO_4)_4(OH)F.2(C_7H_{11}N_2)$
Formula weight	1880.23
Temperature	293(2)K
Wavelength	0.44250Å
Crystal system, space group	Triclinic, $P\bar{1}$
Unit cell dimensions	a = 14.2576(12) Å; α = 61.118(4)°
	b = 14.5490(11) Å; β = 75.696(6)°
	c = 15.3785(3) Å; γ = 74.869(3)°
Volume	2668.6(3) $Å^3$
Z, Calculated density	2, 2.340 Mgm^{-3}

Table 5.21 continued

Absorption coefficient	2.273 mm^{-1}
F(000)	1852
Crystal size / μm	5 x 10 x 15
Theta range for data collection	1.67° to 26.92°.
Limiting indices	$-26 \leq h \leq 28$, $-27 \leq k \leq 29$, $-23 \leq l \leq 30$
Reflections collected / unique	36812 / 27156 [$R_{int} = 0.1434$]
Observed reflections [$F_o > 4\sigma F_o$]	9031
Completeness to theta	26.92, 56.7 %
Refinement method	Full-matrix least-squares on F^2
Data / restraints / parameters	27156 / 4 / 770
Goodness-of-fit on F^2	0.957
Final R indices [$I > 2\sigma(I)$]	R1 = 0.1186, $wR^2 = 0.2496$
R indices (all data)	R1 = 0.2941, $wR^2 = 0.3414$
Largest diff. peak and hole	2.586 and -2.329 $e.A^{-3}$

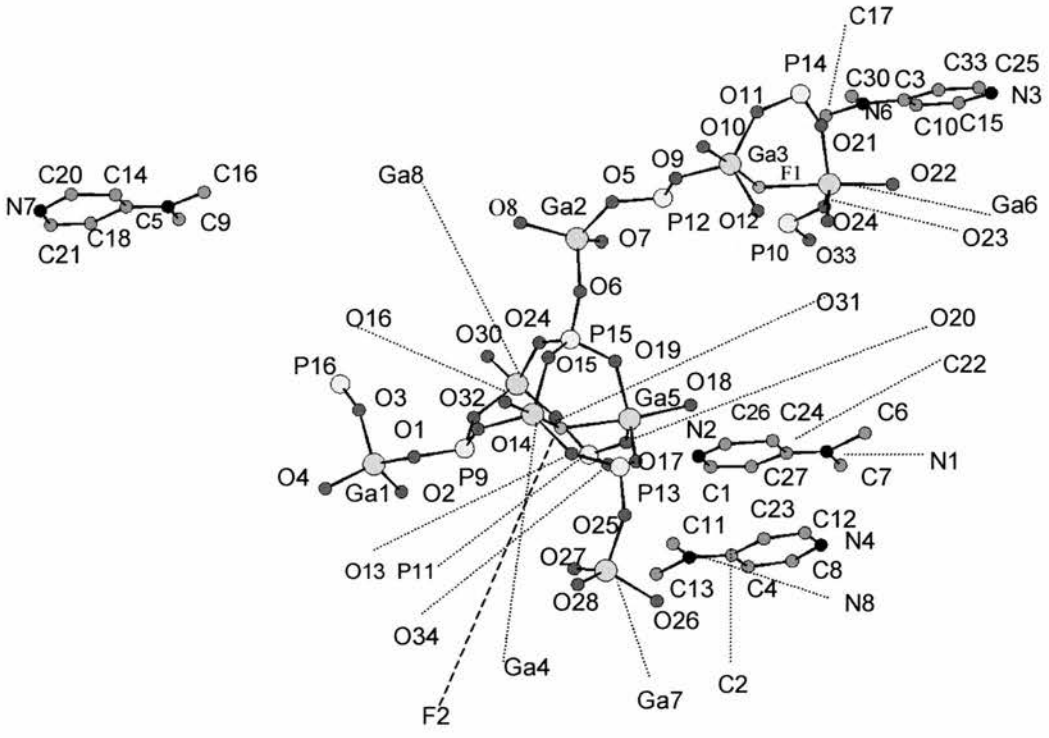

Figure 5.20 *The asymmetric unit of the DMAP-GaPO*

The asymmetric unit (fig. 5.20) of DMAP-GaPO is quite large (88 non-hydrogen crystallographically independent atoms) and due to the limitations of the

data (see table 5.21, above) it was necessary to apply chemically sensible restraints to the DMAP molecules in order to obtain a stable refinement. The refinement is still not of a high standard, however the structure appears sensible and is of interest.

DMAP-GaPO consists of layers of fluorinated gallium phosphate separated by layers of DMAP molecules, which are arranged in a 'herringbone' pattern. The layer structure is clearly visible when viewed in the (100) direction (fig 5.21).

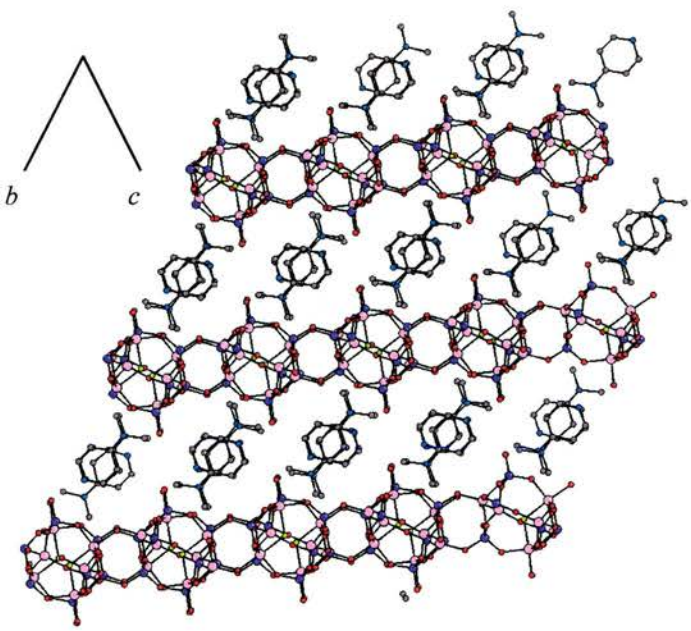

Figure 5.21 *The layer structure of DMAP-GaPO viewed along the (100) axis. The alternating layers of GaPO and DMAP are clearly visible. Colour scheme for atoms: gallium pink, phosphorus blue, oxygen red, fluorine green, carbon grey, nitrogen dark blue*

The GaPO layers are formed from an SBU similar to that of [pyr,F]-GaPO-3. The unit is also related to the D4R, as observed in cyclam-GaPO (see chapter 4) and can be visualised as a D4R containing a central fluorine atom displaced toward two of the Ga atoms (as in cyclam-GaPO, see chapter 4), which has been opened on one edge

(fig. 5.22). These units are linked into chains by the opened edge joining to the opposite complete edge of the next unit.

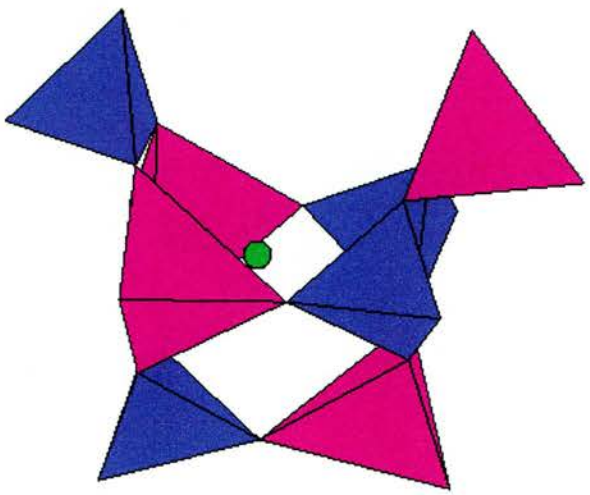

Figure 5.22 *The SBU of DMAP-GaPO, which resembles a side opened D4R cube. Purple tetrahedra GaO_4, blue tetrahedra PO_4, green sphere fluorine. Note that the fluorine is in a non-central position*

The chains are lined by four-rings to form sheets (figure 5.23) which interact with the organic molecules by pendant –OH groups (these are visible in figure 5.21, projecting into the interlayer region). As for [pyr,F]-GaPO-3 the assignment of OH and F cannot be determined for certain from the XRD data, however it is though that the Ga-Ga bridges are formed by fluorine and the terminal groups hydroxyl. For charge balancing reasons only half of the terminal oxygen atoms can be protonated. Because this material has only been synthesised in small batches no thermal analysis has been carried out. Atom positions, selected bond lengths and angles and anisotropic thermal parameters for DMAP-GaPO are given in tables 5.22 to 5.24.

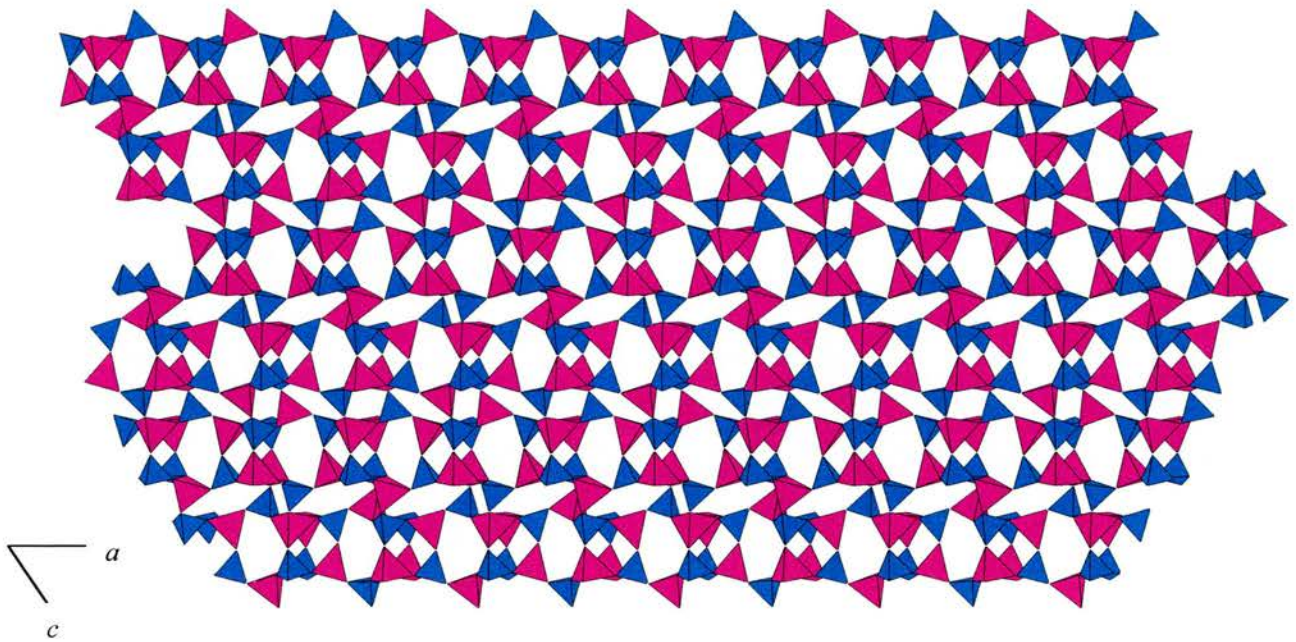

Figure 5.23 *The gallophosphate layer of DMAP-GaPO viewed in the (010) direction. The chains of side opened D4Rs run across the page, linked downwards by four rings*

Table 5.22 *Atomic coordinates (x 10^4) and equivalent isotropic displacement parameters ($Å^2$ x 10^3) for DMAP-GaPO. U(eq) is defined as one third of the trace of the orthogonalized U_{ij} tensor*

	x	y	z	U_{eq}
Ga(1)	991(1)	8383(1)	555(1)	13(1)
Ga(2)	4555(1)	13393(1)	-4460(1)	13(1)
Ga(3)	5067(1)	16758(1)	-8649(1)	14(1)
Ga(4)	928(1)	11783(1)	-3657(1)	15(1)
Ga(5)	409(1)	14271(1)	-3567(1)	15(1)
Ga(6)	4191(1)	19253(1)	-8573(1)	15(1)
Ga(7)	-2863(1)	13109(1)	-3561(1)	15(1)
Ga(8)	1921(1)	11936(1)	-1479(1)	16(1)
P(9)	717(2)	10381(2)	-1389(2)	14(1)
P(10)	3758(2)	18527(2)	-6268(2)	14(1)
P(11)	56(2)	13563(2)	-1281(2)	16(1)
P(12)	4867(2)	15359(2)	-6386(2)	14(1)
P(13)	-732(2)	13635(2)	-4582(2)	14(1)
P(14)	6225(2)	18628(2)	-9584(2)	15(1)
P(15)	2415(2)	12991(2)	-3816(2)	14(1)
P(16)	3005(2)	7946(2)	1226(2)	15(1)
O(1)	828(7)	9181(6)	-746(5)	18(2)
O(2)	331(6)	9131(7)	1228(6)	23(2)
O(3)	2269(6)	8196(7)	559(6)	23(2)
O(4)	707(8)	7127(9)	974(8)	37(3)
O(5)	5072(6)	14166(6)	-5749(6)	18(2)
O(6)	3362(6)	13268(7)	-4502(6)	21(2)

Table 5.22 continued

	x	y	z	U_{eq}
O(7)	4459(6)	14144(8)	-3800(6)	24(2)
O(8)	5209(6)	12102(7)	-3958(7)	27(2)
O(9)	5126(7)	15537(6)	-7463(6)	19(2)
O(10)	5494(6)	15978(6)	-9339(5)	15(2)
O(11)	6049(7)	17521(7)	-9259(7)	25(2)
O(12)	3848(6)	17220(8)	-9036(6)	23(2)
O(13)	-182(7)	12521(7)	-4214(6)	22(2)
O(14)	975(6)	10567(7)	-2460(6)	19(2)
O(15)	2077(6)	12299(8)	-4103(7)	22(2)
O(16)	1246(6)	10983(6)	-4311(5)	14(1)
O(17)	-611(6)	14183(7)	-4015(6)	23(2)
O(18)	369(6)	15746(6)	-4315(6)	17(2)
O(19)	1715(6)	14014(6)	-4013(7)	26(2)
O(20)	43(8)	14337(7)	-2373(6)	27(2)
O(21)	5489(6)	19171(7)	-9019(6)	18(2)
O(22)	3824(6)	20730(6)	-9308(6)	20(2)
O(23)	3846(7)	19286(7)	-7378(5)	22(2)
O(24)	3315(7)	18976(7)	-9058(7)	29(2)
O(25)	-1810(6)	13612(7)	-4440(6)	23(2)
O(26)	-3805(6)	14246(7)	-3880(6)	20(2)
O(27)	-2542(6)	12561(8)	-2319(6)	24(2)
O(28)	-3097(7)	12254(8)	-3952(7)	28(2)
O(29)	2605(6)	12403(8)	-2727(6)	27(2)
O(30)	2768(6)	11461(7)	-613(6)	21(2)
O(31)	1054(7)	12882(9)	-1126(8)	36(2)
O(32)	1404(7)	10783(7)	-1099(7)	27(2)
O(33)	3364(8)	19124(7)	-5678(7)	26(2)
O(34)	-179(7)	14152(8)	-683(7)	29(2)
F(1)	4521(5)	17589(5)	-7825(5)	21(2)
F(2)	589(5)	12623(5)	-2828(5)	19(1)
C(1)	-732(16)	16680(20)	-1179(17)	67(7)
C(2)	-2948(11)	16640(10)	-2469(11)	31(3)
C(3)	5863(11)	21685(12)	-7586(10)	28(3)
C(4)	-3211(13)	17158(15)	-1844(13)	42(4)
C(5)	8043(11)	3325(12)	2521(12)	33(3)
C(6)	-975(17)	20230(20)	-3870(30)	121(15)
C(7)	-1380(20)	19840(30)	-2110(30)	130(16)
C(8)	-3326(13)	18216(14)	-2291(14)	42(4)
C(9)	7590(20)	4740(30)	3020(20)	96(9)
C(10)	5772(15)	22108(17)	-6921(15)	47(5)
C(11)	-2467(18)	15100(20)	-2754(18)	72(6)
C(12)	-2934(14)	18320(16)	-3848(13)	46(4)
C(13)	-2870(20)	14920(20)	-1026(19)	79(7)
C(14)	8277(18)	2948(17)	1838(15)	55(6)
C(15)	5594(16)	23146(16)	-7280(16)	55(5)
C(16)	7880(20)	5120(30)	1230(20)	98(9)
C(17)	6000(20)	19890(30)	-6280(20)	92(8)
C(18)	7943(15)	2558(18)	3536(16)	52(5)
C(20)	8519(19)	1880(20)	2160(20)	71(7)
C(21)	8108(15)	1577(19)	3795(18)	58(6)
C(22)	-918(12)	18410(13)	-2521(12)	37(4)
C(23)	-2842(14)	17322(13)	-3498(11)	38(4)
C(24)	-662(14)	17965(16)	-3213(13)	44(4)
C(25)	5663(16)	23401(15)	-8866(17)	57(5)
C(26)	-478(14)	16820(20)	-2755(18)	65(7)
C(27)	-948(15)	17678(17)	-1520(13)	51(5)
C(30)	6126(18)	20270(20)	-8030(20)	92(10)
C(33)	5827(12)	22395(14)	-8584(13)	39(4)

Table 5.22 continued

	x	y	z	U_{eq}
N(1)	-1093(10)	19397(14)	-2798(16)	66(6)
N(2)	-519(12)	16280(11)	-1820(14)	53(5)
N(3)	5564(12)	23826(12)	-8228(16)	62(5)
N(4)	-3210(9)	18805(12)	-3285(11)	37(3)
N(5)	7835(10)	4350(11)	2288(13)	48(4)
N(6)	5993(10)	20673(12)	-7316(13)	50(4)
N(7)	8396(13)	1226(15)	3133(19)	74(7)
N(8)	-2771(10)	15607(11)	-2121(10)	38(3)

Table 5.23 *Selected bond lengths (Å) and angles (°) for DMAP-GaPO*

Ga(1)-O(4)	1.742(9)	O(11)-Ga(3)-O(12)	123.5(4)
Ga(1)-O(3)	1.772(8)	O(10)-Ga(3)-O(12)	93.9(4)
Ga(1)-O(2)	1.792(10)	O(11)-Ga(3)-O(9)	123.0(4)
Ga(1)-O(1)	1.802(7)	O(10)-Ga(3)-O(9)	90.2(4)
Ga(3)-O(11)	1.797(8)	O(12)-Ga(3)-O(9)	112.8(4)
Ga(3)-O(10)	1.808(8)	O(11)-Ga(3)-F(1)	89.5(4)
Ga(3)-O(12)	1.827(7)	O(10)-Ga(3)-F(1)	176.7(3)
Ga(3)-O(9)	1.833(7)	O(12)-Ga(3)-F(1)	84.4(3)
Ga(3)-F(1)	2.043(8)	O(9)-Ga(3)-F(1)	87.8(3)
P(9)-O(2)#1	1.494(9)	O(2)#1-P(9)-O(14)	108.4(5)
P(9)-O(14)	1.497(9)	O(2)#1-P(9)-O(32)	112.7(6)
P(9)-O(32)	1.506(8)	O(14)-P(9)-O(32)	112.3(5)
P(9)-O(1)	1.522(8)	O(2)#1-P(9)-O(1)	109.1(5)
		O(14)-P(9)-O(1)	106.7(5)
O(4)-Ga(1)-O(3)	106.5(5)	O(32)-P(9)-O(1)	107.4(4)
O(4)-Ga(1)-O(2)	117.3(5)	P(9)-O(1)-Ga(1)	130.6(5)
O(3)-Ga(1)-O(2)	110.0(4)	P(9)#1-O(2)-Ga(1)	134.6(5)
O(4)-Ga(1)-O(1)	109.4(5)	P(16)-O(3)-Ga(1)	142.0(6)
O(3)-Ga(1)-O(1)	104.8(4)	P(11)#1-O(4)-Ga(1)	149.1(8)
O(2)-Ga(1)-O(1)	108.1(4)	Ga(3)-F(1)-Ga(6)	119.1(3)
O(11)-Ga(3)-O(10)	93.8(4)		

Table 5.24 *Anisotropic displacement parameters ($Å^2$ x 10^3) for DMAP-GaPO. The anisotropic displacement factor exponent takes the form:*
$-2\pi^2 [h^2 a^{*2} U_{11} + ... + 2 h k a^* b^* U_{12}]$

	U_{11}	U_{22}	U_{33}	U_{23}	U_{13}	U_{12}
Ga(1)	12(1)	11(1)	13(1)	-2(1)	-3(1)	-4(1)
Ga(2)	13(1)	12(1)	13(1)	-2(1)	-2(1)	-6(1)
Ga(3)	15(1)	12(1)	12(1)	-2(1)	-2(1)	-4(1)
Ga(4)	16(1)	13(1)	13(1)	-1(1)	-4(1)	-6(1)
Ga(5)	14(1)	15(1)	13(1)	-3(1)	-1(1)	-6(1)
Ga(6)	16(1)	14(1)	14(1)	-3(1)	-4(1)	-4(1)
Ga(7)	14(1)	15(1)	15(1)	-4(1)	-2(1)	-5(1)
Ga(8)	14(1)	16(1)	15(1)	-4(1)	-2(1)	-5(1)
P(9)	17(1)	13(1)	11(1)	-1(1)	-3(1)	-5(1)
P(10)	19(1)	11(1)	12(1)	-3(1)	-2(1)	-3(1)
P(11)	18(1)	11(1)	16(1)	-2(1)	-4(1)	-4(1)
P(12)	18(1)	10(1)	13(1)	-3(1)	-5(1)	-3(1)
P(13)	12(1)	15(1)	13(1)	-2(1)	-2(1)	-8(1)
P(14)	14(1)	11(1)	15(1)	-1(1)	-5(1)	-4(1)
P(15)	10(1)	16(1)	13(1)	-4(1)	0(1)	-4(1)
P(16)	11(1)	19(1)	14(1)	-6(1)	-4(1)	-3(1)

Table 5.24 Cont'd

	U_{11}	U_{22}	U_{33}	U_{23}	U_{13}	U_{12}
O(1)	36(4)	11(3)	7(3)	-1(3)	-6(3)	-6(3)
O(2)	19(3)	23(4)	24(4)	-8(3)	-5(3)	0(3)
O(3)	19(3)	26(4)	24(4)	-8(3)	-11(3)	1(3)
O(4)	26(5)	30(5)	52(7)	-15(5)	14(5)	-22(5)
O(5)	27(4)	9(3)	16(4)	-4(3)	-4(3)	-2(3)
O(6)	11(3)	32(5)	14(3)	-3(3)	2(3)	-10(3)
O(7)	17(3)	32(5)	23(4)	-6(4)	-2(3)	-16(4)
O(8)	22(4)	15(4)	35(5)	-1(3)	-16(4)	1(3)
O(9)	31(4)	8(3)	14(3)	-3(3)	-6(3)	2(3)
O(10)	25(4)	7(3)	9(3)	-7(2)	5(3)	2(3)
O(11)	23(4)	17(4)	35(5)	-15(4)	7(4)	-6(4)
O(12)	15(3)	38(5)	26(4)	-22(4)	-8(3)	1(4)
O(13)	32(4)	19(4)	23(4)	-6(3)	-16(4)	-10(3)
O(14)	26(4)	13(4)	14(3)	-6(3)	0(3)	0(3)
O(15)	17(3)	31(5)	28(4)	-20(4)	4(3)	-14(4)
O(16)	18(3)	13(3)	10(3)	-8(3)	3(3)	-1(3)
O(17)	25(4)	24(4)	21(4)	-8(3)	-1(3)	-15(4)
O(18)	21(3)	8(3)	12(3)	-2(3)	6(3)	1(3)
O(19)	17(3)	7(3)	39(5)	4(3)	-4(4)	-5(3)
O(20)	53(6)	15(4)	16(4)	-4(3)	-5(4)	-15(4)
O(21)	17(3)	20(4)	17(4)	-9(3)	2(3)	-4(3)
O(22)	29(4)	13(3)	15(3)	-2(3)	-6(3)	-6(3)
O(23)	38(5)	19(4)	6(3)	-3(3)	1(3)	-9(4)
O(24)	33(5)	19(4)	36(5)	0(4)	-19(4)	-14(4)
O(25)	15(3)	23(4)	25(4)	-2(3)	-3(3)	-9(3)
O(26)	16(3)	21(4)	15(4)	-6(3)	4(3)	1(3)
O(27)	18(4)	32(5)	18(4)	-3(3)	-4(3)	-14(4)
O(28)	26(4)	38(6)	33(5)	-24(4)	12(4)	-23(4)
O(29)	16(3)	39(5)	19(4)	-1(4)	-7(3)	-18(4)
O(30)	14(3)	23(4)	18(4)	-5(3)	-7(3)	6(3)
O(31)	28(4)	42(6)	46(6)	-30(5)	-21(5)	14(5)
O(32)	35(5)	18(4)	26(4)	-2(3)	-18(4)	-6(4)
O(33)	41(5)	16(4)	22(4)	-8(3)	4(4)	-15(4)
O(34)	27(4)	24(5)	32(5)	-11(4)	-9(4)	4(4)
F(1)	27(3)	13(3)	23(3)	-6(3)	-10(3)	-2(3)
F(2)	23(3)	16(3)	13(3)	-5(2)	3(3)	-6(3)
C(1)	53(11)	65(15)	63(13)	2(11)	-30(10)	-19(11)
C(2)	38(7)	13(5)	38(7)	-3(5)	-17(6)	-5(5)
C(3)	38(7)	28(7)	27(6)	-18(5)	-5(6)	-8(6)
C(4)	46(9)	42(10)	42(9)	-22(8)	-4(8)	-11(8)
C(5)	34(7)	31(7)	49(9)	-27(7)	-15(7)	-2(6)
C(6)	39(11)	43(13)	220(40)	-7(19)	-16(17)	-16(11)
C(7)	63(16)	130(30)	300(50)	-50(20)	14(18)	180(30)
C(8)	46(9)	39(9)	52(10)	-27(8)	-13(8)	-4(8)
C(10)	52(10)	55(12)	53(10)	-37(9)	4(9)	-20(10)
C(12)	48(10)	49(11)	33(8)	-16(8)	10(8)	-16(9)
C(14)	83(16)	44(11)	47(10)	-20(9)	-11(10)	-23(12)
C(15)	69(13)	50(11)	75(14)	-45(11)	-23(11)	-11(11)
C(18)	45(10)	64(14)	62(12)	-47(11)	6(9)	-6(10)
C(20)	69(15)	62(16)	110(20)	-71(16)	10(15)	-8(14)
C(21)	39(9)	52(13)	69(14)	-31(11)	29(10)	-10(10)
C(22)	39(8)	32(8)	45(9)	-19(7)	-17(7)	-1(7)
C(23)	57(10)	35(8)	26(7)	-15(6)	-2(7)	-16(8)
C(24)	47(9)	47(11)	36(8)	-23(8)	-6(8)	2(9)
C(25)	58(11)	25(8)	64(13)	-10(9)	-10(10)	11(9)
C(26)	37(9)	100(20)	90(16)	-65(15)	-15(10)	-15(12)
C(27)	61(12)	54(12)	35(9)	-12(8)	-20(8)	-9(10)
C(30)	59(14)	90(20)	190(30)	-120(20)	-14(17)	3(14)

Table 5.24 Cont'd

	U_{11}	U_{22}	U_{33}	U_{23}	U_{13}	U_{12}
C(33)	39(8)	40(9)	43(9)	-31(8)	2(7)	5(8)
N(1)	30(7)	46(10)	120(16)	-37(11)	9(9)	-20(8)
N(2)	59(9)	25(6)	92(12)	-30(7)	-54(9)	13(6)
N(3)	43(8)	20(7)	110(15)	-23(9)	-9(10)	0(7)
N(4)	22(5)	34(7)	48(8)	-20(6)	3(6)	-2(5)
N(5)	45(8)	24(6)	90(12)	-40(7)	-19(8)	8(6)
N(6)	48(8)	33(8)	74(11)	-27(8)	-8(8)	-9(7)
N(7)	39(8)	37(9)	131(19)	-22(12)	-16(11)	-7(8)
N(8)	47(8)	39(8)	35(7)	-19(6)	12(6)	-27(7)

5.4 Possible Mechanisms For Synthesis Of Small Molecule Templated Gallophosphates

As discussed in chapter 1 two mechanisms have been proposed for the formation of this type of material; the chain to layer transformation mechanism of Ozin[11] and the PNBU mechanism of Férey.[12] For the formation of [pyr,O]-GaPO-4 the choice is simple. The structure could not be explained by any argument other than the existence in solution of oxygen centred D4R PNBUs with a structure very similar to that of the final product. In the case of the fluoride route we cannot form a definitive conclusion by looking at the final solids. The three [pyr,F]-GaPO structures form around three slightly different template groupings and clearly the equilibrium between the pyridinium ion (template of [pyr,F]-GaPO-3) and the pyridinium-water complex ([pyr,F]-GaPOs 1 and 2) is of some significance, however, it seems more important that the two types of structure (UT-6 analogues [pyr,F]-GaPOs 1 and 2 and [pyr,F]-GaPO-3) have very different SBUs. [pyr,F]-GaPOs 1 and 2 are composed of D6R units while the unit of [pyr,F]-GaPO-3 seems to be related to the double four ring. For the D6R based structures there are two possible arguments, firstly that the materials could be formed from chain type precursors, linked by the octahedral $Ga_2O_8F_2$ unit found in the final structure (fig. 5.24) and secondly that D6R-like PNBUs are formed in solution which then link via both Ga-F-Ga and Ga-O-P bonds to form the final structure (fig 5.25). The second argument may be supported by the

larger template clusters found for [pyr,F]-GaPOs 1 and 2 would probably stabilise large PNBUs like the D6R, however, some of the evidence from the synthesis study (section 5.2.3 above) seems to support the chain theory.

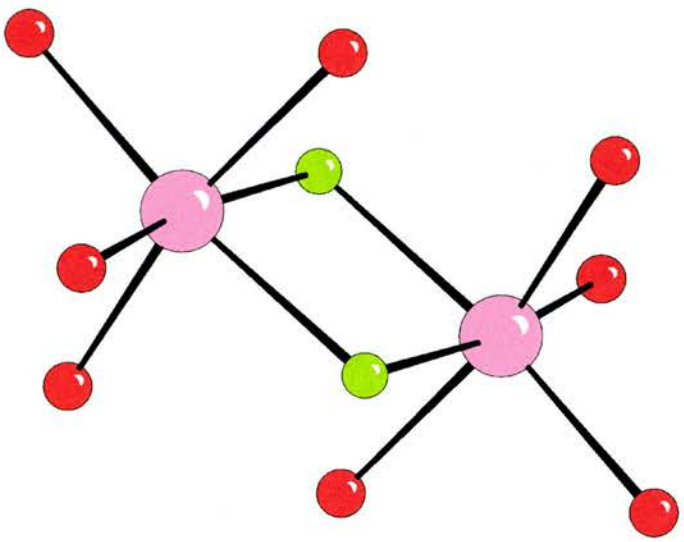

Figure 5.24 *The Double octahedral gallium unit in which the fluorine atoms of [pyr,F]-GaPOs 1 and 2 are located. A similar unit may exist in solution prior to crystallisation of these materials.*

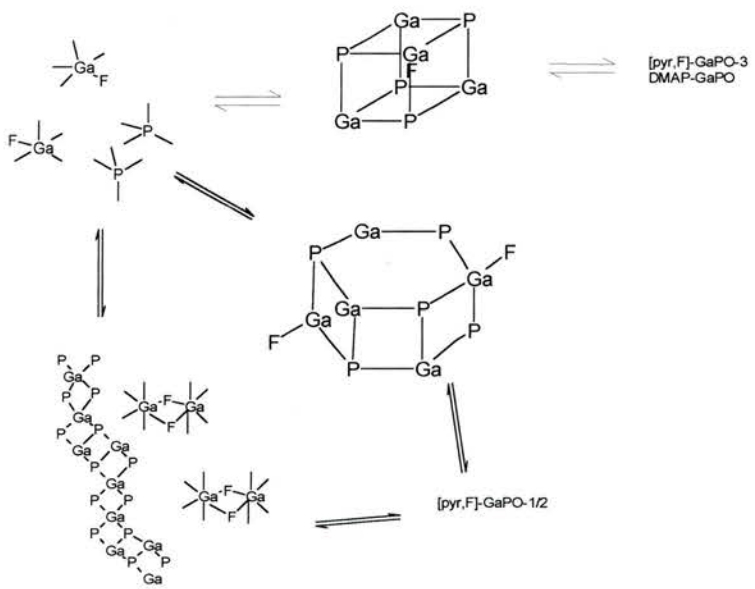

Figure 5.25 *Possible precursors to pyridine and DMAP-GaPO structures. Both the chain and the D6R unit can lead to the structure (see below). Oxygen atoms are omitted for clarity.*

Mechanisms for the formation of [pyr,F]-GaPOs 1 and 2 can be postulated. The chain mechanism is that described by Ozin for the formation of AlPO UT-6, with chains of single four rings being linked by $Ga_2O_8F_2$ dimers with the loss of water. A further condensation then takes place to give the Ga-O-P linkages between the chains (fig. 5.26).

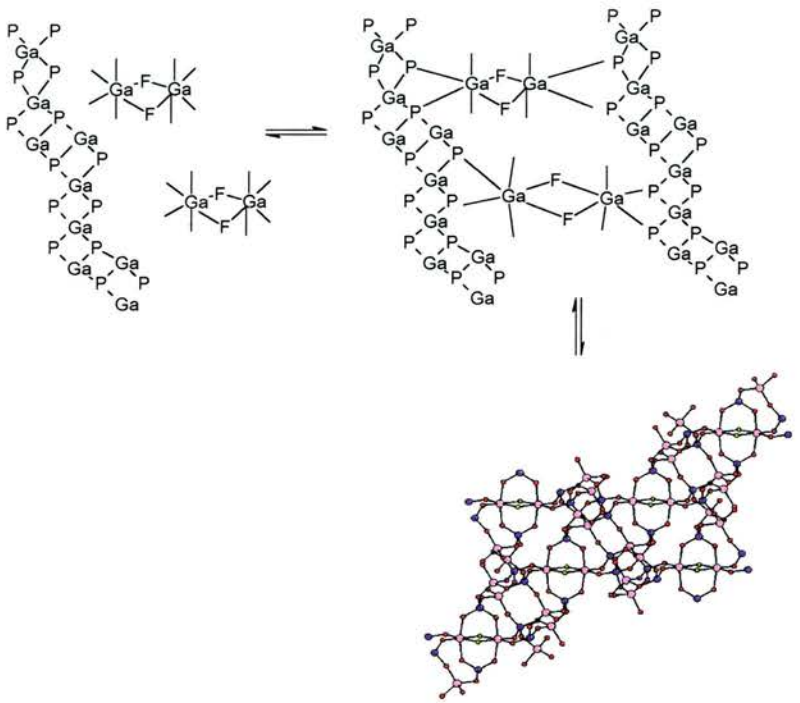

Figure 5.26 *Schematic diagram of the formation of [pyr,F]-GaPO-1/2 from chain precursors*

The mechanism involving D6R PNBUs is similar to the chain mechanism. The pendant fluorine atoms of the D6R units come into close proximity, possibly via some direction by the pyridinium-water complex, these then form chains linked by the $Ga_2O_8F_2$ dimers. Condensation between parallel chains then occurs giving the single four ring linkages (fig 5.27)

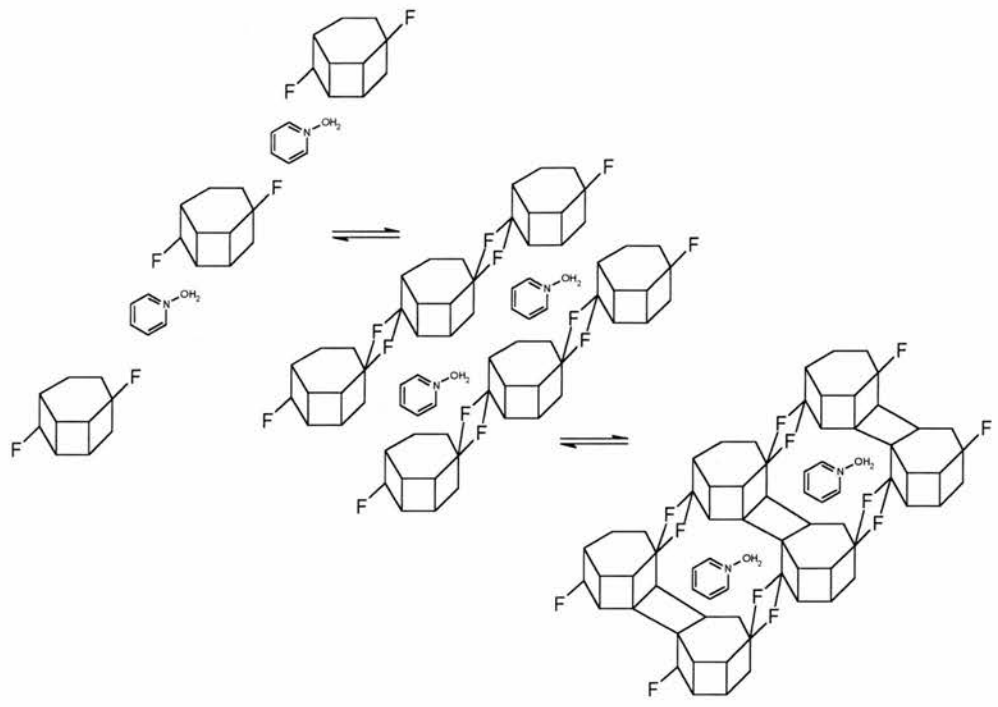

Figure 5.27 *Schematic diagram of the formation of [pyr,F]-GaPO-1/2 from D6R PNBUs*

The similarity between the D4R and the SBU of [pyr,F]-GaPO-3 leads us to believe that this material is almost certainly produced by a mechanism in which a fluorine centred D4R PNBU isomerises to form the unit and the final structure in a similar manner to that observed in AlPO-CJ2.[13] These units are common in GaPO materials (fig.5.28, table 5.25) and it has been suggested that the fluoride ion acts as a template for the D4R;[14] it is therefore highly likely that they are present in the solution.

Table 5.25 *GaPO materials containing fluoride encapsulated D4Rs*

Material	Reference
MU-15	14
GaPO-LTA	15
Cloverite	16
Mu-1	8
Mu-3	17
Cyclam-GaPO	18
ULM-5	19
ULM-18	20

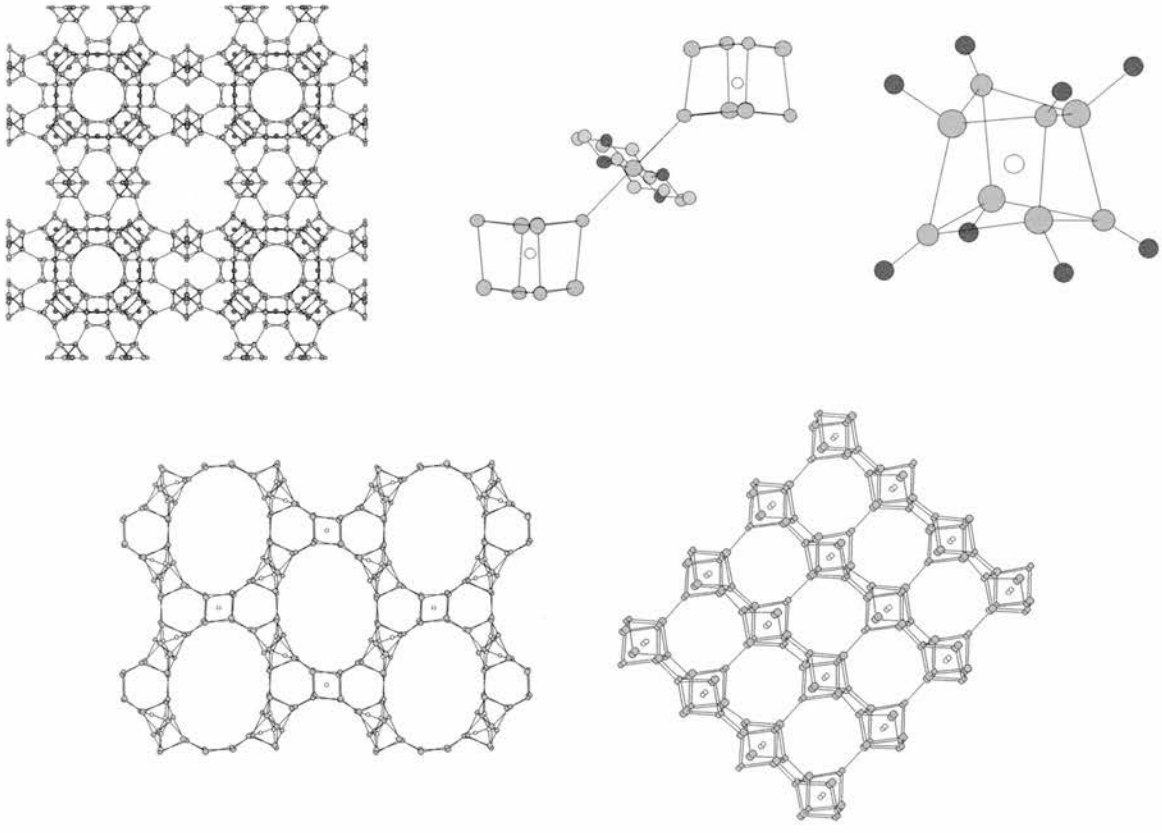

Figure 5.28 *Some of the GaPO structures based on the D4R unit with encapsulated fluoride. Cloverite, cyclam-GaPO and MU-1 (cubic anion, ULM-5 (two types of SBU) and MU-15 . Large grey spheres represent gallium, small phosphorus; white spheres fluorine. In the cyclam ring pale grey spheres represent carbon and dark grey nitrogen other organics omitted. Oxygen and hydrogen atoms are omitted for clarity.*

The side opening of D4Rs has been observed for polyhedral oligomeric silsesquioxanes[21] (POSS, see chapter 1) and is thought to reduce strain in the silicate D4R cage. In POSS systems side opening occurs under proton attack, this could also be the case for the formation of the [pyr,F]-GaPO-3 unit with proton attack on a fluoride centred D4R followed by stabilisation of the unit by a second fluoride ion; alternatively the initial attack could be by fluoride. A similar type of SBU is observed

in DMAP-GaPO and this could again be formed by proton attack on a fluoride centred D4R. In this case however, there is no further fluorine in the structure (fig. 5.29). It is possible that the concentration of fluoride ions influences the final structure.

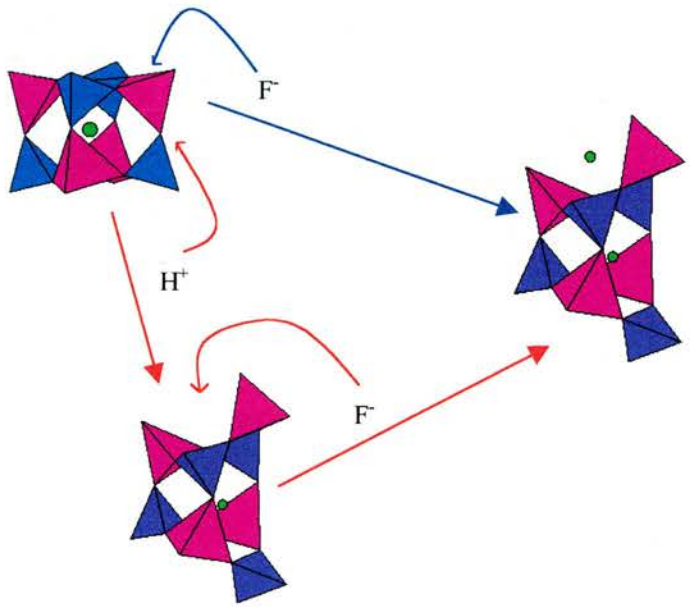

Figure 5.29 *Possible mechanisms for the formation of the side opened D4R units of [pyr,F]-GaPO-3 (a) and DMAP-GaPO (b). As shown the proton attack which forms the DMAP-GaPO SBU could also lead to the [pyr,F]-GaPO-3 SBU if followed by fluoride attack.*

It seems that a very complex set of equilibria are present in the synthesis mixture of a pyridine-GaPO preparation. D4R PNBUs are almost certainly present along with pyridinium ions, possibly complexed with water molecules. In addition there exists either a mixture of GaPO chains and $Ga_2O_8F_2$ units or D6R PNBUs. The crystallisation of one of the product phases leads to its precursors being favoured at the expense of the others in the equilibrium, leading to single phase products. Fluoride in this case does not seem to directly template the D4R unit as suggested by some but undoubtedly plays a role in the formation of the D4R PNBUs of [pyr,F]-GaPO-3 and

DMAP-GaPO. The difference between [pyr,F]-GaPOs 1 and 2 is extremely small, and it is very difficult to determine what favours one over the other in terms of the mechanisms of formation. It is possible as discussed above in section 5.2.3 that one is simply a kinetic product or that greater possibility of hydrolysis favours the more twisted [pyr,F]-GaPO-1.

References

1. R.M. Szostak, *Molecular Sieves, Principles of Synthesis and Identification,* Van Nostrand Rienhold, New York, 1989, Ch. 1.
2. S.J. Weigel, T. Louiseau, G. Férey, V. Munch, F. Taulelle, R.E. Morris, G.D. Stucky and A.K. Cheetham, *Proc. 12th Intl. Zeolite Conference*, 1999, 2453.
3. S. Oliver, A. Kupermann, A. Lough and G.A., *J. Mater. Chem.*, 1997, **7**, 807.
4. A.J. Lough, P.S. Wheatley, G. Fergusonand C. Glidewell, Acta Crystallogra. B, 2000, **56**, 261.
5. S. Kallus, J. Patarin, and B. Marler, *Microporous Mater.,* 1996, **7**, 89.
6. J.R.D De Bord, W.M. Reiff, C.J. Warren, R.C. Haushalter and R.C. Zubieta, *J. Chem. Mater.,* 1997, **9**, 1994.
7. F. Taulelle, J-P. Probet and M. Bernaud, *J. Am. Chem. Soc.,* In Press.
8. T. Louiseau, D. Riou, M. Licheron and G. Ferey, *J. Solid State Chem.,* 1994, **111** 397.
9. T. Louiseau, R. Retoux, P. Lacorre and G. Ferey, *J. Solid State Chem.,* 1994, **111**, 427.
10. S. Feng, X. Xu, G. Yang, R. Xu and F. P. Glasser, *J. Chem. Soc. Dalton Trans.,* 1995, 2147.
11. S. Oliver, A. Kuperman and G.A. Ozin, *Angew. Chem. Int. Ed.*, 1998, **37**, 46.
12. (a) G. Férey, *J. Fluorine Chem.*, 1995, **7**, 187; (b) G. Férey, *C.R. Acad. Sci. Ser. C.*, 1998, **1**, 1.
13. F. Taulelle, M. Pruski, J.P. Amoureaux, D. Lang, A. Bailly, C. Hugenard, M. Haouas, C. Geradin, T. Lousieau and G. Férey, *J. Am. Chem. Soc.,* 1999, **121**, 12148.
14. A. Matijasic, J-L. Paillaud, J. Patarin, *J. Mater. Chem.,* 2000, **10**, 1345.

15. A. Simmen, J. Patarin and Ch. Baerlocher, *Proc. 9th Intl. Zeolite Conference*, 1992, 433.

16. M. Estermann, L.B. McCusker, Ch. Baerlocher, A. Merrouche and H. Kessler, *Nature*, 1991, **352**, 320.

17. P. Rienert, J. Patarin, T. Loiseau, G. Férey and H. Kessler, *Microporous Mesoporous Mater.*, 1998, **22**, 43.

18. D.S. Wragg, G.B. Hix and R.E. Morris, *J. Am. Chem. Soc.*, 1998, **120**, 6822.

19. T. Loiseau and G. Férey, *J. Solid State Chem.*, 1994, **111**, 407.

20. F. Taulelle, A. Samoson, T. Loiseau and G. Férey, *J. Phys. Chem. B*, 1998, **102**, 8588.

21. F.J. Feher, D. Soulivong, A.G. Eklund, *J. Chem. Soc.Chem. Commun.*, 1998, 399.

CHAPTER 6

CONCLUSIONS AND FURTHER WORK

6.1 Conclusions

Several conclusions may be drawn from this thesis. The first is that there are still many new open-framework materials to be discovered in the GaPO system, illustrated by the discovery of an entirely new structural type, cyclam-GaPO. We also conclude that the use of macrocycles as templates for zeolite-type materials could be developed much further and that it is possible to modify the structure of cyclam-GaPO by the substitution of transition metal ions or gallium. This type of modification may also lead to new structural types.

The work presented on the synthesis of gallophosphates with small molecule templates illustrates the complexity of the mechanisms of hydrothermal synthesis, however we have again reached some conclusions:

- D4R PNBUs are present in solution with or without the presence of fluoride ions
- [pyr,O]-GaPO-4 crystallises directly from a D4R PNBU
- The D4R unit is probably the precursor to the SBUs of DMAP-GaPO and [pyr,F]-GaPO-3
- Fluoride does not necessarily stabilise the D4R unit

The mechanism of formation for [pyr,F]-GaPOs 1 and 2 remains unclear.

6.2 Further Work

Further work resulting from this project is currently underway in the synthesis of macrocycle templated open-framework materials. It is hoped that this will lead to a greater knowledge of the conditions under which these materials form and a better understanding of the role of the macrocycle as a structure directing agent.

It is possible that the mechanisms of formation of the various pyridine-GaPO phases may be elucidated by *in-situ* NMR or XRD experiments. It could well be possible to detect the $Ga_2O_8F_2$ unit, the D4R and the D6R as distinct moieties by the use of ^{19}F NMR, as the fluorine environments in each of these units would be expected to have very different chemical shifts. It may also prove possible to isolate the PNBU species as in the case of [pyr,O]-GaPO-4. The equilibrium between pyridinium and the pyridinium water complex could also be investigated and may prove crucial to the final understanding of this system. Work is already under way to attempt to pinpoint the location of the protons in [pyr,O]-GaPO-4 by means of isotope labelling NMR studies. It is hoped that the knowledge gained from the study of this series of compounds can eventually be applied to other zeolite-type materials.

Appendix

The compact disc below contains crystal structure data for the new structures reported in this thesis in CIF format. In addition an electronic copy of the manuscript is included.